

LI-ION BATTERY ENERGY STORAGE SYSTEMS: Effect of Separation Distances based on a Radiation Heat Transfer Analysis

A Graduate Independent Study Research Project

Submitted by:

Victoria Hutchison
WPI Graduate Student

Submitted to:

Professor Milosh Puchovsky PE, FSFPE
Department of Fire Protection Engineering
Worcester Polytechnic Institute
Worcester, MA 01609



WPI

12 JUNE 2017

Table of Contents

Table of Figures	iv
List of Tables	vi
Table of Equations	vii
Abbreviations and Acronyms	viii
Symbols	ix
Acknowledgement	xi
Disclaimer	xi
Abstract	xii
1. Introduction	13
2. Background	15
2.1 Overview of Energy Storage Systems	15
2.1.1 Makeup of a Lithium-Ion Battery ESS	16
2.1.1.1 Cell	17
2.1.1.2 Module	17
2.1.1.3 Rack	18
2.1.1.4 Containerized Energy Storage System	18
2.1.1.5 Other Components	19
2.1.2 Utility Scale Containerized Li-Ion ESS Installations	19
2.2 Lithium-Ion Battery (LIB) Technology	21
2.2.1 LIB Components	21
2.2.2 Applicability of Lithium-Ion Batteries for Energy Storage Systems	22
2.3 The Fire Safety Concerns with Lithium-Ion Battery ESS	22
2.3.1 Failure Modes Resulting in Fire	23
3. Lithium-Ion Battery Fire Events	26
3.1 Arizona ESS Fire	26
3.2 Union Pacific Train Car Explosion Involving LIB's	26
3.3 Two Fires in Boeing 787 Lithium-ion Battery Units	27
3.4 S&C Electric Lithium-Ion ESS fire in Wisconsin	28
3.5 Impact of Previous Fire Events on this Study	28
4. Research and Testing of Lithium-Ion Batteries and ESS	29
4.1 FPRF/Exponent Hazard Assessment of Lithium-Ion Battery ESS	29
4.2 US FAA-Style Flammability Assessment of Lithium-Ion Cells and Battery Packs in Aircraft Cargo Holds	29
4.3 FAA Energetics of Lithium-Ion Battery Failure	30
4.4 DNV GL Considerations for ESS Fire Safety	30
5. Fire Safety Regulations	32
6. Scope of Heat Transfer Analysis	33
7. Methodology of Heat Transfer Analysis	35
7.1 Governing Radiation Heat Transfer Equation	35

7.2 Properties of Radiant Bodies	36
7.2.1 Emissivity of Steel Containers.....	37
7.2.2 Emissivity of Flame	38
7.3 Configuration/View Factor	38
7.3.1 Shape	39
7.3.2 Orientation	39
7.3.3 Dimensions	39
7.3.4 View Factor Calculation	40
7.3.4.1 Parallel Rectangular Plates View Factor.....	40
7.3.4.2 Cylinder to Rectangular Plate View Factor.....	42
7.4 Temperature of Radiant Body.....	44
7.4.1 Wall Temperature of ESS Fire Source	44
7.4.1.1 Heat Transfer Coefficient	45
7.4.1.2 Thermal Conductivity of Steel.....	46
7.4.2 Gas Layer Temperature of ESS Fire Inside Compartment.....	46
7.4.2.1 Forced Ventilation.....	48
7.4.3 Characterization of ESS Fire	49
7.4.3.1 Ignition	50
7.4.3.2 Growth Phase: Fire Propagation throughout ESS	52
7.4.3.3 Fully Developed Fire.....	57
7.4.3.4 Decay Phase	59
7.4.4 Flame Temperature	59
7.5 Total Radiant Flux from ESS Fire Source	59
7.6 Heat Transfer Between ESS Fire Source and Target ESS.....	61
7.6.1 Thermal Threshold of Exposed ESS.....	61
7.6.2 Inside Air Temperature of Target ESS.....	62
7.6.3 Surface Temperature of Target ESS	63
8. Results.....	65
8.1 Results for 20 ft Exposed ESS Containers.....	65
8.2 Results of 40 ft Exposed ESS Containers	69
8.3 Results of 53 ft Exposed ESS Containers	73
8.4 Discussion of Results	77
9. Conclusions	80
10. Recommendations for Future Work.....	80
Bibliography.....	81
Appendix A: Additional Reference Material.....	88
Appendix B: NFPA 2017 C&E Presentation.....	91

Table of Figures

Figure 1 Deployed Li-Ion Based ESS (DOE Energy Storage Strategic Plan, (2014).	16
Figure 2 Lithium-Ion Cells: Cylindrical, Prismatic, and Pouch Cell (Respectively) [13].....	17
Figure 3 Prismatic Li-Ion Battery Module (ALEVO)	17
Figure 4 LIB Enclosed Rack (Left [14]), LIB Open Frame Rack (Right [15]).....	18
Figure 5 Containerized Energy Storage System [14]	19
Figure 6 AES 30 MW (120 MWh) Li-Ion ESS Installation in San Diego, CA [19].....	20
Figure 7 Principal Operation of Lithium-Ion Battery during Charge/Discharge [23].....	21
Figure 8 Lithium-Ion Battery Thermal Runaway Chain of Events	24
Figure 9 Explosion in Union Pacific Train Car filled with Lithium-Ion Batteries.....	26
Figure 10 Boeing 787 APU Li-Ion Battery Module after Thermal Runaway (FAA/NTSB).....	27
Figure 11 Fire involving Li-ion ESS inside S&C Electric Manufacturing Facility	28
Figure 12 Schematic of Approach to Heat Transfer Analysis	35
Figure 13 Absorptivity, reflectivity, and transmissivity of incident heat flux.....	37
Figure 14 Parallel Rectangular Plate View Factor.....	41
Figure 15 Cylinder to Vertical Rectangular Plate View Factor.....	42
Figure 16 HRR Curve Demonstrating Stages of ESS Fire [62].....	50
Figure 17 Area under the curve - Peak Heat Release Rate (Mowrer & Williamson, 1990).....	56
Figure 18 Radiation Heat Transfer Exchange.....	61
Figure 19 – Interior Temperature Profile of Exposed 20 ft ISO Container (500 kWh Exposure)	65
Figure 20 – Interior Temperature Profile of Exposed 20 ft ISO-Container (1 MWh).....	66
Figure 21 – Interior Temperature Profile of Exposed 20 ft ISO-Container (2 MWh).....	66
Figure 22 - Interior Temperature Profile of Exposed 20 ft ISO-Container (3 MWh)	67
Figure 23 - Interior Temperature Profile of Exposed 20 ft ISO-Container (4 MWh)	67
Figure 24 - Interior Temperature Profile of Exposed 20 ft ISO-Container (5 MWh)	68
Figure 25 - Time to Reach Thermal Threshold for Exposed 20 ft ISO Containers.....	68
Figure 26 – Interior Temperature Profile of Exposed 40 ft ISO Container (500 kWh Exposure)	69
Figure 27 – Interior Temperature Profile of Exposed 40 ft ISO Container (1 MWh Exposure)..	70
Figure 28 - Interior Temperature Profile of Exposed 40 ft ISO Container (2 MWh Exposure)..	70
Figure 29 - Interior Temperature Profile of Exposed 40 ft ISO Container (3 MWh Exposure)..	71
Figure 30 - Interior Temperature Profile of Exposed 40 ft ISO Container (4 MWh Exposure)..	71
Figure 31 - Interior Temperature Profile of Exposed 40 ft ISO Container (5 MWh Exposure)..	72
Figure 32 - Time to Reach Thermal Threshold for Exposed 40 ft ISO Containers.....	72
Figure 33 – Interior Temperature Profile of Exposed 53 ft ISO Container (500 kWh Exposure)	73
Figure 34 - Interior Temperature Profile of Exposed 53 ft ISO Container (1 MWh Exposure)..	74
Figure 35 - Interior Temperature Profile of Exposed 53 ft ISO Container (2 MWh Exposure)..	74
Figure 36 Interior Temperature Profile of Exposed 53 ft ISO Container (3 MWh Exposure).....	75
Figure 37- Interior Temperature Profile of Exposed 53 ft ISO Container (4 MWh Exposure)..	75
Figure 38 - Interior Temperature Profile of Exposed 53 ft ISO Container (5 MWh Exposure)..	76
Figure 39 - Time to Reach Thermal Threshold for Exposed 53 ft ISO Containers.....	76
Figure 40 - Time to Failure for 20 ft, 40 ft, 53 ft ISO Containers (2 MWh Energy Capacity Exposure).....	77
Figure 41 - Time to Failure for 20 ft, 40 ft, 53 ft ISO Containers (3 MWh Energy Capacity Exposure).....	78

Figure 42 - Time to Failure for 20 ft, 40 ft, 53 ft ISO Containers (4 MWh Energy Capacity Exposure)	78
Figure 43 - Time to Failure for 20 ft, 40 ft, 53 ft ISO Containers (5 MWh Energy Capacity Exposure)	79
Figure 44 Grid-tied MW scale Li-Ion ESS installations.....	89
Figure 45 20 ft ISO Container	89
Figure 46 40 ft ISO Container	89
Figure 47 53 ft Modified ISO-Container	90

List of Tables

Table 1 Parallel Rectangular Plate Emitting/Receiving Areas	39
Table 2 Cylinders to Vertical/Horizontal Rectangular Plates Emitting/Receiving Areas	40
Table 3 View Factors for Parallel Rectangular Plates at Various Separation Distances	42
Table 4 Cylinder to Rectangular Plate View Factors.....	43
Table 5 Forced Ventilation Rates	48
Table 6 Mass Loss Rates for Various Battery Formats	55
Table 7 Heat Release Rates.....	56
Table 8 Quantity of Gas released for systems of various Energy Capacities	57

Table of Equations

Equation 1 Stefan-Boltzmann Law of Thermal Radiation.....	36
Equation 2 Governing Radiant Heat Flux Equation	36
Equation 3 Radiation Conservation of Energy Principle	37
Equation 4 Principle of Blackbody Radiation	37
Equation 5 Absorptivity of Steel Panel	37
Equation 6 Emissivity of Steel Panel	38
Equation 7 Emissivity of Flame	38
Equation 8 Flame Height	39
Equation 9 Parallel Plate View Factor	41
Equation 10 Intermediate equation for Parallel Plate View Factor	41
Equation 11 Intermediate equation for Parallel Plate View Factor	41
Equation 12 Intermediate equation for Parallel Plate View Factor	41
Equation 13 Intermediate equation for Parallel Plate View Factor	41
Equation 14 Cylinder to Parallel Plate View Factor (Vertical)	43
Equation 15 Cylinder to Rectangular Plate View Factor (Horizontal).....	43
Equation 16 Intermediate equation for Cylinder to Rectangular Plate View Factor	43
Equation 17 Intermediate equation for Cylinder to Rectangular Plate View Factor	43
Equation 18 Intermediate equation for Cylinder to Rectangular Plate View Factor	43
Equation 19 Intermediate Equation for Cylinder to Rectangular Plate View Factor.....	43
Equation 20 Lumped Solid Analysis of Container Wall	44
Equation 21 Temperature Rise of Wall of ESS Fire Source	45
Equation 22 Heat Transfer Coefficient for Hot Side of Wall (Steel Plate)	45
Equation 23 Heat Transfer Coefficient on Ambient Side of Wall (Steel Plate)	46
Equation 24 Thermal Conductivity of Steel ($20^{\circ}\text{C} < T_w < 800^{\circ}\text{C}$).....	46
Equation 25 Thermal Conductivity of Steel ($T_w > 800^{\circ}\text{C}$)	46
Equation 26 MQH Correlation of Hot Gas Layer Temperature	46
Equation 27 FPA Correlation for Hot Gas Layer Temperature - Forced Ventilation.....	48
Equation 28 Growth Function to Peak Heat Release Rate.....	54
Equation 29 Peak Heat Release Rate.....	55
Equation 30 Mass Flow Rate of Gas Layer.....	55
Equation 31 Change in Pressure.....	58
Equation 32 Velocity of Flammable Gases Out of Vent.....	58
Equation 33 Temperature Dependent Density	58
Equation 34 Adjusted Velocity for Temperature Dependent Density.....	58
Equation 35 Total Radiant Heat Flux.....	59
Equation 36 Received Radiant Heat Flux from Heated Steel Panel of ESS Fire Source	59
Equation 37 Received Radiant Heat Flux from Externally Vented Flames.....	60
Equation 38 Conservation of Energy "Storage" Term for Heat Absorbed into Surface	62
Equation 39 Enthalpy Flow between Heated Surface and Air.....	62
Equation 40 Internal Air Temperature	62
Equation 41 Temperature of Steel Panel of Exposed ESS.....	63

Abbreviations and Acronyms

AC	Alternating Current
APS	Arizona Public Service Company
APU	Auxiliary Power Unit
CO	Carbon Monoxide
CO ₂	Carbon Dioxide
DOE	Department of Energy
DC	Direct Current
ESS	Energy Storage System
FAA	Federal Aviation Administration
FM	FM Global
FPA	Foote, Pagni, Alvarez Correlation for Forced Ventilation Fires
FPRF	Fire Protection Research Foundation (Affiliate of NFPA)
GW	Gigawatts
H ⁺	Hydrogen
HRR	Heat Release Rate
IBC	International Building Code
IFC	International Fire Code
IRC	International Residential Code
ISC	Internal Short Circuit
ISO	International Organization for Standardization
kW	Kilowatts
kWh	Kilowatt-hour
LFP	Lithium Iron Phosphate
LIB	Lithium Ion Batteries
LiCoO ₂	Lithium-Cobalt Oxide
LiMn ₂ O ₄	Lithium Manganese Oxide
LiPF ₆	Lithium Fluorophosphate
MQH	McCaffrey, Quintiere, Harkleroad Correlation
MW	Megawatts
MWh	Megawatt-hour
NaS	Sodium-Sulfur Battery
NCA	Lithium Nickel-Cobalt Aluminum Oxide
NCM	Lithium Nickel-Cobalt Manganese Oxide
NFIRS	National Fire Incident Reporting System
NFPA	National Fire Protection Association
NiCd	Nickel-Cadmium Battery
NTSB	National Transportation and Safety Board
OC	Oxygen Consumption Calorimetry
SDG & E	San Diego Gas & Electric
SEI	Solid Electrolyte Interface
SFPE	Society of Fire Protection Engineers
SOC	State of Charge
THC	Total Hydrocarbons
UL	Underwriter's Laboratories

Symbols

A_w	Area of wall exposed to heat (m^2)
A_s	Surface area of container boundary surfaces (m^2)
α	Absorptivity
α_g	Fire Growth Rate Constant (kW/s^2)
$c_{p,air}$	Specific heat of air ($kJ/kg-K$)
$c_{p,steel}$	Specific heat of the steel panel ($kJ/kg-K$)
dt	Time step (s)
ε	emissivity (flame and surface)
$F1_{p,2p}$	Rectangular Parallel Plate Geometric View Factor
$F1_{c,2p}$	Cylindrical Flame to Rectangular Plate View Factor
g	Gravity (m/s^2)
H	Separation distance between parallel plates (m)
h	Heat Transfer Coefficient (kW/m^2K)
H_c	Height of Compartment (m)
H_f	Flame Height (m)
H_r	Flame Height (m)
ΔH_c	Effective Heat of Combustion (MJ/kg)
k	Thermal Conductivity ($kW/m-K$)
k_a	Absorption coefficient (m^{-1})
l	Flame thickness (m)
\dot{m}	Mass flow rate (kg/s)
\dot{m}_{air}	Mass flow rate of air through compartment (kg/s)
\dot{m}_{fuel}	Mass loss rate of fuel (kg/s)
p	Pressure (Pa or N/m^2)
ρ_{air}	Density of air (kg/m^3)
ρ_s	Density of steel (kg/m^3)
ρ	Reflectivity
\dot{Q}	Heat Release Rate (kW)
\dot{q}''	Radiant Heat Flux (kW/m^2)
R_1	Radius of cylindrical externally vented flame (m)
R_2	Separation Distance between cylindrical flame and parallel plate (m)
σ	Stefen-Boltzman Constant (kW/m^2K^4)
T_{air}	Temperature of Inside Air of Exposed ESS (K)
T_{fl}	Temperature of Flame (K)
T_g	Temperature of Hot Gas Layer (K)
$T_{S,Hot}$	Temperature of Exposed ESS Steel Panel (K)
T_w	Temperature of Heated Boundary Layer of ESS Fire Source (K)
T_∞	Ambient Temperature (K)
t	Time (s)
τ	Transmissivity
u	Vent flow velocity (m/s)
V	Volume (m^3)

\dot{V}	Volumetric Flow Rate of Air (m^3/s)
W_1	Length of container (m)
W_2	Height of container (m)
Δx_s	Thickness of steel (m)
Δx_{air}	Thickness of air gap between container wall and battery racks (m)

Acknowledgement

The author would like to gratefully acknowledge the support of the National Fire Protection Association (NFPA) that provided a fellowship used to fund this graduate independent research study. It is noted that NFPA did not direct how the funds of the fellowship were to be used. The author would also like to thank Professor Nicholas Dembsey at Worcester Polytechnic Institute for his input.

Disclaimer

This report reflects research conducted as part of a graduate independent study project within the Department of Fire Protection Engineering at Worcester Polytechnic Institute (WPI). The views and conclusions presented in this document are solely those of the authors and should not be interpreted as being necessarily representative of NFPA or WPI.

Abstract

The global market for Energy Storage Systems (ESS) continues to grow significantly. ESS facilities pose unique challenges with respect to fire safety. They can be the source of fast developing fires of significant heat release. A uniform and definitive approach regarding the relevant fire hazards and how to address them is not fully established. This study summarizes the growing use of ESS specific to lithium-ion battery technology, addresses and characterizes the associated uncontrolled fire hazards, and correlates heat release rate to ESS energy density. Through a radiation heat transfer analysis separation distances between adjacent ESS containers are examined. The results of this study can be used to inform the development of standardized spacing practices for ESS containers based on associated energy capacity and container size.

1. Introduction

Energy storage is an emerging market that plays an integral role for attaining a resilient and efficient electrical grid [1]. The evolution of the electrical grid is anticipated to require a variety of services such as energy management, backup power, load leveling, frequency regulation, voltage support, grid stabilization, etc. all of which can be facilitated through energy storage systems (ESS) [1]. The anticipated increase in demand for these ESS drives manufacturers to produce products with greater efficiency at a lower cost – promoting the greater deployment of ESS worldwide.

The Paris Agreement as part of the United Nations Framework on Climate Change, has put forth an aggressive clean energy initiative to reduce 80% of the greenhouse gas emissions by 2050 [2]. This 80 x 50 initiative is driving accelerated investments into renewable energy sources such as solar and wind farms, which are supplemented with energy storage systems [3]. Government entities and many organizations worldwide are in favor of the implementation of renewable energy – providing tax incentives for the use of renewable energy and energy storage systems – as part of the overall clean energy initiative [8].

The energy storage market is composed of four general technologies: electrochemical, chemical, thermal, and mechanical [4]. This report focuses on the electrochemical technology of secondary rechargeable batteries, with a specific focus on the lithium-ion technology. In recent years, there has been a marked increase in the use of lithium ion batteries in ESS's – accounting for nearly 50% of deployed battery-based energy storage systems [1]. The family of lithium-ion batteries are favorable in the energy storage industry due to their high energy densities, high efficiency, and cycle life.

Although ESS's play an integral role in being able to store the energy generated by renewable energy sources, such ESS facilities have the potential for fast developing fires of significant heat release. In general, storing large amounts of energy in a confined space is a challenge, due to the physics behind energy. Energy wants to be elsewhere – it naturally wants to spread out [5]. So packing large quantities of energy into a small confined space presents the potential for a violent energy release in the form of a fire or explosion. This report focuses on an analysis of the fire propagation hazard between adjacent ESS containers.

The potential impact of a fire in a lithium-ion battery ESS is significant based on the quantities of energy contained. Although battery and ESS manufacturers incorporate safety features into the designs to prevent a catastrophic event in a lithium-ion ESS, fire events in lithium-ion battery applications have occurred and have resulted in fires of significant duration. Similar risks are present in ESS installations.

A conclusive approach regarding how to address and quantify the relevant fire hazards in ESS containers is lacking due to the limited availability of technical studies and research reports. Beyond the internal safety mechanisms of LIB ESSs, the siting and spacing of ESS containers plays a significant role in fire safety. A radiation heat transfer analysis can be used to assess separation distances between adjacent ESS containers.

The overall approach to the radiation heat transfer analysis of an ESS container fire on an exposed ESS container include:

- Intensity of emitted radiation from the ESS Fire (Heat Flux) which is dependent upon:
 - Emissivity of Flame and Heated Surface
 - View Factor at Surfaces of Adjacent ESS Container
 - Separation Distance
 - Flame/Surface Temperature
 - Internal Gas Temperature (Fire Plume Temperature)
 - Temperature of Boundary Layers of Compartment (Walls)
 - Quantification of Fire Event within ESS
 - Ignition
 - Fire Growth Rate
 - Peak Heat Release Rate
- Inside air temperature of exposed ESS with respect to thermal threshold
 - Temperature rise of the exposed steel panel
 - Total Radiant Heat Flux Absorbed

This report applies an analytical radiation heat transfer analysis for the evaluation of separation distances between outdoor lithium-ion ESS containers. This analysis quantifies a fully involved, uncontrolled fire event in a lithium-ion battery ESS container and presents thermal thresholds at which an ESS becomes unstable when exposed to a radiant energy source.

2. Background

Scientific literature and available research reports related to lithium-ion batteries and li-ion energy storage systems were gathered and analyzed to provide an understanding of the technology itself, along with the associated hazards and gaps in analysis. The Department of Energy's Strategic Plan [1], codes and standards addressing ESSs [6,7,14], LIB/ESS fire incident reports, and other lithium-ion focused research reports and test data were used as the basis for this analysis.

2.1 Overview of Energy Storage Systems

An energy storage system is a system capable of storing electrical energy for use at a later time [4]. Energy storage systems are changing how energy is generated and delivered around the world. For utility applications, an ESS stores energy during low periods of demand and utilizes the stored energy by putting it onto the power grid during peak periods of demand. Energy storage systems allow the generation and distribution of electrical energy to be balanced based on the demand of the end user – maximizing the use of generated energy.

The four major types of energy storage systems include: electrochemical, chemical, mechanical, and thermal [4].

- *Electrochemical* ESSs are systems and/or devices that can provide electrical energy upon demand. Example of this technology are secondary batteries (such as Li-Ion, NiCd, Lead-Acid), electrochemical capacitors, flow batteries, and hybrid battery-capacitor systems.
- *Chemical* ESSs consists of fuel supply equipment combined with a fuel cell power system or generator to convert the fuel to electrical energy.
- *Mechanical* ESSs utilize a mechanical means of generating energy to run an electric generator to provide electric energy upon demand. Mechanical ESS technology include compressed air, pumped-water, fly wheels, etc.
- *Thermal* ESSs use heated fluids to generate energy and run an electric generator to provide energy on demand.

Of the four categories of energy storage systems discussed above, this report focuses on electrochemical energy storage. According to the U.S. Department of Energy, nearly 50% of the deployed electrochemical energy storage systems utilize a lithium-ion or lithium iron phosphate chemistry [1]. See the breakdown of deployed battery ESS systems in Figure 1 below.

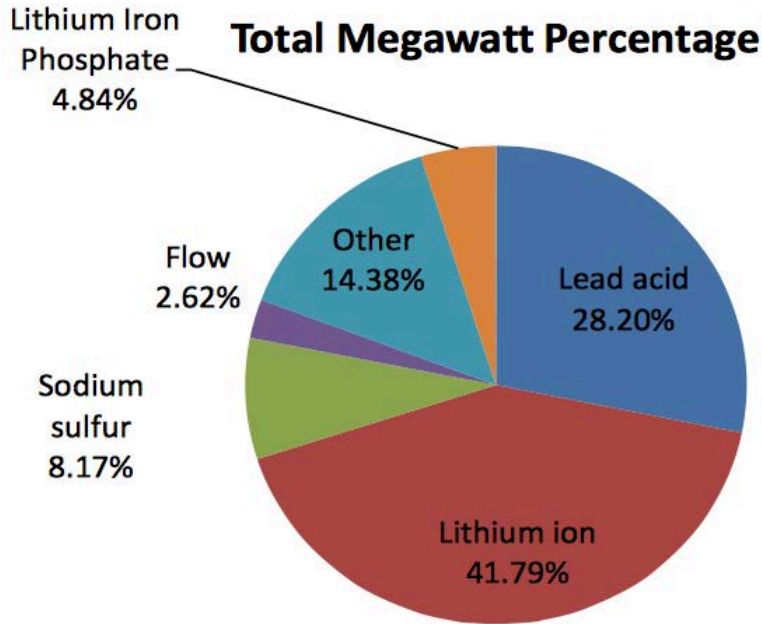


Figure 1 Deployed Li-Ion Based ESS (DOE Energy Storage Strategic Plan, (2014).

The electrochemical energy storage industry still utilizes other chemistries such as lead acid, sodium sulfur, nickel-cadmium, flow batteries, and others; however, lithium-ion batteries have become the battery of choice in recent years due to their high energy densities, high efficiency, size, etc. [1].

The energy storage market presents a vast variety of electrical energy storage systems for both commercial and residential applications. Of the lithium-ion based energy storage systems, there are various designs and sizes available. Lithium-ion batteries have been deployed in a wide range of energy-storage applications. On the residential scale, ESS are typically comprised of energy-type batteries of a few kilowatt-hours up to 100 kilowatt-hours commonly combined with photovoltaic systems. Whereas ESSs for utility and commercial applications are typically multi-megawatt containerized battery units for the provision of grid ancillary services [9].

Manufacturers are currently developing batteries with higher energy densities, allowing the energy capacity of an ESS container to nearly double [12,15,16]. However, this study focuses on the range of system sizes currently deployed in ESS installations to date – this range was determined to be between 500 kWh and 5 MWh [10]. Since the fire hazard intensifies with increased energy capacities, this study focuses on megawatt scale, containerized, lithium-ion battery ESSs.

2.1.1 Makeup of a Lithium-Ion Battery ESS

Great variation exists in the designs of containerized energy storage systems, however the components and general orientation is consistent throughout the ESS industry. The number of batteries can range between thousands to tens of thousands of lithium-ion batteries (LIB) within an ESS container [11,12,15,16]. Different manufacturers utilize different sizes and cell formats

which alters the designs of ESSs. Multiple cells are connected in series and parallel to comprise a module of batteries. Multiple modules are then electrically interconnected to form a rack. The ESSs are lined with an array of racks along each side of the container to form a large-scale battery energy storage system. The individual components of lithium-ion battery ESSs are described below.

2.1.1.1 Cell

A cell is essentially a single lithium ion battery. These batteries come in various formats such as cylindrical, prismatic, or pouch cells as shown in Figure 2 below [13]. Of the formats shown below, each cell format is available in various sizes corresponding to variation in the cell mass, energy density, amperage, etc.

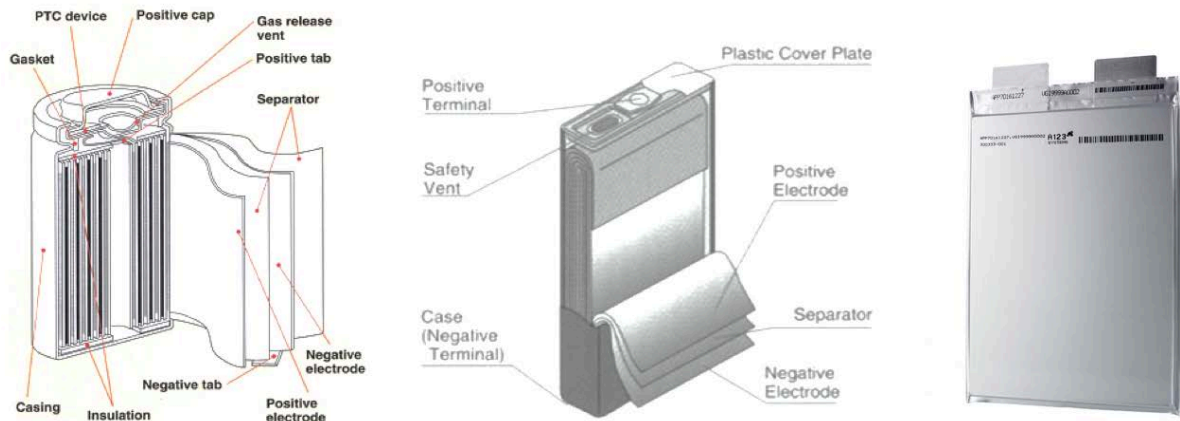


Figure 2 Lithium-Ion Cells: Cylindrical, Prismatic, and Pouch Cell (Respectively) [13]

2.1.1.2 Module

A module is a series of cells electrically interconnected in series and/or parallel [4]. A string of batteries is electrically connected to provide higher voltages and capacities. An example of multiple lithium-ion battery modules utilizing prismatic cells is shown in Figure 3 below.



Figure 3 Prismatic Li-Ion Battery Module (ALEVO)

2.1.1.3 Rack

A rack within an energy storage system consists of a series of modules electrically interconnected to provide a larger energy output at the required voltage. A rack typically has multiple drawers/trays as shown in Figure 4 below. Within each drawer there will be single or multiple modules depending on the size and formats of the cells utilized. Figure 4 illustrates the difference in rack designs. The figures display battery racks with multiple modules in an enclosed steel/aluminum cabinet (left) [14] and an open frame rack (right) [15].

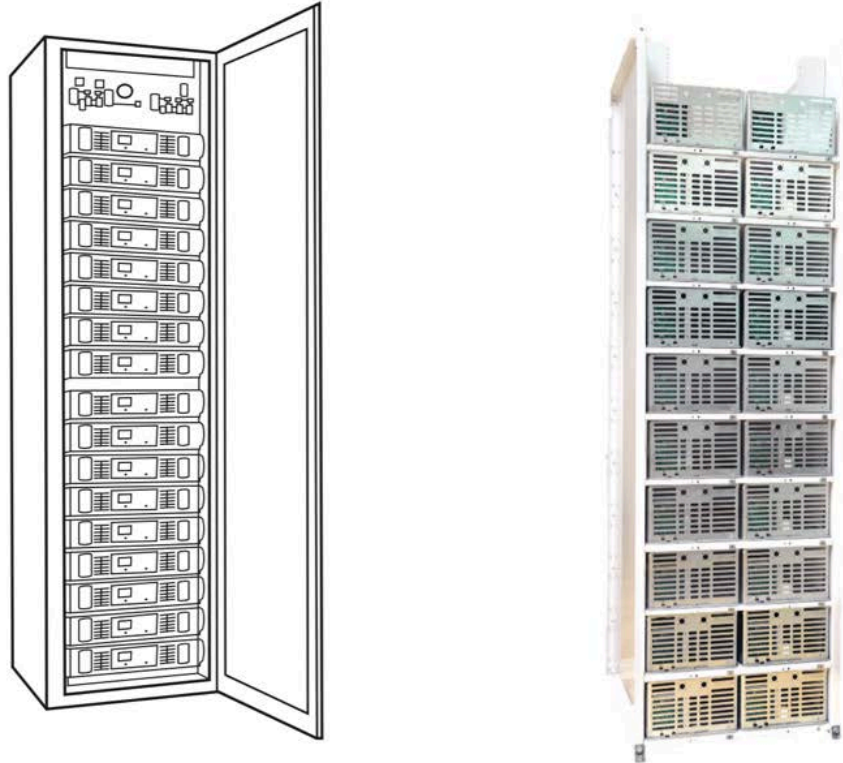


Figure 4 LIB Enclosed Rack (Left [14]), LIB Open Frame Rack (Right [15])

2.1.1.4 Containerized Energy Storage System

A containerized energy storage system consists of arrays of lithium-ion battery racks aligned along the walls of the container to obtain a desired energy/power output. Within this system will be a converter unit to convert the energy from DC to AC and vice versa to allow the stored energy to be utilized on the electrical grid. A schematic of a typical design of a containerized, mega-watt scale energy storage system is shown in Figure 5 below.

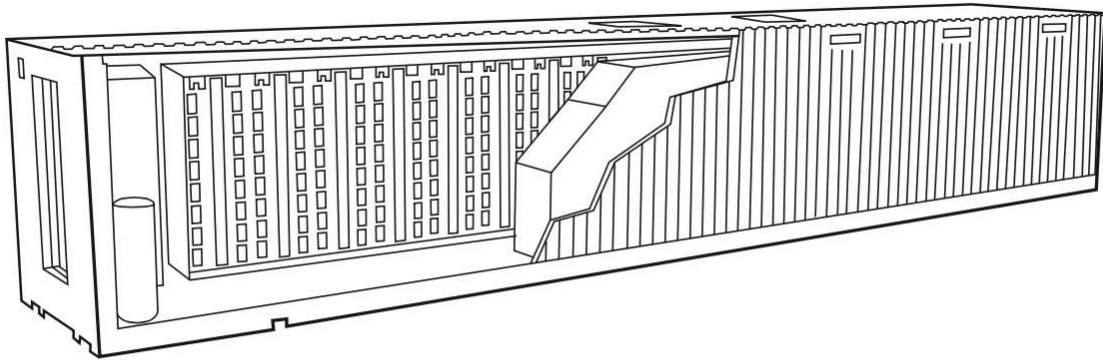


Figure 5 Containerized Energy Storage System [14]

2.1.1.5 Other Components

From a review of containerized ESS installations, there appears to be mechanical ventilation systems for each container that is intended to provide thermal conditioning to the energy storage system. There are also vents on the containers, in locations varying for different manufacturers. For standard ISO containers, there are multiple pressurization vents on each side of the container of approximately 3 inches by 8 inches in size [20]. However, modifications for ESS containers often contain vents larger than those on standard ISO-shipping containers to account for high pressures in the event of a fire.

2.1.2 Utility Scale Containerized Li-Ion ESS Installations

The designs of various vendors and manufacturers of containerized ESS's were considered to understand the universe of deployed lithium-ion ESS installations. Figure 44 of Appendix A shows the numerous installations worldwide that utilize lithium-ion batteries in utility scale ESSs [10]. According to the Department of Energy Global Energy Storage Database, there are currently 695 lithium-ion battery ESS installations – accounting for 1.64 GW of power [10].

Utility scale containerized ESSs are commonly contained within standard ISO-Containers. The International Organization of Standardization (ISO) has a standard that addresses intermodal shipping containers: ISO 1496-1:2013 Part 1. An intermodal shipping container is a rectangular container made of corrugated steel that is intended to transport or store materials without unloading the cargo. These shipping containers have standardized dimensions of either 20 ft or 40 ft in length by 8 ft wide and 8.5 ft high and are composed of a strong, durable, weatherproof corten steel [17]. Manufacturers have also modified the 40 ft ISO container to make a larger container of 53 ft in length – shown in Figure 47 of Appendix A.

These containers are favorable to the energy storage industry because it allows the ESS to be manufactured and installed at the manufacturer's facility, transported to the installation location, and commissioned onsite as a fully functional system. They also provide a weatherproof and

secure enclosure to store extensive quantities of energy. Although the energy storage industry is beginning to shift towards specially manufactured containers, the dimensions, shape, and materials used are consistent with standardized ISO containers and are therefore the focus of this analysis. All energy storage systems vary slightly in their designs; however, this study assumes that the ESSs are contained in uninsulated standardized ISO-containers. Deployed ESS containers range in size, however, the most common sizes are 20 ft, 40 ft, or 53 ft long, with standard widths of 8 ft and height of 8.5 ft [20]. All three sizes are analyzed in the radiation heat transfer analysis of this study. Figures 45, 46, and 47 in Appendix A show the different size containers utilized in the energy storage industry.

In large ESS facilities, there are often multiple containers placed adjacent to each other. The number of ESS containers is dependent on the power/energy demand of the facility. Figure 6 below shows a typical layout for a large energy storage facility with multiple ESS containers. This particular SDG&E installation in San Diego, CA consists of 24 lithium-ion ESS containers capable of providing 30 MW of power/120 MWh of energy [18]. Each ESS container has a maximum rated energy capacity of 5 MWh. There are approximately 400,000 lithium-ion batteries installed within this ESS facility – amounting to approximately 16,666 lithium-ion batteries/container and 20 batteries/module. This ESS installation provides an equivalent amount of energy as to serve 20,000 customers for 4 hours [19].



Figure 6 AES 30 MW (120 MWh) Li-Ion ESS Installation in San Diego, CA [19]

2.2 Lithium-Ion Battery (LIB) Technology

The term “lithium-ion” does not represent a specific battery, but rather a family of batteries with a wide array of different chemistries. However, this group of batteries are all characterized by the transfer of lithium ions between the electrodes during the charge and discharge cycles [20].

A lithium-ion battery contains three fundamental components: the electrodes, separator and electrolyte. Between the positive electrode (cathode) and negative electrode (anode) lies a separator, typically composed of a micro-perforated plastic [23]. During the charging process, lithium-ions move between the anode and the cathode. The liquid electrolyte, commonly composed of a lithium salt and a flammable organic solvent, allows the lithium-ions to move through the separator from the cathode to the anode [23]. There are two tabs per lithium-ion cell, one per electrode –cathode and anode [31]. These tabs allow an electrical connection to be made during the transfer of lithium-ions. During the charge/discharge process, the electrons flow through the external electrical circuit, while lithium-ions move between the cathode and the anode. See Figure 7 below.

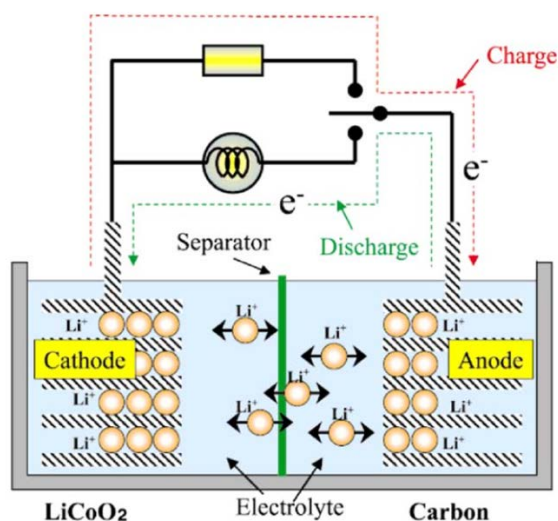


Figure 7 Principal Operation of Lithium-Ion Battery during Charge/Discharge [23]

2.2.1 LIB Components

The cathode is a key component of the charging process in a lithium-ion battery as it accepts lithium ions during discharge and releases them during the charge cycle. The cathode is typically composed of a metal oxide, such as Lithium-Cobalt Oxide, but it can also be a polyanion such as Lithium-Iron Phosphate, or a spinel such as Lithium-Manganese Oxide [23]. There are a variety of cathode materials that can be used in a lithium-ion battery including LiCoO_2 , LiMn_2O_4 , NCA, NCM, LFP, and others [23]. One of the most common cathode materials is LiCoO_2 due to its high voltages and corresponding high energy densities. However, studies indicate that other cathodes such as lithium-iron phosphate are inherently safer yet have significantly lower voltages and energy densities [23].

The anode, negative electrode, is another one of the primary components of a lithium-ion battery cell, which accepts lithium-ions while charging, and releases lithium-ions to the cathode during discharge [23]. Graphite and hard carbon are the most common anode materials due to their high capacity and ability to work closely to lithium [34].

The electrolyte is typically composed of an organic solvent and a lithium-based salt for high voltage lithium-ion batteries [31]. The most common lithium-based salt used in the electrolyte is LiPF_6 which is combined with a blend of two of the following organic carbonates – ethylene carbonate, asdimethyl carbonate, dimethyl carbonate, or ethyl methyl carbonate [41].

In between the cathode and the anode lies a separator. The separator is a polymer that encases the electrons from both the cathode and the anode. The separator functions as a barrier between the two conductive electrodes that allows the electrons to safely pass through the electrolyte to and from the cathode and anode [23].

2.2.2 Applicability of Lithium-Ion Batteries for Energy Storage Systems

Lithium-ion batteries are an ideal battery to use for energy storage because of their ability to retain charge. As batteries age, their capacity fades not allowing the batteries to be fully charged due to the loss in capacity of the battery. However, lithium-ion batteries only lose $\frac{1}{4}$ the amount of charge typically lost per month in other standard batteries such as lead-acid or nickel-cadmium. Lithium-ion batteries potential for storage has been optimized by their high energy density and energy efficiency [45]. As defined by the Energy Storage Association, a battery and/or ESSs energy density is “the amount of energy that a storage system can store per unit volume occupied by the system” [21]. As battery manufacturers continue to evolve the li-ion technology, higher energy densities are being developed which far surpass that of other battery types such as lead-acid, NiCd, or NaS. Lithium-ion batteries have energy densities ranging between 100 Wh/l to over 400 Wh/l depending on the specific chemistry, whereas lead-acid and NiCd batteries energy densities are typically 100 Wh/l or less [22]. Lithium-ion batteries also suffer no memory loss, therefore they are able to achieve nearly 100% charge and discharge efficiency which gives them a longer cycle life [22]. As this technology continues to evolve, lithium-ion batteries storage capabilities are expected to advance, increasing their applicability for energy storage applications.

2.3 The Fire Safety Concerns with Lithium-Ion Battery ESS

The fire hazards associated with lithium-ion battery energy storage systems are centered on the LIBs flammable organic electrolyte and its highly reactive electrodes [31]. The high performance of lithium-ion batteries is attributed to the unique combination of materials used, which under normal operating conditions does not pose a problem. However, when lithium-ion batteries undergo a failure, the separation layer is breached allowing the electrodes to react with the electrolyte, producing high temperatures, pressures, and eventually resulting in a fire [47]. The heat released from LIB fires can be significant, posing fire propagation hazards which accumulates with subsequent failures [48]. A few minor incidents may combine to severely

threaten safe operation of a lithium-ion ESS – for there are a variety of failures or defects that lead to hazardous conditions, making the batteries unsafe for operation [45].

The unsafe condition of a lithium-ion cell is a result of compiling defects, failures, and reactions that cause the battery to be in a hazardous state. The generalized breakdown of a lithium ion cell during failure are based on the combination of four conditions: sufficient state of charge, self-sustaining exothermic reactions, a localized heat source, and heat generation as a result of insufficient cooling [45].

2.3.1 Failure Modes Resulting in Fire

A lithium-ion battery can result in a fire due to electrical, mechanical, or thermal failures [49].

Electrical Failures

- Overcharge
- Over-discharge

An electrical failure is most commonly due to overcharge or over-discharge. During overcharge, the lithium intercalated into the crystallographic structure of the anode disassociates and plates on the surface of the anode. A thermal runaway reaction is then initiated within a lithium-ion cell due to the violent reaction of the overcharged anode (deposited lithium) and electrolyte solvent at high temperatures which was a result of the rapid exothermic reaction between the de-lithiated cathode and the electrolyte [24].

Mechanical Failures

- Internal short circuit
- Physical Damage
- Manufacturing Defect

Mechanical failures include physical damage, an internal short circuit, or a manufacturing defect. The batteries can be physically damaged if they are punctured in some way, as to dent or tear through the battery components, which causes an internal short circuit and an internal localized heat source [49]. Other conditions such as low ambient pressure, vibration, shock, corrosion, or impact can also initiate a mechanical failure event within a LIB. A lithium-ion battery can also encounter a mechanical failure if a particle is inadvertently lodged into the cell during the manufacturing process. A dendrite or “particle” in the cell will cause localized resistance heating around the particle, which causes an internal short-circuit, and an increase in internal temperature and pressure within the cell [49].

Thermal Failures

- Overheating
- Internal Localized Heating

Thermal failure modes include overheating or internal localized heating. The batteries can become overheated by an external fire/heat source or from ambient temperatures that exceed their thermal stability limits (60°C) [49]. Both electrical and mechanical failures develop internal

localized heating within a lithium-ion battery which contributes to a thermal degradation of the cell.

The age of a cell also plays an important role in the safety of lithium-ion batteries. Issues arise as minute amounts of corrosion begin to appear after numerous reaction cycles – causing an internal localized heat source. The built up corrosion can cause defects and an internal localized heat source within the cell [34]. The closer the battery is to the end of its life, the faster it can thermally degrade [45]. Although it is a preconceived notion that batteries become safer over time due to their reduced performance, this does not prove to be true for lithium-ion batteries. The hazards of lithium-ion batteries increase with age – their potential for failure rises as the battery degrades allowing them to reach unstable thermal conditions with less abuse [45].

All failure modes within lithium-ion batteries generate heat and stimulate further thermally-driven chemical reactions within the cell until it reaches an ultimate failure point known as thermal runaway – resulting in fire.

Fire can erupt in a lithium-ion battery once it undergoes one of the failure modes. A thermal, electrical, or mechanical failure, or combination of, can lead to thermal runaway [51]. A lithium-ion battery goes into thermal runaway when the “cell temperature reaches a threshold that causes an uncontrollable rapid release of energy and corresponding temperature rise resulting in a thermal event, such as a fire” [31]. The stability of a lithium-ion cell is primarily dependent on temperature. The temperature of the cell is determined based on the heat generation/dissipation rates. If the heat cannot be dissipated linearly at an equivalent rate of generation, then the internal chemical reactions become stimulated by the increasing temperature and induce the cells into thermal runaway [23]. The chain of events from the initial failure mode to the thermal runaway event within an energy storage system is illustrated in Figure 8 below.

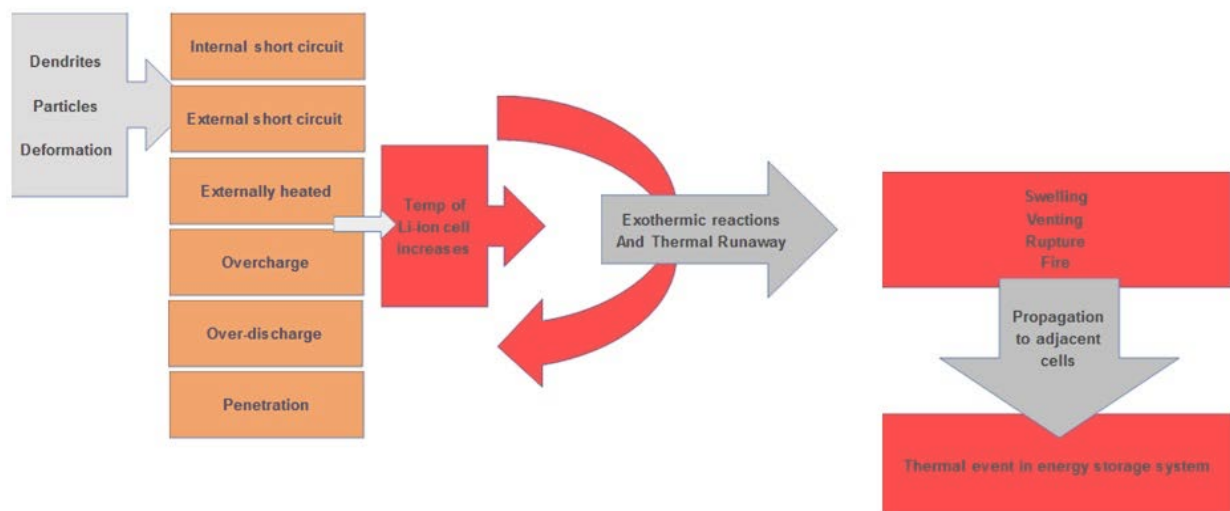


Figure 8 Lithium-Ion Battery Thermal Runaway Chain of Events

There are several internal chemical reactions during a lithium-ion battery failure that build up to thermal runaway. First, the solid electrolyte interface decomposes at a low temperature allowing the electrolyte to react with the anode, causing a spike in temperature [23, 47]. The increasing temperature causes a chemical reaction between the flammable organic electrolyte and the intercalated-lithium of the negative electrode. The electrolyte breaks down during this reaction, releasing various hydrocarbon gases and causing rapid, internal pressure build up within the cell [23]. As the temperature continues to rise, the separator melts allowing the electrodes begin to short circuit due to contact, and the electrolyte breaks down. The collapse of the electrolyte initiates a reaction between the electrolyte and the cathode, causing the cathode to decompose [23,47]. The decomposition of the cathode releases the oxygen within the metal oxide, which then oxidizes the flammable electrolyte. As the temperature continues to rise, hot and flammable gases are vented from the cell and readily ignite [23]. Once combustion is sustained in one cell, it can propagate heat to adjacent cells and induce thermal runaway in other cells/modules/racks within the energy storage system [48].

A fire within a lithium-ion cell is a result of a series of internal degradation reactions within the cell [47]:

- (1) Reactions begin within the anode around 80°C.
- (2) Between 100°C and 120°C the solid electrolyte interface (SEI) layer diminishes causing the negative electrode (anode) and electrolyte to undergo a reduction.
- (3) At 120-140°C the positive electrode (cathode) endures exothermic reactions resulting in a rapid release of oxygen from the decomposition of the metal oxide.
- (4) Between 140 and 180°C the electrolyte undergoes an oxidation process while the positive electrode decomposes at a rate of 100°C/min.

Thermal runaway will typically occur at 180°C at low states of charge, 120°C at 100% state of charge, or 80°C when overcharged [60]. The increased temperature causes a rapid increase in pressure within the battery. Under these conditions, the pressure initiates a violent ejection of the flammable volatiles – resulting in a self-sustaining fire [54]. As combustion endures, the cells continue to swell and release bursts of flames. More flames continue to be produced from the batteries with greater intensity and magnitude, while gaseous products from the lithium-ion combustion reaction are emitted [60]. Once a lithium-ion battery within an ESS ignites, the other cells have the potential to overheat and initiate propagating thermal runaway reactions between adjacent batteries, modules, and racks within the ESS. During a propagating thermal runaway event, the energy release is extremely hazardous and difficult to control – signifying the ultimate failure point of a Li-ion ESS.

3. Lithium-Ion Battery Fire Events

A general review of past fire events involving lithium-ion batteries is presented to help characterize the relevant fire hazards. According to the National Fire Incident Reporting System (NFIRS) and a general search of ESS related fires, only one fire involving a fully-operational energized ESS utilizing the lithium-ion technology is documented – Arizona ESS fire. However, other incidents involving large quantities of lithium-ion batteries were analyzed to obtain insight into the energy release and duration of a lithium-ion ESS fire.

3.1 Arizona ESS Fire

On November 26, 2012, a fire was ignited inside a 1.5 MW containerized LIB ESS atop McMillian Mesa in Arizona [25]. The Arizona Public Service Company (APS) was utilizing this solar-tied lithium-ion battery ESS to test its ability to store energy and utilize it during peak periods of electricity demand. The firefighters let the fire burn for an extended period of time, until an APS employee was able to shut off the power to the system. The fire caused significant damage to the ESS, however the power substation and nearby structures were not damaged because the ESS was placed a significant distance away from other structures [25]. Further information regarding how the fire started, specified burn duration, type/format/size of batteries involved, etc. is not publicly available at this time.

3.2 Union Pacific Train Car Explosion Involving LIB's

On April 27, 2017 in Houston, Texas a Union Pacific train car was transporting used lithium-ion batteries from various consumer products to a recycling facility [26]. The conductor noticed smoke coming from one of the rail cars, so he stopped the train to inspect the situation. At this time, fire was coming from a rail car that was filled with lithium-ion batteries. Shortly after, the rail car exploded, producing a blast that was felt up to 1.5 miles away. The explosion event had so much force behind it that it completely blew off the walls of the shipping container and broke windows and cracked walls in nearby homes. The batteries continued to burn and smolder for hours [26]. The fire department was able to control the fire within a few hours. However, how the fire started is still under investigation. The result of this event is shown in Figure 9 below.



Figure 9 Explosion in Union Pacific Train Car filled with Lithium-Ion Batteries

3.3 Two Fires in Boeing 787 Lithium-ion Battery Units

Two events occurred involving the lithium-ion battery systems within the Boeing 787 Dreamliner. On January 7, 2013 the first fire event occurred in the lithium-ion battery auxiliary power unit (APU) of a Japan Airlines plane at the gate of Logan International Airport in Boston, Massachusetts [27]. When parked at the gate, the APU is the sole source of power. Smoke was first observed in the aft cabin of the aircraft. Immediately after, a maintenance manager in the cockpit saw that the APU had shut down automatically. To inspect the power loss of the APU, a mechanic opened the aft electronic equipment bay and found heavy smoke and fire coming from the front of the APU battery case [27]. A firefighter reported that the APU battery case was glowing, with radiant waves coming off the battery case due to the extreme heat – identified by a thermal imaging camera. This APU battery unit consisted of 8 prismatic lithium-ion batteries. The entire module was approximately the size of a shoe box. All eight batteries were involved in the fire and it took approximately 1 hour and 40 minutes to control and extinguish the fire [28]. The mechanic that initially spotted the fire stated that he attempted to fight the fire with a fire extinguisher but it had no impact on the fire itself and the environment within the compartment was too dangerous to stay any longer.

Nine days later on January 16, 2013, a fire event erupted in the main battery within the aircraft that provides power to specific electrical/electronic equipment during ground and flight operations. Shortly after take-off, a “serious incident” occurred in the main battery and required an emergency landing [27]. All 184 passengers were able to evacuate the plane safely. However, since the main battery is the same design as the APU battery unit, the cause of the incident was likely similar. The findings from the investigation are provided below.

The NTSB Materials Laboratory’s results indicated that the event was initiated by an internal short circuit (ISC) of one cell within the battery pack [27]. This ISC lead the initiating cell into thermal runaway, which propagated to all neighboring cells within the battery pack as shown in Figure 10 below. The investigation determined that all cells had undergone a thermal runaway event due to the mechanical deformation, thermal damage, and ruptured vent discs of the cells [27]. Further investigation is still ongoing to determine the cause of the ISC in the initiating lithium-ion cell.



Figure 10 Boeing 787 APU Li-Ion Battery Module after Thermal Runaway (FAA/NTSB)

3.4 S&C Electric Lithium-Ion ESS fire in Wisconsin

In Franklin, WI around 11:00 AM on August 10, 2016 a fire was reported from the S&C Electric facility [29]. Reports indicated large billows of black smoke pouring out of the facility. Within this facility, energy storage systems are designed, assembled, and operated before being deployed. The fire was initially assumed to have initiated with the lithium-ion batteries, however, the investigation later determined that the fire started in the battery manufacturer's DC power and control compartment – not the batteries themselves [30]. The DC power and control unit that started the fire was part of a larger system that was being assembled – therefore the safety features normally integrated into an ESS were not yet installed in this particular fire event. Even though the batteries did not start the fire, they became involved shortly after. Prior to the fire department arrival, the lithium-ion batteries were burning and producing significant amounts of smoke as shown in Figure 11 below. Even though the batteries were not connected (i.e. not charging or discharging) at the time of the fire, they still significantly contributed to the overall severity of the event. It took the fire department several hours to control the fire and reduce the temperature of the batteries below dangerous levels [30].



Figure 11 Fire involving Li-ion ESS inside S&C Electric Manufacturing Facility

3.5 Impact of Previous Fire Events on this Study

The fire events discussed in sections 3.1 through 3.4 informed how we approached this study – specifically the duration of the radiation heat transfer analysis. These fires revealed that as more batteries become involved, the severity of the heat release from the fire and the duration of the event significantly increases. However, firefighting tactics appeared to control the fires within a few hours. Therefore, this radiation heat transfer analysis examines a fire duration of up to 3-hours to correlate with firefighting operations referenced in the fire events previously discussed.

4. Research and Testing of Lithium-Ion Batteries and ESS

Full-scale testing of a large containerized lithium-ion battery energy storage system has yet to be conducted. However, other testing has been conducted to provide insight into the fire hazards associated with lithium-ion battery energy storage systems. A few of the larger-scale testing and research reports will be summarized below:

- (1) FPRF/Exponent Hazard Assessment of Lithium-Ion Battery Energy Storage Systems
- (2) FAA *Fire Hazards of Lithium-Ion Batteries* – testing of pallet load of lithium-ion batteries in an aircraft cargo hold
- (3) DNV GL/Con-Edison *Considerations for ESS Fire Safety*

4.1 FPRF/Exponent Hazard Assessment of Lithium-Ion Battery ESS

Exponent, Inc. and the NFPA's Fire Protection Research Foundation conducted a full-scale fire test of a Tesla Powerpack – 100kWh lithium-ion ESS at 100% SOC [4]. Two tests were conducted, one with an external ignition source of 400 kW and another with an internal ignition by heater cartridges. The internal test set individual cells into thermal runaway to simulate an internal failure, and the external test led the internal cells into failure through heat exposure [4]. The key results from this test are summarized below, which aids in the understanding of an ESS fire.

The results of the external ignition test determined the following:

- (1) A fire in the Powerpack resulted in internal temperatures exceeding 2,000 °F.
- (2) External temperatures reached 450 °F.
- (3) Flames were observed coming out of the exhaust vent and out of the ESS front door.
- (4) Flames several feet high was observed from the exhaust vent of the Powerpack.
- (5) Heat flux of ~ 25kW/m² measured 6 ft from front of ESS.
- (6) All batteries and electronics of the ESS were damaged.

The internal ignition test gave the following results:

- (1) A fire in the Powerpack resulted in internal temperatures exceeding 2,000 °F.
- (2) Temperatures at pods below the initiator pod showed temperature ranges between 80 and 180°F.
- (3) External temperatures reached 70 °F.
- (4) Initiator pod was damaged, but other cells were not damaged.

4.2 US FAA-Style Flammability Assessment of Lithium-Ion Cells and Battery Packs in Aircraft Cargo Holds

Exponent conducted flame attack tests on single prismatic batteries and prismatic battery packs inside a cargo hold [32]. The key takeaways from this testing provides insight into battery behavior under fire conditions as well as temperature profiles of the fire events.

Key findings from these small scale tests include the following:

- (1) Frequent battery case rupture events were observed in the prismatic battery back testing.

- (2) Direct flame impingement on small, unpackaged quantities of prismatic battery packs can lead to thermal runaway of individual cells and venting of gases. The vent gases are generally ignited by the pre-existing flame, increasing the total heat flux produced by the fire.
- (3) Testing of 4 cell li-ion battery packs produced ceiling temperatures between 400°C and 600°C.

4.3 FAA Energetics of Lithium-Ion Battery Failure

The Federal Aviation Administration (FAA) has worked to quantify the hazard of lithium-ion batteries under a fire event since a fleet of the Boeing 787 Dreamliner were grounded as a result of hazards associated with LIB fires. In addition to the fire events, large numbers of lithium-ion batteries are being shipped as cargo on aircraft. Although the failure of a single cell is a low probability event (1/1,000,000), the large quantity of batteries on aircraft and the severe impact of an event on the survivability of the aircraft make the risk a safety concern to the passengers [33].

To analyze the hazard of lithium-ion batteries undergoing a thermal runaway event in an aircraft, a pallet load of 18650 cylindrical batteries were forced into thermal runaway within a cargo hold of an aircraft. This test showed that all of the batteries became involved in the fire. This testing provided data regarding the energetics of lithium-ion battery fires and heat release rate curves providing insight into the growth function of a fire involving multiple packs of lithium-ion batteries [33]. This study is applicable to quantifying a fire event in a ESS due to the number of batteries in a confined compartment.

4.4 DNV GL Considerations for ESS Fire Safety

DNV GL and Rescue Methods were contracted by Con-Edison Power and the New York State Energy Research and Development Authority (NYSERDA) to address a series of frequently asked questions regarding ESS Fire Safety [46]. This work included testing of lithium-ion batteries of various chemistries as individual cells and battery modules. The individual cells were exposed to a 4 kW radiant heat source until they vented inside DNV GL's Large Battery Destructive Testing Chamber. For the module testing, modules between 7.5 and 55 kWh were ignited inside a partially closed metal container by direct flame impingement from a propane torch [46]. The module testing provided data concerning the effect of oxygen, toxicity, and heat release rate of the fire.

A few key findings from this testing are discussed below:

- (1) Batteries are more volatile at higher states of charge (SOC).
 - a. Mass loss rate is proportional to SOC.
 - i. Average mass loss rate: 18% mass loss over 41.7 min.
- (2) If flames are visible and temperature is rising, the ESS is likely to have multiple batteries and/or modules involved in the fire. Rising temperatures within the ESS is an indication of increasing risk.
- (3) The batteries themselves emit flammable gases.

- a. Fully involved/improperly ventilated spaces pose a lower explosive limit hazard.
 - b. Recommended Ventilation Rate Correlation of 0.2 - 0.32 cfm/Wh.
- (4) Flammable gas flashover observed; energy released was proportional to the concentration of gases in the enclosed volume.
- (5) HRR produced variable results; Range was between 2.5 – 80 kW/kg.
- a. Dependent on volume of gases, duration of release, rate of ignition, and gaseous mixture.
- (6) Partially burned systems can continuously emit flammable gases as long as the cells retain their heat – even if the fire has been extinguished.

5. Fire Safety Regulations

Codes such as NFPA 855 Standard for Stationary Energy Storage Systems (in development), NFPA 1 Fire Code, International Fire Code (IFC), International Building Code (IBC), International Residential Code (IRC), FM Global standards and UL standards are in the development stages of providing guidance on the implementations of electrochemical energy storage systems.

Although the regulations are being developed for all types of ESS, this report focuses specifically on outdoor, containerized, megawatt scale energy storage systems, which is addressed by NFPA 1 [7], NFPA 855, the International Fire Code (IFC) [6], FM Global Data Sheet 5-33 [14], and UL 9540.

The upcoming editions of NFPA 855, NFPA 1, and IFC are consistent in their recommendations regarding the siting and location of outdoor containerized ESSs as shown below.

*Separation: Stationary storage battery systems located outdoors shall be separated by a minimum **5 feet** from the following:*

- *lot lines*
- *public ways*
- *buildings*
- *stored combustible materials*
- *Hazardous materials*
- *High-piled stock*
- *Other exposure hazards*

Exception: The fire code official (AHJ) is authorized to approve smaller separation distances if large scale fire and fault condition testing conducted or witnessed and reported by an approved testing laboratory is provided showing that a fire involving the system will not adversely impact occupant egress from adjacent buildings, or adversely impact adjacent stored materials or structures.

The other publicly available guidance on separation distances for containerized energy storage systems was published by FM Global in Data Sheet 5-33 Electrical Energy Storage Systems [14]. Their separation guidance is indicated below:

*Construction and Location: Provide a minimum space separation between ESS enclosures of **20 ft**.*

If the space separation between ESS enclosures is less than 20 ft, provide a thermal barrier, rated a minimum of 1 hour, on the inside or outside of the enclosure, in accordance with Data Sheet 1-21.

Since the intent of this report is to evaluate separation distances between adjacent ESS units during a fire event, the radiation heat transfer analysis examines the radiant exposure at distances varying between 3 and 20 feet.

6. Scope of Heat Transfer Analysis

Predicting fire behavior through analytical modelling has been evolving for quite some time. In recent years, the capabilities of analytical models have grown extensively and have become a common tool for unique engineering projects. The focus of analytical models is to describe in mathematical language the various phenomena observed during fire events [54]. These individual equations usually describe a small part of a fire. However, when combined, they can create a complex computer code intended to give an estimate of the expected behavior and duration of a fire based upon given input parameters [54]. These analytical models have progressed to the point of providing accurate predictions of fire behavior suitable for unique engineering applications – such as energy storage system fires.

This project utilizes a detailed analytical heat transfer model to analyze the impact of a fire in an ESS on an exposed ESS container. During a fire, there are three modes of heat transfer: conduction, convection, and radiation.

- *Conduction* – The transfer of heat from the direct contact of a solid of higher temperature to a solid of lower temperature [35].
 - Dominant in cell to cell fire propagation.
- *Convection* – The transfer of heat through the movement of hot smoke and gases to solid surfaces of lower temperature [35].
 - Dominant in heating boundary surfaces of container.
- *Radiation* – The transmission of heat energy by electromagnetic waves through the space between a body at a higher temperature to a body at a lower temperature [35].
 - Dominant mode of heat transfer outside the container to an adjacent ESS.

All three modes of heat transfer contribute to the development and behavior of a fire, however, each mode takes precedence in different phases of the fire. Conduction and convection are applicable to the ignition and growth phases of the fire within the ESS container, however radiation becomes dominant when the container reaches temperatures exceeding 400°C [37]. Radiation heat transfer is considerably different than conduction or convection in that a material medium is not required for two objects to exchange heat [39]. Since conduction is not applicable outside the container and convection is negligible at remote distances, this study focuses on radiation heat transfer between an ESS fire source and an exposed ESS unit. As a fire develops in an ESS, a temperature difference will develop between the radiant bodies and the target surface. This variance in temperature over time will determine the rate at which the radiant interchange occurs [39]. Therefore, the impact of thermal radiation from flames or heated surfaces on an adjacent ESS container must be analyzed through a detailed heat transfer analysis to determine how quickly the exposed lithium-ion batteries become unstable, presenting conditions for a delayed ignition event in the exposed ESS container.

This analytical heat transfer model requires an analysis of the compartment fire, external burning, the shape, size, and configuration of the radiant body, the radiant heat flux emitted from the ESS fire and received at the target, and the impact of the radiant exposure at various separation distances. This analysis uses a solid flame radiation model to analyze the radiant exposure from a fire in an ESS container ranging between 500 kWh and 5 MWh of rated energy capacity to determine when the exposed ESS container reaches its thermal threshold over

separation distances ranging between 3 ft and 20 ft. The thermal threshold of the exposed ESS container is established as the point at which the inside temperature of the exposed ESS container is raised to 80°C – the temperature at which self-generating thermal reactions within LIB's are initiated, compromising the safety of the individual LIB cells.

Key parameters for the radiation heat transfer analysis include the following:

- Intensity of emitted radiation from the ESS fire (Radiant Heat Flux) at the surface of exposed ESS container
 - Emissivity
 - View Factor
 - Separation Distance
 - Flame/Surface Temperature
 - Temperature of Boundary Layers of Compartment (Walls)
 - Internal Gas Temperature (Fire Plume Temperature)
 - Quantification of Fire Event within ESS
 - Ignition
 - Growth Phase (Rate of Fire Propagation)
 - Peak Heat Release Rate (Fully Developed Fire)
- Inside Air Temperature of Exposed ESS with respect to Thermal Threshold
 - Temperature Rise of the Exposed Steel Panel
 - Total Radiant Heat Flux Absorbed

7. Methodology of Heat Transfer Analysis

The solid-flame radiation model is currently a common approach to analyze thermal radiation hazards for large fires. The solid-flame radiation model approximates the fire or radiant source as a geometric shape based on analytically derived values and correlations for the mass burning rate, fire size, flame height, etc. The intensity of the thermal radiation received at an exposed ESS is determined through corresponding geometric view factors for the approximated shapes of the radiant bodies, their temperatures, and efficiency of emitting and/or absorbing radiation [36].

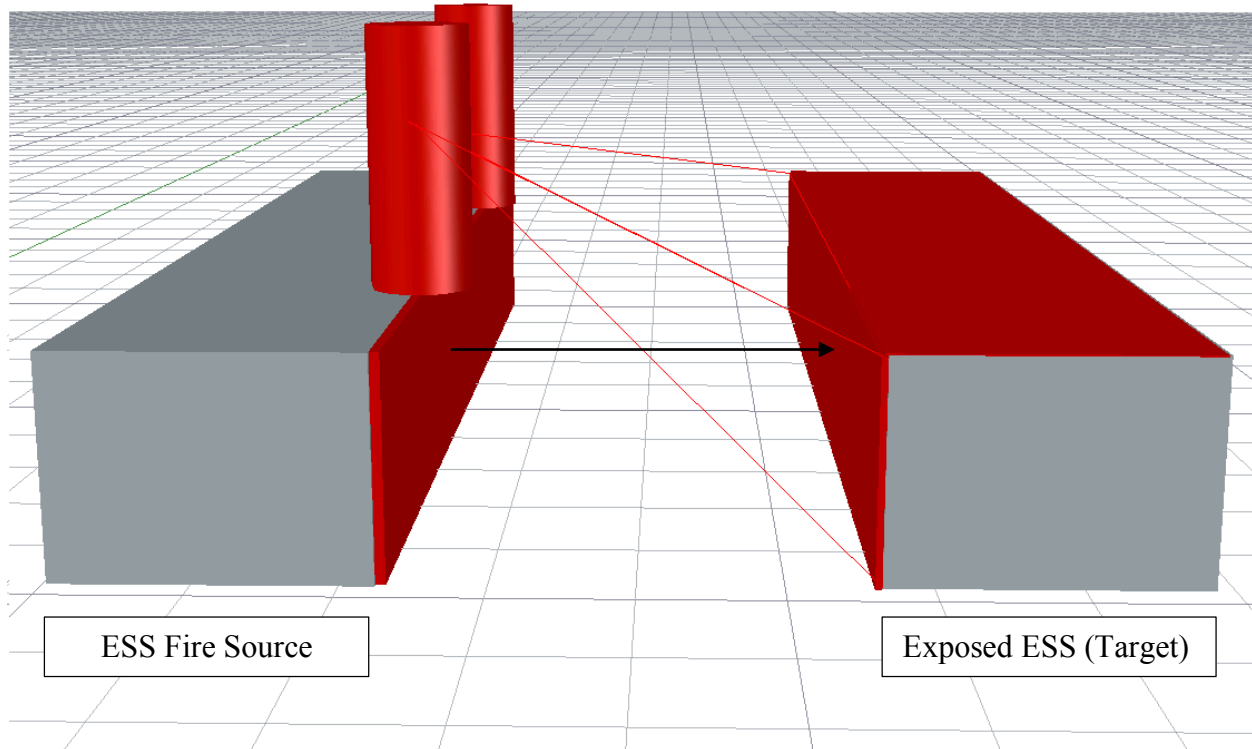


Figure 12 Schematic of Approach to Heat Transfer Analysis

Based on the schematic shown in Figure 12, the intent of this solid flame radiation model is to determine the intensity of the radiation emitted from the ESS container fire source, as a function of its heat release rate, to determine the impact of the absorbed radiation into an exposed ESS container. The radiant bodies of the ESS container fire source are the cylindrical geometric flames exiting the vents and the heated surface (wall) as a function of the fire source inside. The exposed ESS will be radiantly heated from the visible radiant bodies of the ESS fire source. The red surfaces in Figure 12 represent the surfaces that are either emitting or receiving radiation.

7.1 Governing Radiation Heat Transfer Equation

Thermal radiation is primarily a function of temperature – as all matter with a temperature above absolute zero emits radiation. The measurement of the maximum amount of radiation emitted from a surface or flame as a function of its temperature is represented as its heat flux (\dot{q}'') [37].

$$\dot{q}'' = \sigma T^4 \quad (1)$$

σ = Stefan-Boltzman Constant (5.67×10^{-11} kW/m²K⁴)

T = Temperature of Radiant Body (K)

Equation 1 above indicates that the radiant source is a perfect radiator; however, this is not always the case. Since this study examines the impact of an incident radiant heat flux on a target ESS at a remote location, this equation is too simplistic to accurately depict the radiation absorbed by a target.

It is assumed that as a fire develops within the ESS container, the temperatures of the steel panels will be heated and flames will escape the compartment through the vents of the container; this phenomenon is analyzed in section 7.4.3.3.1. The heated panel and the externally vented flames are assumed to be the radiant sources of the ESS fire. However, to account for their efficiency as a radiator and the impact of the separation distance between the ESS containers, two additional variables must be considered - the emissivity and geometric view factor. The emissivity (ϵ) is a property that represents the fraction of energy emitted with respect to a perfect radiator [37]. The separation distance between ESSs are accounted for by a geometric view factor, which indicates the fraction of radiation that can be seen by the target relative to the total radiation emitted by the radiant sources [37].

Therefore, according to Quintiere's *Principles of Fire Behavior* Equation 3-5, the radiant heat flux absorbed at a target is expressed through the following equation:

$$\dot{q}'' = \epsilon \sigma F T^4 \quad (2)$$

Where:

q_{rad}'' = radiative heat flux (kW/m²)

ϵ = emissivity

σ = Stefan-Boltzman Constant (5.67×10^{-11} kW/m²K⁴)

F = Geometric View Factor

T = Temperature Radiant Body (K)

Equation 2 accounts for the emissivity of the radiant body (surface and flame), Stefan-Boltzman Constant, geometric view factors between the radiant bodies and the target, and the temperature of the radiant bodies (surface/flame). Sections 7.2, 7.3, and 7.4 quantifies and discusses the methodology for determining the emissivity, view factor, and temperature of the radiant sources, respectively.

7.2 Properties of Radiant Bodies

Thermal radiation is essentially an energy exchange between surfaces. A radiant body will emit a portion of its total radiative energy, known as the incident radiation, on a target surface [39]. Of the incident (emitted) radiation, a fraction of it will be absorbed, reflected, and transmitted at the exposed surface [69], as shown in Figure 13 below.

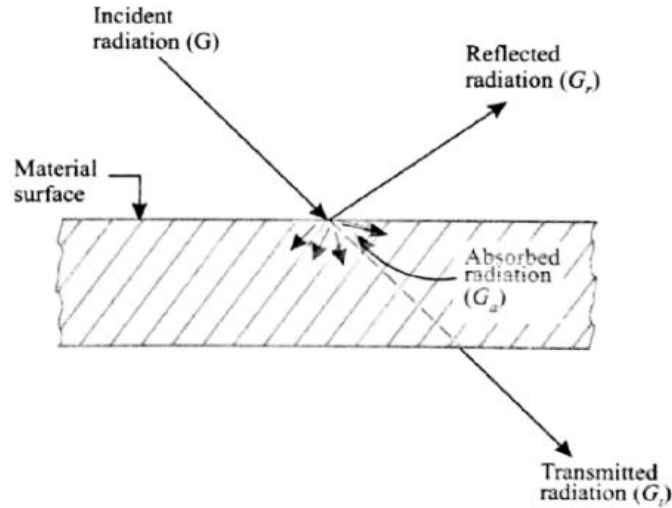


Figure 13 Absorptivity, reflectivity, and transmissivity of incident heat flux

From the conservation of energy principal, we see that the sum of absorptivity, reflectivity and transmissivity is equal to 1 as shown in Equation 3 below [69].

$$\alpha + \rho + \tau = 1 \quad (3)$$

Where:

α = fraction of radiant energy absorbed

ρ = fraction of radiant energy reflected

τ = fraction of energy transmitted through the interface

Therefore, to determine the fraction of radiation received at the exposed ESS, the absorptivity, reflectivity, and transmissivity of the absorbing surface as well as the emissivity of the radiant sources.

7.2.1 Emissivity of Steel Containers

Since this model analyzes steel containers, it can be assumed that the containers are opaque surfaces; therefore, the transmissivity – the amount of radiation transferred directly through the exposed ESS – would be equal to zero. These containers also have large surface areas from which heat will be radiated from. According to a radiation heat transfer study, opaque surfaces with a large surface area behave as radiant black bodies [65]. A black body is defined as an opaque object that emits the maximum thermal radiation and absorbs all incoming light (heat) [69]. Since the steel panel is assumed to behave as a radiant blackbody, we can also assume that the reflectivity is equal to zero. Therefore, we can assume that all radiation received by the target ESS is absorbed into the exposed steel panels as shown in Equations 4 and 5 below.

$$\alpha + \overset{0}{\rho} + \overset{0}{\tau} = 1 \quad (4)$$

$$\alpha = 1 \quad (5)$$

Based on the principles of black body radiation, the maximum radiation absorbed is equivalent to the radiation emitted [65,69]. Therefore, it is assumed that the emissivity and absorptivity of the steel containers are both equal to 1 as shown in Equation 6 below.

$$\alpha = \varepsilon = 1 \quad (6)$$

Where:

$$\begin{aligned} \alpha &= \text{absorptivity of steel} \\ \varepsilon &= \text{emissivity of steel} \end{aligned}$$

According to Drysdale's *An Introduction to Fire Dynamics*, the emissivity of a rough steel plate is approximately between 0.92 and 0.97 [57]. Therefore, to assume the steel plates are perfect radiators with an emissivity and absorptivity of 1 is a conservative approach, however it is relatively consistent with material properties. Since the emissive properties of the materials used by ESS manufacturers varies, this model assumes the containers behave as blackbody radiators, which encompasses the maximum potential radiation exposure from the heated steel panel.

7.2.2 Emissivity of Flame

The emissivity of a flame is a value that is relatively difficult to quantify, and a very active area of research. The fuels and combustion products of the flame give off radiation. However, the efficiency of the flames emitted energy is a function of the flames thickness and an absorption coefficient [37].

$$\varepsilon = 1 - \exp(-kl) \quad (7)$$

Where:

$$\begin{aligned} k &= \text{absorption coefficient (m}^{-1}\text{)} \\ l &= \text{flame thickness (m)} \end{aligned}$$

The absorption coefficient indicates how easily radiation can leave the flame. Since there is limited data on accurately quantifying an absorption coefficient for lithium-ion battery fires, an accurate flame emissivity could not be calculated based on Equation 7 above. However, the absorption coefficient of turbulent diffusion flames of common fuels is frequently 1 m^{-1} , which corresponds to high flame emissivity values of nearly 1 [37]. As a conservative assumption, this model assumes the flames behave as a blackbody radiator with an emissivity of 1, which is consistent with flame emissivity values commonly used in fire modelling.

7.3 Configuration/View Factor

The view factor is the variable that determines the fraction of radiation received by the target, with respect to the total radiation emitted from the source [37]. The view factor accounts for the shape, orientation, and size of both the emitter and the target as well as the separation distance between them. Since this model accounts for the radiation coming from the heated ESS container and the externally vented flames, two view factors are calculated.

7.3.1 Shape

This analysis treats the radiant sources as geometric shapes – modelling the externally vented flames as a cylindrical radiant body and the heated side panel of the ESS container as a rectangular plate.

7.3.2 Orientation

The orientation of the radiant source and the target influences the fraction of radiation that is visible to the target. The flames are expected to form a buoyant fire plume that resembles a vertical cylinder radiating to both a vertical rectangular plate and a horizontal rectangular plate. Since the base of the cylindrical flame will be at the top of the fire source container, two surfaces of the target ESS will be visible to the cylindrical radiant body – top and side panel. The view factor that accounts for the radiation emitted from the heated rectangular plate of the fire source to the target ESS is represented as two vertical parallel plates.

7.3.3 Dimensions

Since this study focuses on ESS within ISO-Containers, their standard dimensions of 8 ft in width, 8.5 ft in height, and lengths of 20 ft, 40 ft, and 53 ft will be used as the dimensions of the receiving surfaces for the view factors for the external flames and the radiating panel. The dimensions of the vertical plate (8.5 ft in height x length) will be used as the area of the emitting panel. See the emitting and receiving surface areas in Table 1 below.

Table 1 Parallel Rectangular Plate Emitting/Receiving Areas

	Area of Emitting Body dA_1			Area of Receiving Body dA_2		
	Width(ft)	Height (ft)	Total(ft ²)	Width(ft)	Height (ft)	Total(ft ²)
Parallel Plates: 20 ft	20	8.5	170	20	8.5	170
Parallel Plates: 40 ft	40	8.5	340	40	8.5	340
Parallel Plates: 53 ft	53	8.5	450.5	53	8.5	450.5

The dimensions of the external flames, represented as a cylinder, are dependent on the flame height and the radius of the flames. These are time dependent variables that change throughout different phases of the fire. However, the flame height was approximated through the Heskestad's flame height correlation, shown in Equation 8 below [78], which is a function of the heat release rate of the fire and the diameter of the vented flame.

$$H_f = 0.235\dot{Q}^{\frac{2}{5}} - 1.02D \quad (8)$$

Where:

$$\begin{aligned} H_f &= \text{Flame Height (m)} \\ D &= \text{Diameter of Flame (m)} \\ \dot{Q} &= \text{Heat Release Rate (kW)} \end{aligned}$$

The flame height and diameter of the flame are used to calculate the area of the emitting body, and the area of the ESS receiving radiation is a summation of the area of the horizontal and vertical panels of the exposed ESS. This is put forth in Table 2 below.

Table 2 Cylinders to Vertical/Horizontal Rectangular Plates Emitting/Receiving Areas

	Area of Emitting Body dA_1			Area of Receiving Body dA_2		
	Width(ft)	Height (ft)	Total(ft ²)	Width (ft)	Height (ft)	Total (ft ²)
Cylinder to Vertical Plate: 20 ft	Flame Radius and Flame Height Calculation. - Time dependent			20	8.5	170
Cylinder to Horizontal Plate: 20 ft				20	8	160
Total: 20 ft						330 ft²
Cylinder to Vertical Plate: 40 ft	Flame Radius and Flame Height Calculation. - Time dependent			40	8.5	340
Cylinder to Horizontal Plate: 40 ft				40	8	320
Total: 40 ft						660 ft²
Cylinder to Vertical Plate: 53 ft	Flame Radius and Flame Height Calculation. - Time dependent			53	8.5	450.5
Cylinder to Horizontal Plate: 53 ft				53	8	424
Total: 53 ft						874.5 ft²

7.3.4 View Factor Calculation

The view factor from the radiant bodies to adjacent containers is a critical component of this radiation heat transfer analysis. It is within this factor that the various separation distances are accounted for. In general, we know that a fire's intensity reduces with distance. The view factor will account for the angle, separation distance, area of radiating surface/flame and the area of the target surface. The view factors for the radiating panel and cylindrical vented flames are calculated through the methods shown below:

7.3.4.1 Parallel Rectangular Plates View Factor

The geometric view factor between the side panels of the ESSs can be calculated through the mathematically derived equation {Eq. 9} that analyzes the view factor between two rectangular parallel plates aligned at their center across specific separation distances [57], as depicted in Figure 14 below.

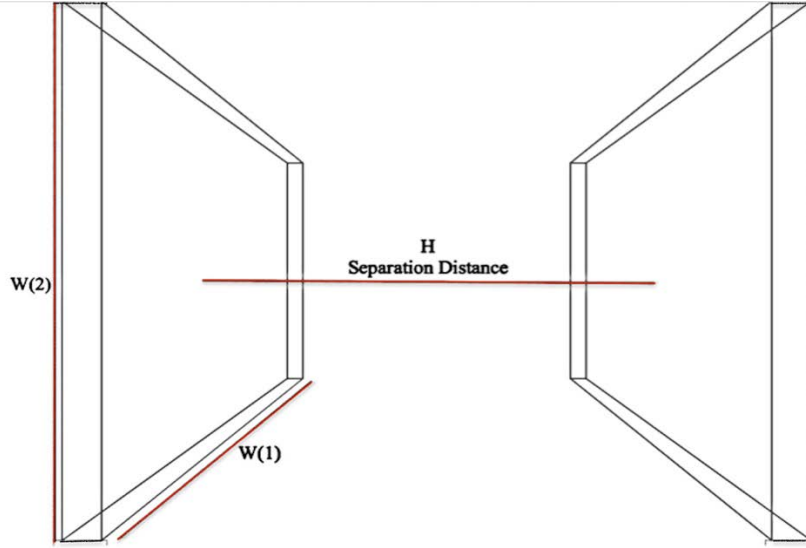


Figure 14 Parallel Rectangular Plate View Factor

$$F_{1(p),2} = \frac{1}{\pi xy} \left[\ln \frac{x_1^2 y_1^2}{x_1^2 + y_1^2 - 1} + 2x(y_1 \arctan \frac{x}{y_1} - \arctan x) + 2y(x_1 \arctan \frac{y}{x_1} - \arctan y) \right] \quad (9)$$

A series of intermediate equations are required to determine the view factor between the rectangular plates: x_1 , y_1 , x , and y . These variables are calculated through equations 10 – 13 shown below [57].

$$x_1 = \sqrt{1 + x^2} \quad (10)$$

$$y_1 = \sqrt{1 + y^2} \quad (11)$$

Equations 10 and 11, representing x_1 and y_1 , are a function of x and y , shown in equations 12 and 13 below. X is a function of the length of the containers (W_1) and the separation distance between the containers, and Y is a function of the height of the container wall and the separation distance between the ESS containers.

$$x = \frac{W_1}{H} \quad (12)$$

$$y = \frac{W_2}{H} \quad (13)$$

Integrating the intermediate equations {Eq. 10 – 13} back into the governing rectangular parallel plate view factor calculation will provide a fractional value that indicates the portion of radiation received at the target surface based on the container size and separation distance. See the calculated view factor values for 20 ft, 40 ft, and 53 ft containers across a range of separation distances in Table 3 below.

Table 3 View Factors for Parallel Rectangular Plates at Various Separation Distances

Separation Distance	20 ft Container	40 ft Container	53 ft Container
3 ft	0.6298	0.5543	0.5297
5 ft	0.5028	0.4533	0.4327
6 ft	0.4490	0.4132	0.3944
7 ft	0.4010	0.3789	0.3616
8 ft	0.3583	0.3492	0.3336
9 ft	0.3203	0.3233	0.3094
10 ft	0.2867	0.3005	0.2884
12 ft	0.2308	0.2618	0.2536
15 ft	0.1697	0.2155	0.2137
20 ft	0.1078	0.1585	0.1656

7.3.4.2 Cylinder to Rectangular Plate View Factor

To represent the externally vented flames escaping the ESS container, the flames were modelled as an elevated geometric cylinder emitting radiation onto a rectangular plate in the vertical and horizontal orientation. Figure 15 below represents the view factor between the elevated cylindrical flame and the vertical rectangular plate. This view factor accounts for the amount of visible radiation emitting from the area of the cylindrical flames to the entire area of the steel panels.

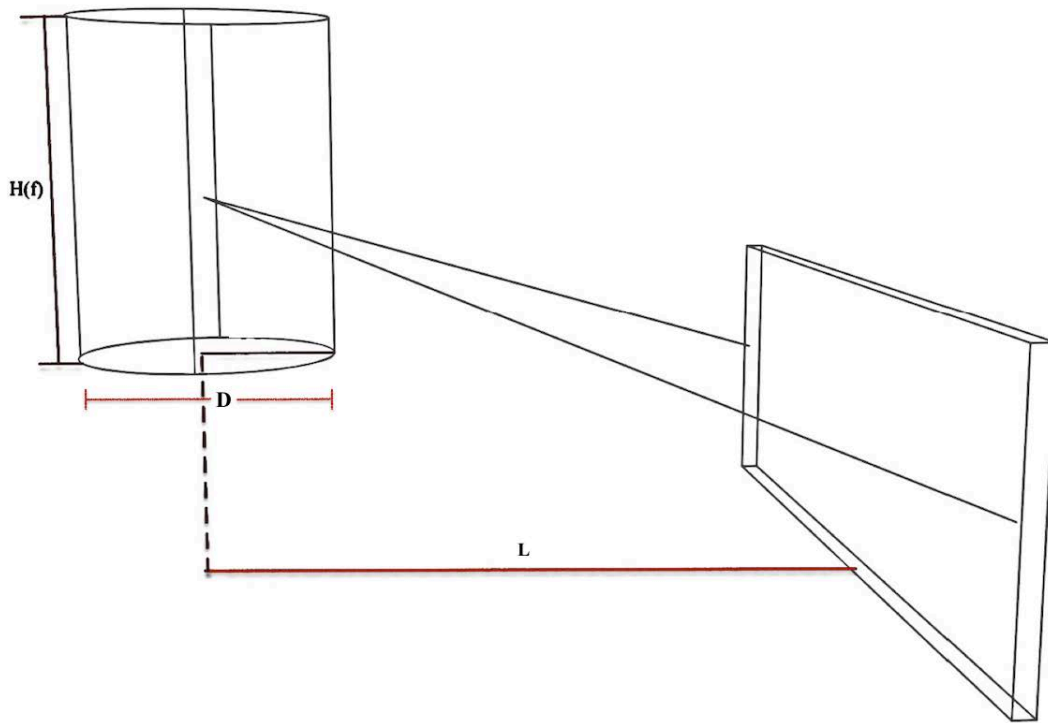


Figure 15 Cylinder to Vertical Rectangular Plate View Factor

The fraction of the radiation received at the rectangular plates is based on the derived function shown in Equations 14 and 15 below between a cylindrical radiant body and a rectangular plate of vertical orientation for the side panel of the exposed ESS {Eq. 14} and horizontal orientation for the top panel of the exposed ESS {Eq. 15} [78].

$$F_{1_c, 2_{p,V}} = \frac{1}{\pi S} \tan^{-1} \left(\frac{h}{\sqrt{S^2-1}} \right) - \frac{h}{\pi S} \tan^{-1} \sqrt{\frac{S-1}{S+1}} + \frac{Ah}{\pi S \sqrt{A^2-1}} \tan^{-1} \sqrt{\frac{(A+1)(S-1)}{(A-1)(S+1)}} \quad (14)$$

$$F_{1_c, 2_{p,H}} = \frac{(B-1)/S}{\pi \sqrt{B^2-1}} \tan^{-1} \sqrt{\frac{(B+1)(S-1)}{(B-1)(S+1)}} - \frac{A-1}{S} \tan^{-1} \sqrt{\frac{(A+1)(S-1)}{(A-1)(S+1)}} \quad (15)$$

The intermediate equations to calculate the geometric view factors are shown in Equations 16, 17, 18 and 19 below. This factor accounts for the separation distance between the cylindrical radiant body (L), and the size of the flame (diameter (D) and flame height (H_f)) [78].

$$S = \frac{2L}{D} \quad (16)$$

$$h = \frac{2H_f}{D} \quad (17)$$

$$A = \frac{h^2 + S^2 + 1}{2S} \quad (18)$$

$$B = \frac{(1+S^2)}{2S} \quad (19)$$

Table 4 below shows the summation of the calculated view factors from the cylindrical flames to the top and side panel of the exposed ESS.

Table 4 Cylinder to Rectangular Plate View Factors

Separation Distance	500 kWh	1 MWh	2 MWh	3 MWh	4 MWh	5 MWh
3 ft	0.837	0.835	0.834	0.834	0.834	0.834
5 ft	0.624	0.638	0.639	0.640	0.640	0.640
6 ft	0.579	0.598	0.600	0.601	0.602	0.602
7 ft	0.549	0.573	0.576	0.576	0.577	0.577
8 ft	0.528	0.553	0.557	0.558	0.559	0.559
9 ft	0.513	0.539	0.543	0.544	0.545	0.546
10 ft	0.502	0.528	0.532	0.534	0.535	0.535
12 ft	0.486	0.512	0.517	0.519	0.520	0.520
15 ft	0.475	0.498	0.501	0.504	0.505	0.506
20 ft	0.467	0.482	0.487	0.489	0.490	0.491

A summation of both view factors was calculated to accurately depict the intensity of radiation imposing on the container based on both radiant sources – the cylindrical flame exiting the vent and the radiant heat from the panel. The summation of the view factors will indicate the intensity

of radiation received at the adjacent container, allowing the surface temperature and internal air temperature of the exposed container to be calculated.

7.4 Temperature of Radiant Body

At the core of radiation heat transfer is the temperature of the radiating body [53]. Therefore, as the fire grows within the ESS, a hot gas layer will form within the container as a function of the emitted combustion products of the fire plume. The temperature of the hot gas layer will continue to rise as a function of the heat release rate, discussed in section 7.4.2, 7.4.3.2.1, and 7.4.3.2.2. This hot gas layer will heat the boundary layers of the compartment (container walls) through means of convection and radiation heat transfer [40]. The temperature of the heated steel panel will serve as the rectangular radiant body. The temperature of the externally vented flames will serve as the cylindrical radiant body. The methods of determining the temperatures of the radiant sources are put forth within this section.

7.4.1 Wall Temperature of ESS Fire Source

The approach to calculating the wall temperature of the fire involved ESS container was through the method of Peatross and Beyler. This method modifies the MQH correlation and Beyler and Deal methods which are based on the assumption that the walls are composed of normal insulating materials. Whereas, Peatross and Beyler modified these two correlations to account for the wall material being a highly conductive steel – applicable to this ESS fire scenario which ignores insulation of the container walls [41].

The rise of the wall temperature of the container is a function of the heat transfer between the hot gas layer and the steel panel. The temperature of the panel is a function of the heat stored within the panel with respect to the steel's material properties (density, specific heat, thickness, surface area). However, the rise in the wall temperature is dependent on the enthalpy flow through the wall – heat into the wall from the developed compartment fire and the outflow of heat from the wall to the atmosphere. This approach assumes that the temperature of the gas layer throughout the compartment is uniform, which heats the boundary layers (walls) at a constant rate [42]. This analyzes the heat flow into the wall from the radiant and convective heat from the hot gas layer and the heat outflow of the convective losses from the wall to the outside.

Storage = Enthalpy flow

$$\text{Storage} = \rho_s c_s \Delta x A_w \frac{dT_{w,1}}{dt} \quad (20)$$

$$\text{Enthalpy Flow} = \text{heat into wall} - \text{heat out of wall} = \dot{q}''_{in,rad+conv} - \dot{q}''_{out,conv losses}$$

According to Quintiere's *Fundamentals of Fire Phenomena* [63], the temperature rise of the wall of the ESS fire source is represented through the energy exchange shown in Equation 21 below.

$$\frac{dT_{w,1}}{dt} = \frac{1}{\rho_s c_s \Delta x A_w} [\varepsilon \sigma (T_g^4 - T_w^4) + h_{hot} A_w (T_g - T_w) - h_{\infty} A_w (T_w - T_{\infty})] \quad (21)$$

$dT_{w,1}/dt$ = change in wall temperature above ambient over time

ρ_s = density of steel panel (kg/m^3)

c_s = specific heat of steel ($kJ/kg - K$)

Δx = thickness of steel panel (m)

A_w = Surface Area of Container Surfaces (m^2)

ε = emissivity (dimensionless)

σ = Stefan – Boltzman Constant ($5.67e^{-11} kW/m^2 K^4$)

T_g = Temperature of Hot Gas Layer (K)

T_w = Temperature of Heated Steel Panel (Wall) (K)

h_{hot} = heat transfer coefficient (hot) ($kW/m^2 K$)

h_{∞} = heat transfer coefficient (ambient) ($kW/m^2 K$)

Equation 21 above requires the quantification of the heat transfer coefficient at the hot and ambient sides of the wall (h_{hot} , h_{∞}) as well as the calculation of the hot gas layer temperature – a function of the ESS fire. These variables are determined in sections 7.4.1.1 and 7.4.2, respectively.

7.4.1.1 Heat Transfer Coefficient

To quantify the convective heat transfer at the boundary layer between the hot gas layer and the compartment walls, an effective heat transfer coefficient must be calculated. A heat transfer coefficient quantifies that rate at which heat is transferred from the hot gas layer of the fire through the solid wall [43]. The heat transfer coefficient used to represent the energy exchange at the hot side of the walls was based on the following equation [57]:

$$h_{hot} = \sqrt{\frac{kpc}{t}} \quad (22)$$

where:

k = thermal conductivity ($kW/m-K$)

p = density of steel (kg/m^3)

c = specific heat ($kJ/kg-K$)

t = time (s)

Equation 22 represents a heat transfer coefficient that is a function of the temperature dependent thermal conductivity of the steel panel, density, and specific heat of the steel with respect to time.

Under ambient conditions, the heat transfer coefficient is a stagnant value, which is used to represent the convective losses to the outside of the container. This heat transfer coefficient is a function of the thermal conductivity of the steel at ambient condition and the thickness of the steel [57] as shown in Equation 23 below.

$$h_{\infty} = \frac{k}{\Delta x} \quad (23)$$

Where:

k = thermal conductivity

Δx = thickness of steel panel

7.4.1.2 Thermal Conductivity of Steel

The thermal conductivity of a material is defined as its ability to conduct heat. Steel, as analyzed for energy storage systems, has a high thermal conductivity. Therefore, even though the steel structure of the ESS containers are noncombustible, it serves as a great medium for heat transfer. The high thermal conductivity of steel allows heat to be transferred through the panel at a fast rate. The standard thermal conductivity of steel according to the Eurocode 3 [44] is 54 W/m-K. As the temperature of the steel panel increases, the thermal conductivity of the steel will decrease allowing heat to be transferred through the container more rapidly. Equations 24 and 25 below are derived correlations that represent the temperature dependence of the thermal conductivity of steel based on Eurocode 3 and a study on material properties at elevated temperatures [44].

$$k_s = 54 - \left(\frac{T_w}{300}\right) \quad \text{for } 20^{\circ}\text{C} < T_w \leq 800^{\circ}\text{C} \quad (24)$$

$$k_s = 27.3 \frac{W}{m-K} \quad \text{for } T_w > 800^{\circ}\text{C} \quad (25)$$

7.4.2 Gas Layer Temperature of ESS Fire Inside Compartment

A common method for calculating the temperature rise of the upper gas layer is through the method of McCaffrey, Quintiere, and Harkleroad (MQH). This method applies a simple conservation of energy principle to the hot gas layer, which gives the following correlation [40]:

$$\frac{\Delta T_g}{T_{\infty}} = \frac{\dot{Q}}{1 + \frac{h_k A}{m_g c_p} T_{\infty}} \quad (26)$$

$\frac{\Delta T_g}{T_{\infty}}$ = Change in Temperature of the Hot Gas Layer over time

\dot{Q} = Heat Release Rate (kW)

m_g = mass flow rate of gas layer(kg/s)

c_p = specific heat of air $\left(\frac{\text{kJ}}{\text{kg} - \text{K}}\right)$

T_{∞} = Ambient Temperature (K)

h_k = heat transfer coefficient (kW/m²K)

A_T = Surface Area of Compartment Boundaries

This MQH correlation analyzes the compartment temperature with respect to the energy generated by the fire (\dot{Q}), the flow rate of the gas out an opening under natural ventilation (\dot{m}_g), the specific heat of the air (c_p), and the heat lost from the hot gas layer to the surrounding surfaces ($h_k A$).

The MQH correlation represents the hot gas layer temperature under naturally ventilated conditions [40]. In traditional fires, the compartment plays a significant role in limiting fire growth. The size of the openings can restrict the availability of additional oxygen needed to reach full combustion of the fuel [53]. If the oxygen concentration within the compartment is insufficient to reach full combustion, the amount of fuel consumed will be reduced, leaving a substantial amount of unburned fuel. With incomplete combustion, the heat release rate will be lower and the temperature and heat transfer to the fuel surface will also be reduced [40].

Lithium-ion batteries challenge this ventilation-limited scenario because they are able to generate their own oxygen when undergoing thermal runaway [23]. Testing has shown that lithium-ion batteries are capable of producing sparks of flaming combustion in an inert environment along with a release of significant quantities of flammable gases [60]. Therefore, it is assumed that a substantial amount of oxygen can release during each battery failure, as a result of the decomposition of the battery's metal oxide (cathode). However, a limited oxygen concentration within the container will not stop the progression of thermal runaway within the ESS. Once sufficient burning has taken place to raise the compartments ambient temperature above the battery's thermal stability limits, thermal runaway reactions can progress. Although the oxygen released from the individual batteries may not be sufficient to sustain steady combustion within a ventilation-limited compartment, masses of flammable gases from the thermal runaway reactions of LIB's will continue to be released [23]. This scenario poses over-pressurization and explosion hazards due to the mass of unburnt fuel in a closed unventilated compartment [59]; this presents additional hazards that are outside the scope of this report.

A ventilation-limited scenario could underestimate the heat release rate and quantity of fuel burned in an ESS fire. Code councils and researchers are recommending mechanical ventilation systems to cool the ESS and remove flammable and toxic gases during a failure event to mitigate an explosion hazard [6,46]. Therefore, based on the assumption that forced ventilation will be used to mitigate hazards posed by lithium-ion batteries during failure, a forced ventilation scenario can be used to characterize a fully developed fire within an ESS. The continuous air flow into the ESS container will allow the fire to be limited to the quantity of fuel within the compartment – representing a fully-involved ESS fire event.

The hot gas layer temperature is largely impacted by the ventilation conditions within the compartment. Therefore, the MQH correlation for determining the hot gas layer temperature must be modified to account for the effects of forced ventilation. Foote, Pagni, and Alvares conducted a series of 64 fire tests with varying forced ventilation conditions [40]. From these tests, empirical constants that represent the change in the hot gas layer temperature in forced ventilation conditions were derived [79]. Following the basic relationship of the MQH correlation, Foote, Pagni, and Alvares added data for forced ventilation fires – now referred to as the FPA method [40]. Therefore, to represent a ESS forced ventilation fire, the FPA method was

used, as shown in Equation 27 below, to determine the change in temperature of the hot gas layer over time.

$$\frac{\Delta T_g}{dt} = T_\infty + \left(0.63 * \frac{\dot{Q}}{\dot{m}c_p T_\infty}\right)^{0.72} * \left(\frac{h_k A}{\dot{m}c_p}\right)^{-0.36} \quad (27)$$

$\frac{\Delta T_g}{dt}$ = Change in Temperature of the Hot Gas Layer over time (K/s)

T_∞ = Ambient Temperature (K)

\dot{Q} = Heat Release Rate (kW)

\dot{m} = forced ventilation flow rate (kg/s)

c_p = specific heat of air $\left(\frac{\text{kJ}}{\text{kg} - \text{K}}\right)$

h_k = heat transfer coefficient (kW/m²K)

A_T = Surface Area of Compartment Boundaries

This equation is a function of the heat release rate of the fire (\dot{Q}), the forced ventilation flow rate (\dot{m}), specific heat of air (c_p), heat transfer coefficient (h_k), and surface area of the compartment boundaries (A) under varying ventilation conditions. In order to determine the hot gas layer temperature we must define the ventilation within the compartment and the fire source (heat release rate (\dot{Q})).

7.4.2.1 Forced Ventilation

According to the 2018 Edition of the International Fire Code, a minimum ventilation rate of 150 cfm is required within energy storage systems [6]. This value was used as a minimum threshold for a forced ventilation fire scenario. Testing conducted by DNV GL provided data to develop a ventilation rate correlation of 0.32 cfm/kWh for safe operation of an ESS as a function of the energy capacity of the system [46]. This correlation was used as the basis for the forced ventilation rates for various ESS capacities analyzed within this study. See Table 5 below for the forced ventilation air flow rates of corresponding energy capacities.

Table 5 Forced Ventilation Rates

ESS Capacity	Ventilation Factor	Forced Ventilation Air Flow Rate
0.5 MWh	0.32 cfm/kWh	160 cfm
1 MWh	0.32 cfm/kWh	320 cfm
2 MWh	0.32 cfm/kWh	640 cfm
3 MWh	0.32 cfm/kWh	960 cfm
4 MWh	0.32 cfm/kWh	1280 cfm
5 MWh	0.32 cfm/kWh	1600 cfm

Forced ventilation can significantly impact the fire growth, temperature within the compartment, spread of gases from the fire, and the decent of the smoke layer within the compartment [62]. Since this scenario analyzes a fire under forced ventilation conditions, the growth of the fire will

be significantly impacted by the volumetric air flow rate within the ESS container by providing an adequate oxygen supply for the large quantity of fuel. However, it also serves as a limiting factor for the peak heat release rate of a fire in a compartment with uniform air flow.

A compartment fire with forced-ventilation behaves significantly different than a naturally ventilated space. Naturally ventilated fires typically have a stratified thermal hot gas layer that develops from the fire plume and descends toward the floor as the oxygen concentration is reduced within the compartment. However, a forced ventilation compartment may have an unstable gas layer due to the mixing of the combustion products and the air flow which spreads the hot gases throughout the compartment [62].

A forced ventilation scenario also limits the formation of the smoke layer. As in any compartment fire, the depth of the smoke layer increases over time. However, the smoke layer in forced ventilation scenarios descends until it reaches equilibrium; this phenomenon allows for additional fuel to be consumed [62]. Once the fire reaches its peak heat release rate, the fire growth is limited to the ventilation rate throughout the compartment. Since the ventilation rate is constant, the amount of fuel that can be consumed per second becomes constant, allowing the fire to reach a steady-state condition until all fuel within the container is consumed.

7.4.3 Characterization of ESS Fire

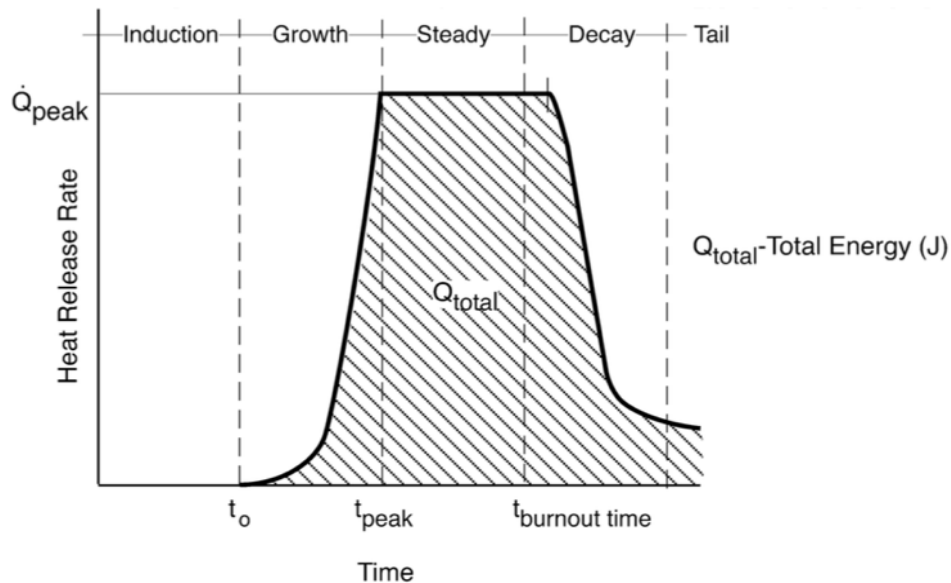
A fire within a lithium-ion ESS container can be characterized by the behavior of individual fire events in cells and/or modules. The means of heat transfer and rate of fire spread between batteries, modules, and racks within a container is analyzed within this study. As previously mentioned, there is significant variation in the design of ESS containers based on the lithium-ion technology. The number of batteries can range between thousands to tens of thousands of lithium-ion batteries (LIB) in an energy storage container [11,15]. Since the variation in specific chemistries, sizes, formats, and quantity of lithium-ion batteries in ESS containers are vast, it's difficult to generalize them. Therefore, the rated energy capacity (Wh) of the ESS was established as a means of characterizing ESS containers. The energy density of the lithium-ion batteries used in ESS containers determines the quantity of energy that can be provided per unit volume. Therefore, the increasing energy capacity (Wh) of the ESS containers examined is a function of the energy density (Wh/l) of the batteries used within a specific container size ($m^3(L)$).

This analysis focuses on the conditions under which a fully involved fire event within an ESS could occur. A fire within an ESS container can be represented as a compartment fire. In general, compartment fires are influenced by the amount of oxygen available to sustain combustion [63]. Since studies have shown that the quantity of combustible gases released during lithium-ion battery fires can present an over pressurization hazard, recommendations for forced ventilation systems are being put forth to provide both cooling to the batteries and to remove toxic gases under failure conditions [46,59]. A forced ventilation scenario considers the possibility of all lithium-ion batteries failing and going into a thermal runaway event; this causes the fire scenario to be dependent on the quantity of fuel within the container.

This scenario ignores the potential control of a fire suppression system, and analyzes the following fire stages of a fully-involved forced ventilation ESS fire [35, 53].

- *Ignition (Induction)* – The early stage of fire development where the fire’s progression is limited to a fuel source and the thermal hazard is localized to the area of burning material.
- *Growth* – The stage of fire development when the heat release rate from an incipient fire has increased to the point where heat transferred from the fire and the combustion products are pyrolyzing adjacent fuel sources.
- *Fully Developed Fire (Steady-State)* – Fire development, within a compartment, has reached its peak heat release rate.
- *Decay* – The stage of fire development within a structure characterized by either a decrease in the fuel load, resulting in lower temperatures and pressure in the fire area.

Figure 16 shown below is expected to be representative of a containerized ESS heat release rate curve of a fully-involved energy storage system fire.



(a) Burnout Time > Time to Peak HRR

Figure 16 HRR Curve Demonstrating Stages of ESS Fire [62]

7.4.3.1 Ignition

This fire scenario assumes a single cell ignition source where one lithium-ion battery undergoes a thermal runaway event initiated by one of the failure modes discussed in section 2.3.1 of this report including overheating, overcharging, internal short circuit, etc. The fire behavior of a few lithium-ion batteries provides insight into the behavior, severity, duration, and rate of fire propagation of a lithium-ion ESS fire. The combustion behavior of a lithium-ion battery is described below to serve as a basis for developing a probable fire scenario within a large ESS.

7.4.3.1.1 Battery Expansion

Regardless of the initiating event, all failure modes result in an increase in temperature and pressure within the cell. The components of lithium-ion batteries are heat sensitive, thus any internal failure or exposure to high ambient temperature will raise the temperature of the battery. As the decomposition of the battery generates heat faster than can be dissipated, pressure will rise internally causing the battery to expand [60].

7.4.3.1.2 Jet Flame

After the battery(s) have expanded, the cells components undergo internal chemical degradation reactions. Testing of 100% SOC lithium-ion batteries indicated a loud hissing sound – typically representative of a thermal runaway reaction – followed by a violent release of large quantities of gas. This flammable vapor ignited immediately after it was released, resulting in an intense jet flame [60]. The initial jet flame is believed to be a result of the decomposition of the SEI layer, compromising the separation between the electrolyte and the anode – which allows for chemical reactivity and a violent ejection of gases [58].

7.4.3.1.3 Stable Combustion

Following the initial flame jet, the batteries typically enter a phase of stable combustion [60]. At this stage, the intensity of the combustion process is significantly reduced, however, the battery components continue to burn as they vaporize and combust with the available oxygen.

7.4.3.1.4 Additional Cycles of Jet Flame/Stable Combustion

Typically, a lithium-ion battery fire will undergo additional cycles of violent jet flames with increasing intensity followed by periods of stable combustion [60]. The additional jet flames are accompanied by large quantities of flammable gas, presenting a large concentration of combustible gases within the compartment. The number of additional jet flames will be dependent on state of charge (SOC), number of batteries involved, and the chemistry. Single cell fires commonly experience three jet flames at 100% and 50% SOC, the three violent ejections correspond to the sequence of reactions within the cell involving the decomposition of the anode, separator, and cathode [60]. The decomposition of the cathode (positive electrode – metal oxide) has shown to be the most violent jet flame – which is attributed to the additional release of oxygen during the decomposition of the metal oxide and electrolyte.

7.4.3.1.5 Decline of Fire Event to Extinguishment

As the internal reactions cease and the flammable vapors are consumed, the fire will slowly begin to decline in its intensity, size, and heat released [60]. The total duration of the combustion of the lithium-ion batteries is dependent on their state of charge (SOC) – which directly correlates to the intensity and rapidity of the reactions, and the number of batteries involved. This is directly related to the amount of energy released as flaming combustion (kW/Wh) as a function of the batteries energy density.

7.4.3.1.6 Why is this behavior unique in comparison to traditional fuels?

The behavior of lithium-ion batteries, as described in sections 7.4.3.1.1 - 7.4.3.1.5, is unique in comparison to traditional fuels. Studies of traditional fires typically focus on liquid pool fires or fires involving solid fuels such as wood or plastics. A pool fire is defined as a turbulent diffusion flame burning above a horizontal pool of vaporizing hydrocarbon fuel where the fuel has zero or very low initial momentum [50,57]. A solid fuel fire is characterized by three phases: time to pyrolysis, time to mix, and time for flammable mixture to proceed to combustion [63]. Lithium-ion batteries, however, do not correspond to the behavior of either category. A pool fire does not appropriately describe this scenario due to the state of the fuel. A lithium-ion battery fire should also not be classified as a solid-fuel fire because the chemical decomposition process of a LIB is not consistent with solid pyrolysis [57]. However, when a lithium-ion battery fails, its flammable volatiles are released with significant momentum and intensity.

Based on the fire behavior of single and/or multiple cell battery packs, observations show that the decomposition products of a lithium-ion battery are released with significant momentum [60]. This behavior aligns with a jet fire phenomenon defined as a “turbulent diffusion flame resulting from the combustion of a fuel continuously released with some significant momentum in a range of directions” [50]. However, since the jet flames of a lithium-ion battery are intermittent – corresponding to individual failures of battery components, the overall fire event of an ESS should be classified as a turbulent diffusion flame fire with intermittent peaks in intensity during released jet flames.

7.4.3.2 Growth Phase: Fire Propagation throughout ESS

Thermal runaway in individual lithium-ion batteries is relatively well studied and understood. Essentially, a failure within a cell induces exponential heat-generation reactions, vents flammable gases, ejects cell contents, and produces extreme temperatures and flaming ignition of the cell and/or battery materials [48]. However, there is a significant lack of understanding concerning how thermal runaway effects a larger system, such as an ESS. Small-scale testing proves that the thermal impact from a lithium-ion battery undergoing thermal runaway is significant enough to spread to adjacent cells resulting in a cascading thermal runaway event [48]. This fire scenario assumes that a lithium-ion cell in thermal runaway produces enough heat to raise the temperature of adjacent batteries above their failure point, initiating thermal runaway in the neighboring batteries, propagating the heat throughout the battery module until all batteries reach a state of thermal runaway. A study that analyzes thermal runaway propagation in large format lithium-ion battery modules confirms the assumption that thermal runaway in one cell can propagate throughout an entire battery module [64]. The testing concluded that only 12% of the heat released from the first battery in thermal runaway was necessary to propagate the failure to an adjacent cell, and only 7% of the heat released was required to propagate to additional cells within the module. This data indicates that as more batteries become involved, more heat will be released, requiring less energy, heat, and time to involve more batteries within the ESS – resulting in an exponential fire growth [64].

Extensive variation in rack design is found through the ESS industry. For example, some racks are enclosed in steel/aluminum cabinets, while others are open frame racks as shown in section

2.1.1. This will impact the fire propagation between modules and racks, however, this scenario assumes a worst case event where the convective and radiative heat coming off a battery module will be sufficient enough to spread to adjacent modules within a rack. Since the flame temperature of lithium-ion battery fires has demonstrated temperatures exceeding 2000°F [4], it is assumed that a fully involved battery rack fire will generate enough heat to involve adjacent racks within a container.

Substantial burning develops as thermal runaway reactions progress throughout the ESS. As subsequent batteries fail, a series of processes occur in the development of flame spread throughout the container. During flaming combustion, heat and free radicals coming from the failing batteries will be transported into the unburned gas region – causing combustion reactions just ahead of the flame, resulting in fire growth [57]. The fire will propagate to adjacent cells through direct flame impingement and/or heat transfer through means of conduction, convection, and radiation. The rapidity and intensity of lithium-ion battery combustion reactions along with their violent ejection of flammable gases is expected to raise the temperature of the developing gas layer. The rising compartment temperature can place batteries not intimate with the fire event into an unstable thermal condition, allowing exothermic self-degradation reactions to begin and lead to thermal runaways in other battery racks within the ESS [48].

7.4.3.2.1 Quantification of Fire Growth

The intermittent peaks in intensity during the growth phase of a lithium-ion ESS fire makes it difficult to assess the propagation rate throughout an ESS. The fire growth rate was concluded to be best represented as a time dependent “t-squared” fire based on HRR curves of multi-cell fire tests [33,52]. Using an at^2 fire growth approximation, the heat release rate is expected to accelerate as an exponential function, until the peak heat release rate is reached [53]. However, arrays of lithium-ion batteries demonstrate a more complicated burning behavior than illustrated by this simple t^2 fire characterization. Their burning behavior is characterized by multiple peaks and valleys associated with the intermittent phases of jet flaming and stable combustion, or the burnout of one module or rack and the growth of fire on a newly exposed set of batteries [60]. However, testing from the FAA concluded that a t^2 characterization was closely correlated to the actual measured heat release rate curve, allowing this representation to be used to predict heat release rate curves for larger systems [33].

To approximate the growth of a t^2 fire, a fire growth constant must be determined to represent the impact of fuel chemistry and orientation on fire growth [53]. Substantial research and testing has been conducted on a variety of different fuels to categorize different rates of fire growth: slow, medium, fast, and ultrafast. Since limited data regarding the fire propagation rate between large quantities of lithium-ion batteries exists, growth constants (α) were derived from the limited small-scale heat release rate data available [33, 52]. These calculations classified the growth rate of multiple battery packs as falling between a slow and medium growth coefficient for t^2 fires [33]. To be conservative, this study models the estimated ESS fire as a medium t^2 fire to account for the compartment effects on fire growth, such as radiation feedback and the dense quantity of fuel within the container. The fire growth constant used to approximate the fire propagation throughout the ESS was 0.0118 kW/s² – medium fire growth constant [53].

Therefore, the heat release rate during the growth phase of the fire is calculated through the power-law fire growth correlation [53] shown below in Equation 28.

$$\dot{Q} = \alpha(t - t_0)^2 \quad (28)$$

\dot{Q} = Heat Release Rate (During Growth Phase) – kW
 α = fire growth constant (0.0118 kw/s²)
 t = time (s)
 t_0 = time at ignition ~ 0

7.4.3.2.2 Quantification of Peak Heat Release Rate of ESS Fire Event

The heat release rate (HRR) of a fully involved ESS fire is the factor that quantifies the fire source within an ESS. The HRR is defined as “the rate at which energy is generated by the burning of a fuel and oxygen mixture. As the heat release rate increases, the heat, smoke production and pressure within the area will increase and spread along available flow paths toward low pressure areas” [35]. The most common method of quantifying the heat release rate is through Oxygen Consumption Calorimetry (OC), which assumes that the HRR is proportional to the oxygen consumed during the combustion of common organic fuels [55]. However, quantifying the heat release rate through OC methods is challenging for lithium-ion batteries due to their ability to release oxygen during failure.

The heat release rate of an LIB ESS fire is dependent on the quantity of fuel, ventilation conditions, and the phase of the fire (incipient, growth phase, steady, decay). In this scenario, the peak heat release rate is assumed to be limited to the forced-ventilation air flow within the compartment. Through a study on thermal runaway in large lithium-ion battery systems, the effective heat of combustion of a lithium-ion battery in air was determined to be approximately 28 kJ/g [59]. The mass flow rate of the gas layer within the compartment is dependent on the mass loss rate of the fuel (kg/s), density of air (1.2 kg/m³) and the range of volumetric airflow rates (m³/s). The ventilation rate within the ESS containers were determined based on a ventilation rate correlation of 0.32 cfm/Wh [46] determined through testing conducted by DNV GL and Consolidated Edison. This ventilation factor allowed the ventilation rates to be dependent on the maximum rated energy of the ESS containers. For ESSs ranging between 500 kWh and 5 MWh, the range of forced ventilation rates were determined to be between 0.133 m³/s (150 cfm) and 0.755 m³/s (1,600 cfm). The minimum airflow value determined by this correlation is consistent with the minimum ventilation rates for stationary battery energy storage systems put forth by the upcoming 2018 edition of the International Fire Code [6].

The peak heat release rate quantifies the heat released for complete combustion of the fuel – peak burning rate [70]. Although, it is uncommon for lithium-ion batteries to reach full combustion, it has been determined that the combustion efficiency for oxygen containing products can be between 90 and 100%. Since lithium-ion batteries release oxygen during combustion, the peak burning rate of a lithium-ion battery ESS fire can be quantified through Equations 29 and 30 below [70].

$$\dot{Q}_{peak} = \Delta H_{c,eff} * \dot{m} \quad (29)$$

$$\begin{aligned} \dot{Q}_{peak} &= \text{Peak Heat Release Rate (kW)} \\ \Delta H_c &= \text{Effective Heat of Combustion (kJ/kg)} \\ \dot{m} &= \text{Mass flow rate(mixed gas layer) (kg/s)} \end{aligned}$$

Where,

$$\dot{m} = \dot{m}_{air} + \dot{m}_{fuel} = (\rho_{air} * \dot{V}) + MLR_{fuel} \quad (30)$$

$$\begin{aligned} \rho_{air} &= \text{density of air (kg/m}^3\text{)} \\ \dot{V} &= \text{Volumetric flow rate(m}^3\text{/s)} \\ MLR &= \text{Mass loss rate of fuel (burning rate of fuel (kg/s))} \end{aligned}$$

Equation 30 above assumes that the gas layer within the compartment, constituting of air flow and the fuel released from the volatiles of the lithium-ion batteries, is well mixed and its temperature is uniform [57]. Therefore, the mass flow rate of the flammable gas within the compartment is dependent on the temperature dependent density of the air and the volumetric flow rate of the mechanical ventilation system in addition to the mass loss rate of the fuel (rate of volatile release from LIB failure) which combine to form the mixed flammable gas layer.

Various small scale tests of various types of lithium-ion batteries have indicated that between 16% and 27% of the battery mass is lost over a time period of 40 to 60 seconds [46,59,60]. Since different battery formats vary in mass, a few different types of commonly used lithium-ion batteries were analyzed to obtain a range of mass loss rates for various battery types. See the data in Table 6 below.

Table 6 Mass Loss Rates for Various Battery Formats

Battery Types	Average Mass	Mass Loss Rate
Cylindrical 18650	0.042 kg	0.000003 kg/s
Cylindrical 26650	0.093 kg	0.00004 kg/s
Prismatic (small)	0.038 kg	0.00002 kg/s
Prismatic (large)	3.65 kg	0.0015 kg/s
Polymer (small)	0.0145 kg	0.000006 kg/s
Polymer (large)	0.15 kg	0.00345 kg/s

The mass loss rate (burning rate) of the battery is an important variable in quantifying the heat release rate; however, in comparison to the volumetric flow rates within the compartment, the mass loss rate plays a somewhat insignificant role in the total heat release rate. Therefore, the mass flow rate of air and the heat of combustion of lithium-ion batteries combusting in air is used to approximate the peak heat release rate. Using equations 29 and 30, the range of heat release rates from forced-ventilation fire scenarios is 2.55 MW to 25.37 MW for 500 kWh to 5 MWh systems. This data is shown in Table 7 below.

Table 7 Heat Release Rates

System Size	\dot{V}_{air}	ρ_{air}	\dot{m}_g	$\Delta H_{c,eff}$	Peak HRR
500 kWh	0.076 m ³ /s	1.2 kg/m ³	0.0912 kg/s	28 MJ/kg	2.55 MW
1 MWh	0.151 m ³ /s	1.2 kg/m ³	0.1812 kg/s	28 MJ/kg	5.07 MW
2 MWh	0.302 m ³ /s	1.2 kg/m ³	0.3624 kg/s	28 MJ/kg	10.15 MW
3 MWh	0.453 m ³ /s	1.2 kg/m ³	0.5436 kg/s	28 MJ/kg	15.22 MW
4 MWh	0.604 m ³ /s	1.2 kg/m ³	0.7248 kg/s	28 MJ/kg	20.29 MW
5 MWh	0.755 m ³ /s	1.2 kg/m ³	0.9060 kg/s	28 MJ/kg	25.37 MW

Once the peak heat release is reached, the ESS compartment will be in a fully-developed fire phase. At this point the fire will burn at a steady rate, driven by the ventilation in the compartment, until nearly all the fuel is consumed and the burnout/decay phase is initiated, as represented in Figure 17 below.

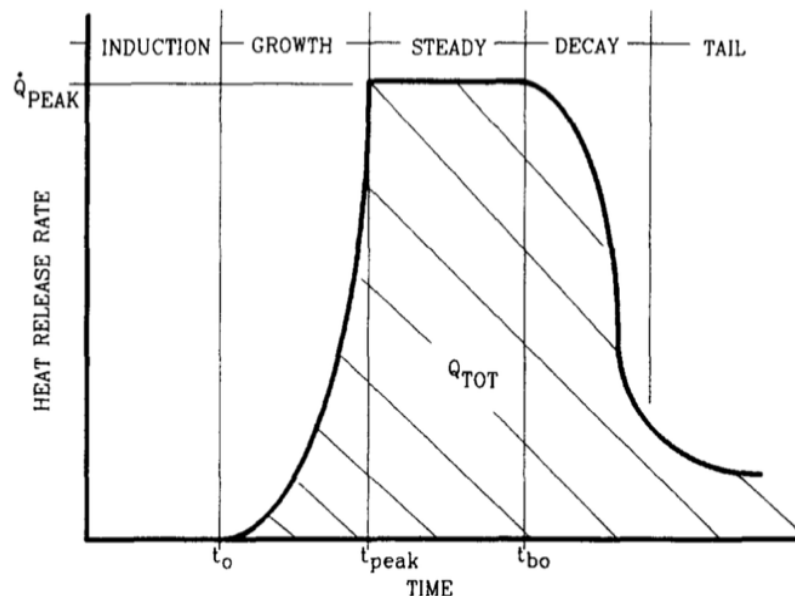


Figure 17 Area under the curve - Peak Heat Release Rate (Mowrer & Williamson, 1990)

During an ESS fire, the separator, packaging, and electrolyte of LIBs are the primary components involved during a thermal runaway reaction; as these components fail, large quantities of flammable gases are released. The gases vented during a thermal runaway reaction are composed of CO₂, CO, H⁺, and an assortment of hydrocarbons [59]. According to a study conducted by Exponent on large lithium-ion battery systems, batteries at 100% SOC can vent a volume of 2.5 L / 0.7 Gal of flammable gas when undergoing thermal runaway – which corresponds to approximately 0.33 liters per watt-hour of energy [59]. The total quantity of flammable gas/fuel released if all batteries in ESS go into thermal runaway is shown in Table 8.

Table 8 Quantity of Gas released for systems of various Energy Capacities

System Size	Flammable Gas released per Watt-hr of energy	Gas released if ALL batteries go into thermal runaway
500 kWh	0.33 L/Wh	165,000 L
1 MWh	0.33 L/Wh	330,000 L
2 MWh	0.33 L/Wh	660,000 L
3 MWh	0.33 L/Wh	990,000 L
4 MWh	0.33 L/Wh	1,320,000 L
5 MWh	0.33 L/Wh	1,650,000 L

With the large quantity of batteries and corresponding energy stored within these systems, a large amount of fuel will be generated within the ESSs. As shown in Table 8 above, between 165,000 and 1,650,000 L of flammable gases can be released through failing lithium-ion batteries within an ESS container for 500 kWh – 5 MWh systems – given that all batteries contained within the ESS become involved in the fire.

As discussed in section 2.3.1 of this report, the driver of lithium-ion degradation and thermal runaway reactions is heat. It is assumed that flammable volatiles will still be released from failing cells even after the peak heat release rate has been reached. However, the rate of fuel consumption is limited to the forced ventilation rate within the container. As the temperature continues to rise in the compartment, excess unburnt fuel vapors will continue to be released, increasing the gas temperature and gaseous mass within the container.

7.4.3.3 Fully Developed Fire

The two main factors that influence fire growth are the heat (energy) released and the burning rate of the fuel (batteries) – which are both driven by the heat transfer throughout the container. As batteries ignite and fire spreads throughout modules and racks, hot flammable gases will be generated and the boundary surfaces of the container will be heated, all radiating back to the fuel surface (batteries) which leads to further thermal reactions. As the radiant and convective heat transfers throughout the container, the ambient temperature within the compartment will rise placing the batteries in an environment that exceeds their stable range. This leads to the initiation of numerous simultaneous reactions within the batteries leading to an uncontrollable energy release within the batteries inside the ESS.

At this point, the fire has reached its peak heat release rate; the corresponding elevated temperatures within the container reach a point at which all exposed batteries and other combustibles can ignite, virtually simultaneously, and the air flow to the compartment is sufficient to sustain intense burning. During this stage, the heat release rate of the fire becomes limited by the ventilation rate within the compartment. Since the ventilation (volumetric) flow rate is a constant value, the fire is expected to burn under steady-state conditions at its peak heat release rate until nearly all the fuel is consumed.

The release of these flammable gases will increase the gaseous mass within the container. This drastic increase in mass is accounted for by a positive increase in pressure within the container. To prevent an explosion due to over pressurization, it is assumed that the built up pressure in the ESS will force the flames and gases out of the vents at a velocity driven by the temperature of the internal gas layer and the pressure difference within the container. Further analysis of vent flows and fire growth outside of the ESS container is provided in section 5.3.1. From an assortment of installations, the most common vent locations are on the side of the containers. The size, orientation and projection distance of the external fire is dependent on the heat release rate and pressure within the container.

7.4.3.3.1 Fire Behavior Outside the ESS Container

As the fire grows within the ESS, the temperature of the gas layer rises. Since gases expand with increasing temperature, the pressure difference over the vent will increase forcing the flammable gases out the vent at a temperature dependent velocity.

According to the SFPE Handbook [73], the pressure difference in the compartment can be calculated by analyzing the pressure difference between the floor and the ceiling, assuming standard atmospheric pressure. This can be determined based on the height of the compartment, gravity, and atmospheric pressure as shown in Equation 31 below.

$$\Delta p = p_f - p_c = p_{amb}gH \quad (31)$$

Where:

Δp = change in pressure
 p_f = pressure at floor
 p_c = pressure at ceiling
 p_{amb} = ambient pressure
 g = gravity
 H = height of compartment

$$flow\ velocity = u = \sqrt{\frac{2\Delta p}{\rho}} \quad (32)$$

To account for the density of the gas flowing through the vent, the density shall be calculated as a function of the gas layer temperature [73], represented by the following correlation:

$$\rho = \frac{352.8}{T_g} \quad (33)$$

Giving,

$$flow\ velocity = u = 0.70\sqrt{T\Delta p} \quad (34)$$

Once vented from the compartment, these flammable gases may ignite with the outside air through an oxidation reaction, causing burning outside the ESS container [61]. Since the vented gases from a LIB failure consists of CO, CO₂, H⁺, and THC (Total Hydrocarbons), the theory of chemical kinetics may be applied. This theory indicates that oxidation reactions cannot occur

outside a compartment efficiently until the gas temperatures are near that of flashover ~ 775 K (500 C) [61].

Once the fire exits through the vents of the containerized ESS, the adjacent containers will be exposed to a radiative heat flux from the fire. The heat flux impinging on the adjacent containers will be a function of the emissivity of the flame, heat released from the fire and its corresponding flame temperature, size of cylindrical flame, and the separation distance between the flame and the target surface.

7.4.3.4 Decay Phase

The fire within the ESS will reach a decay phase once the flammable gases from the failed batteries within the ESS have been consumed [35]. The batteries are expected to smolder until their temperatures are reduced below their thermal threshold of 80°C .

7.4.4 Flame Temperature

The temperature of the externally vented flames is a function of the radiant losses from the compartment. Studies of gases flowing out of compartments indicate that the temperature of the externally vented flames can be represented as being equivalent to the temperature of the hot gas layer within the compartment [63].

7.5 Total Radiant Flux from ESS Fire Source

The incident radiative heat flux emitted from the ESS fire source is a summation of the heat flux from the flame and the heat radiated from the steel panel of the fire involved ESS – giving the following equation.

$$q''_{total} = \sum q''_{rad,panel} + q''_{rad,fire} \quad (35)$$

The radiant heat flux emitted by the heated panel of the ESS fire source is quantified by the correlation shown in Equation 36 below. The radiation emitted from the heated steel panel is a function of the temperature of the steel panel, heated by the fire and its resulting internal gas temperature as discussed in sections 7.4.1 and 7.4.2.

$$q''_{rad,panel} = \varepsilon\sigma F_{1p,2p}(T_w^4 - T_{\infty}^4) \quad (36)$$

Where:

ε = emissivity of surface

σ = Stefan-Boltzman Constant

$F_{1p,2p}$ = View factor of rectangular parallel plates

T_w = Temperature of the wall (steel panel) of the fire source ESS

T_{∞} = Ambient Temperature

The radiant heat flux emitted from the exposed flame leaving the container is quantified as a function of the emissivity of the flame, Stefan-Boltzmann constant, view factor between cylindrical flames and rectangular panels, and the externally vented flame temperature. This correlation is depicted in Equation 37 below.

$$q''_{rad,fire} = \varepsilon\sigma F_{1(fl),2(p)}(T_{fl}^4 - T_{\infty}^4) \quad (37)$$

Where:

ε = emissivity of surface

σ = Stefan-Boltzmann Constant

$F_{1(fl),2(p)}$ = View factor from cylindrical flame exiting ESS to exposed ESS steel panel

T_{fl} = Flame temperature of flames exiting the fire source ESS

T_{∞} = Ambient temperature

7.6 Heat Transfer Between ESS Fire Source and Target ESS

The calculations put forth in sections 7.1 through 7.4 represent the fire behavior of a lithium-ion energy storage system within the compartment and how it escapes as externally vented flames. This section will analyze the impact of the radiant energy emitted onto and absorbed by the exposed ESS, with respect to the rise of the internal air temperature (T_{air}) of the exposed ESS.

Figure 18 below represents the radiation heat transfer exchange between the ESS fire source and the exposed ESS container. The development of the hot gas layer (T_g), as a function of the HRR and forced ventilation rate, heats the wall (T_w) of the ESS fire source and provides sufficient heat and pressure to produce externally vented flames (T_f). The flame and the heated panel will emit radiation onto the exposed ESS, \dot{q}''_{flame} and \dot{q}''_{panel} respectively, as a function of their temperatures, emissivity, and view factor. The internal air temperature (T_{air}) of the exposed ESS will be heated by the radiant exposure, as a function of the surface temperatures of the steel container (T_s) exposed to the radiant energy as demonstrated in the schematic below.

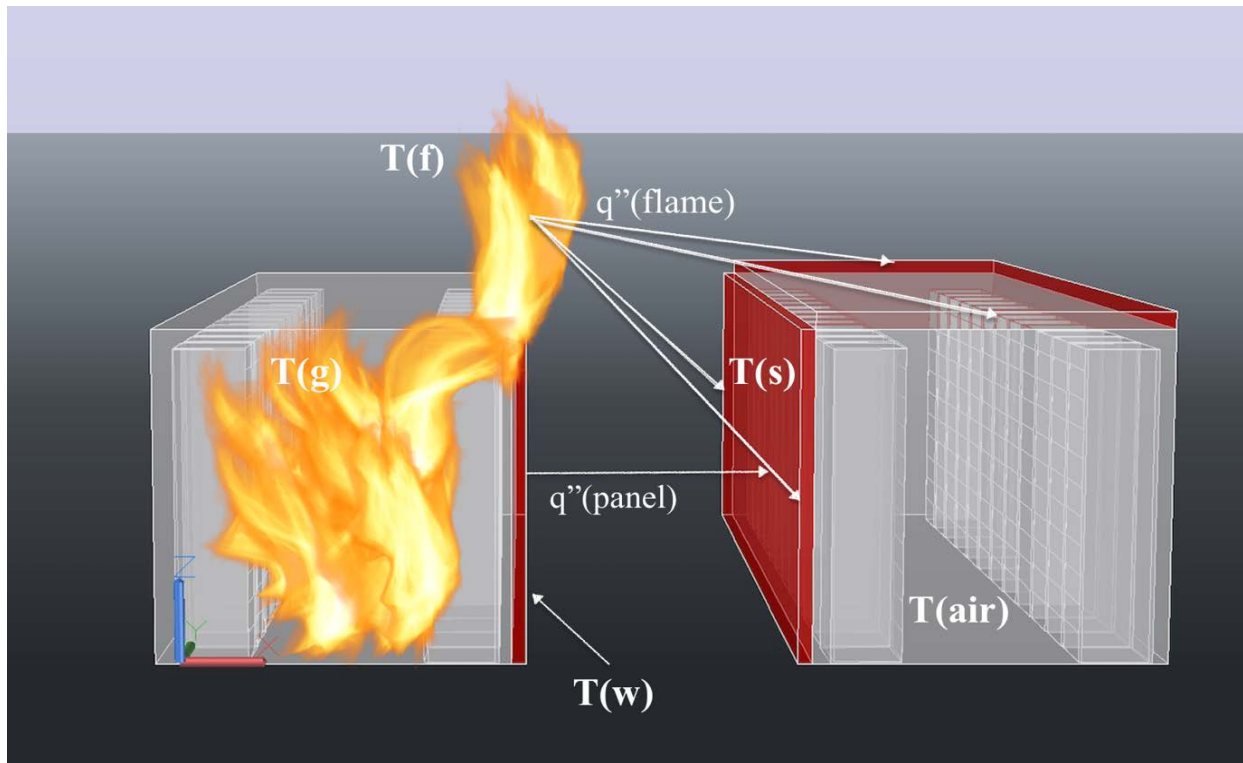


Figure 18 Radiation Heat Transfer Exchange

7.6.1 Thermal Threshold of Exposed ESS

In order to quantify the thermal threshold of the exposed target ESS, the internal air temperature of the exposed ESS must be calculated. This analysis assumes that the air temperature of the exposed ESS container rises uniformly throughout the container when exposed to a radiant energy source. The temperature at which lithium-ion batteries within the ESS container become thermally unstable and allow for self-generating internal heating that will likely lead to a thermal runaway event needs to be established.

According to a literature review of lithium-ion battery failures, 80°C (353 K) is the temperature at which lithium-ion batteries can begin to undergo exothermic reactions and thermally self-decompose [23, 47], as discussed in section 2.3.1. A failure in a single battery cell can lead to a series of thermal runaway events that can propagate into a catastrophic failure within the entire ESS. In order to analyze the point at which an ESS becomes unsafe from a radiant exposure, a thermal threshold of 80°C was set as the critical point of failure for a lithium-ion ESS. While it has been reported that thermal runaway within battery cells occurs at 120°C, a thermal threshold of 80°C was used because a nonreversible thermal reaction occurs within lithium-ion batteries at this temperature. The 80°C threshold also provides for a more conservative approach in the analysis.

7.6.2 Inside Air Temperature of Target ESS

In order to determine when the target ESS reaches its thermal threshold due to the radiant exposure from an adjacent ESS fire, the internal air temperature must be calculated. To analyze the interior temperature of the container that is exposed to a radiant heat source, conduction, convection, and radiation heat transfer must be considered. As the radiant fire source heats up the panels of the exposed ESS, heat will conductively be transferred to the interior side of the steel panel. At this point, the inside air temperature will rise through convection heat transfer between the heated steel surfaces and the air within the compartment.

This scenario treats the ESS container walls as a thermally lumped solid. This allows for the assumption that the temperature of the solid is spatially uniform at any instant during the unsteady heating process, or that the temperature gradients within the body are negligible [40]. This generates an energy balance between the heated solid and its surrounding environment, represented as the storage of heat in the steel panel and the convective enthalpy flow from the heated panel to the inside air [57]. As shown in Equations 38 and 39 below, the enthalpy flow is the inflow of energy into the volume from the heated panels and the outflow of heat losses. Through this energy balance, the rise in internal air temperature of the exposed ESS can be calculated through Equation 40 below.

$$\textit{Storage} = \textit{enthalpy flow}$$

$$\textit{Storage} = \rho c_p V \frac{dT_{air}}{dt} \quad (38)$$

$$\textit{Enthalpy flow} = \dot{q}_{in} - \dot{q}_{out} = [hA(T_{s,hot} - T_{air}) - (hA)_{cold}(T_{air} - T_{\infty})] \quad (39)$$

Giving the following correlation for the internal air temperature:

$$\frac{dT_{air}}{dt} = \frac{1}{\rho c_p V} * [hA(T_{s,hot} - T_{air}) - (hA)_{cold}(T_{air} - T_{\infty})] \quad (40)$$

Where,

$$dT_{\text{air}}/dt = \text{Change in inside air temperature of exposed ESS over time}$$

$$\rho = \text{density of steel panel } \left(\frac{\text{kg}}{\text{m}^3}\right)$$

$$c_p = \text{specific heat of steel panel (kJ/kg-K)}$$

$$V = \text{volume of steel panel – surface area x thickness of steel panel (m}^3\text{)}$$

$$h = \text{heat transfer coefficient (hot and ambient side of steel) (kW/m}^2\text{K)}$$

$$A = \text{surface area of steel panels (m}^2\text{)}$$

$$T_{s,\text{hot}} = \text{Temperature of heated steel panels of exposed ESS container (K)}$$

$$T_{\text{air}} = \text{Inside air temperature of exposed ESS container (K)}$$

$$T_{\infty} = \text{Ambient Temperature (K)}$$

Equation 40 above demonstrates the temperature rise of the air inside the exposed ESS. This correlation assumes uniform temperature rise within the compartment. However, to determine the rise in the internal air temperature of the exposed ESS (T_{air}) over time, the surface temperature of the heated panels ($T_{s,\text{hot}}$) must be computed as a function of the absorbed radiant heat flux.

7.6.3 Surface Temperature of Target ESS

To determine the impact of the incident radiation exposure on the target ESS, the quantity of radiation absorbed into the steel panels must be determined. Although the steel ISO-Containers are noncombustible, they have a high thermal conductivity – the property of a material to conduct heat. As the steel heats up, its thermal conductivity is reduced, lessening its strength, which allows the heat to be transferred through the panel more quickly. Therefore, as the fire grows within the ESS fire source, higher radiant heat fluxes will be emitted and absorbed into the target ESS over time, which will raise the temperature of the steel panel.

According to the SFPE Handbook of Fire Protection Engineering, Equation 41 below demonstrates the relationship between the total impinging radiative flux from the fire source as calculated in section 7.5 through equations 35, 36 and 37 on the temperature of the exposed steel panel over time.

$$T_{s,\text{hot}} = T_{\infty} + \frac{\alpha \dot{q}'' \sqrt{t}}{A_s k \rho c_p} \quad (41)$$

where:

$$T_{s,\text{hot}} = \text{Temperature of the steel exposed to radiative fire source (K)}$$

$$T_{\infty} = \text{Ambient temperature (K)}$$

$$\alpha = \text{Absorptivity}$$

$$\dot{q}'' = \text{Total radiant heat flux (kW/m}^2\text{)}$$

$$t = \text{Time (s)}$$

$$A_s = \text{Surface area of steel exposed to fire source (m}^2\text{)}$$

$$k = \text{Thermal conductivity of the steel panel (kW/m-K)}$$

$$\rho = \text{Density of steel (kg/m}^3\text{)}$$

$$c_p = \text{Specific heat of steel (kJ/kg-K)}$$

By determining the surface temperature of the exposed ESS, the inside air temperature of the exposed ESSs over time can be calculated at various separation distances. This inside air temperature (T_{air}) can then be analyzed with respect to its thermal threshold of 80°C to determine the safety of the ESS exposed to a radiation over time.

8. Results

This section presents the results of the radiation heat transfer calculations described in section 7. ESS's with energy capacities ranging from 500 kWh to 5 MWh inside ISO-shipping containers of 20 ft, 40 ft, and 53 ft nominal sizes were considered at separation distances ranging from 3 ft to 20 ft. The results indicate the rise of inside air temperature within exposed ESS containers and identify the time at which thermal thresholds as previously described are reached. Calculations approximate a fire duration of up to 3-hours to correlate with the length of firefighting operations referenced in section 3.

8.1 Results for 20 ft Exposed ESS Containers

Temperature profiles for 20 ft ESS containers exposed to radiant sources are provided in Figures 19 through 24. The figures indicate if and when the internal air temperature of the exposed 20 ft ESS container reach thermal thresholds of 80°C (353 K) and 120°C (393 K) over a three-hour period.

Figure 25 consolidates the results of the time to reach the thermal threshold of 80°C for 20 ft ESS containers when exposed to adjacent burning ESS containers of 500 kWh (0.5 MWh) to 5 MWh energy capacities.

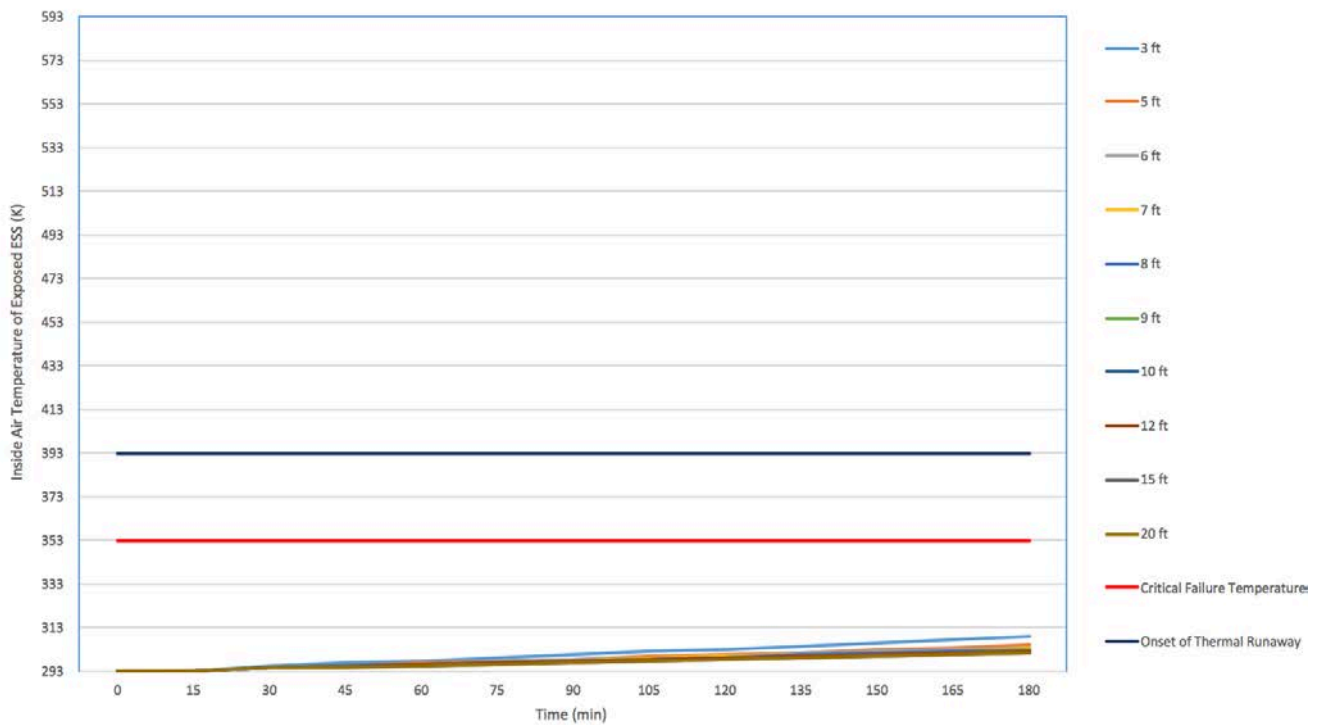


Figure 19 – Interior Temperature Profile of Exposed 20 ft ISO Container (500 kWh Exposure)

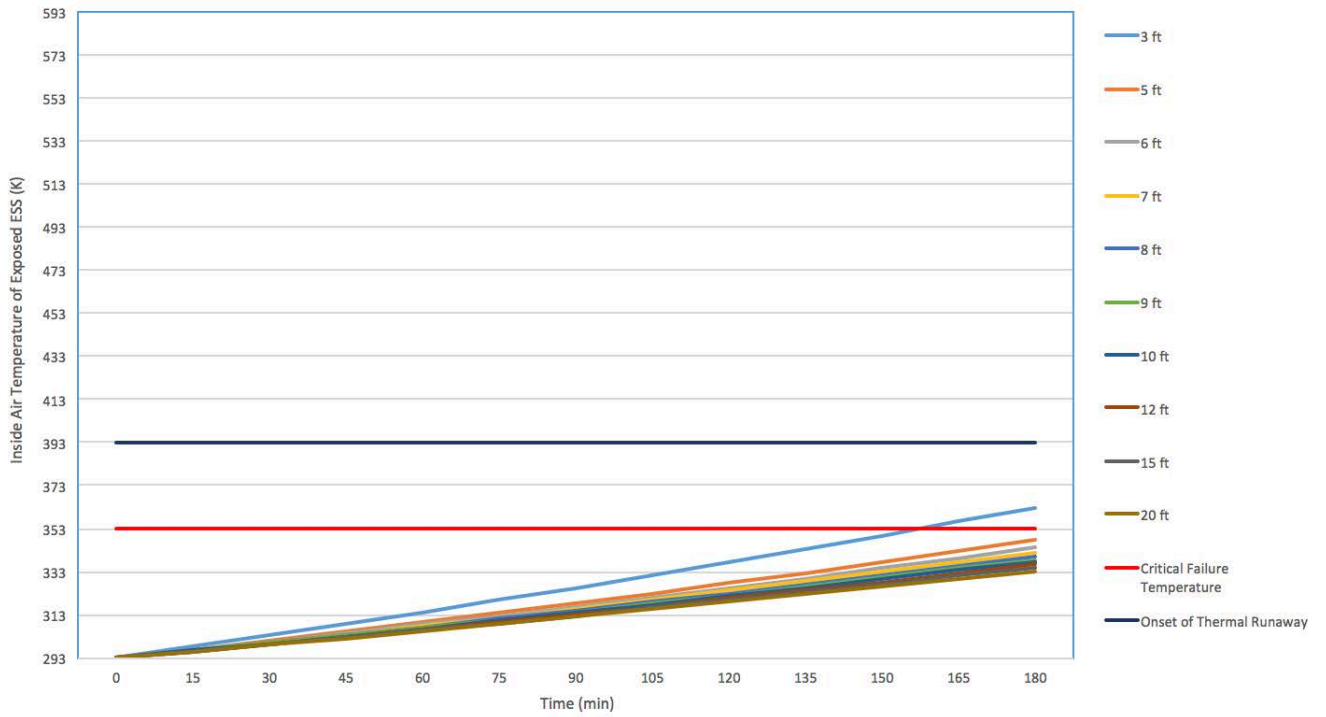


Figure 20 – Interior Temperature Profile of Exposed 20 ft ISO-Container (1 MWh)

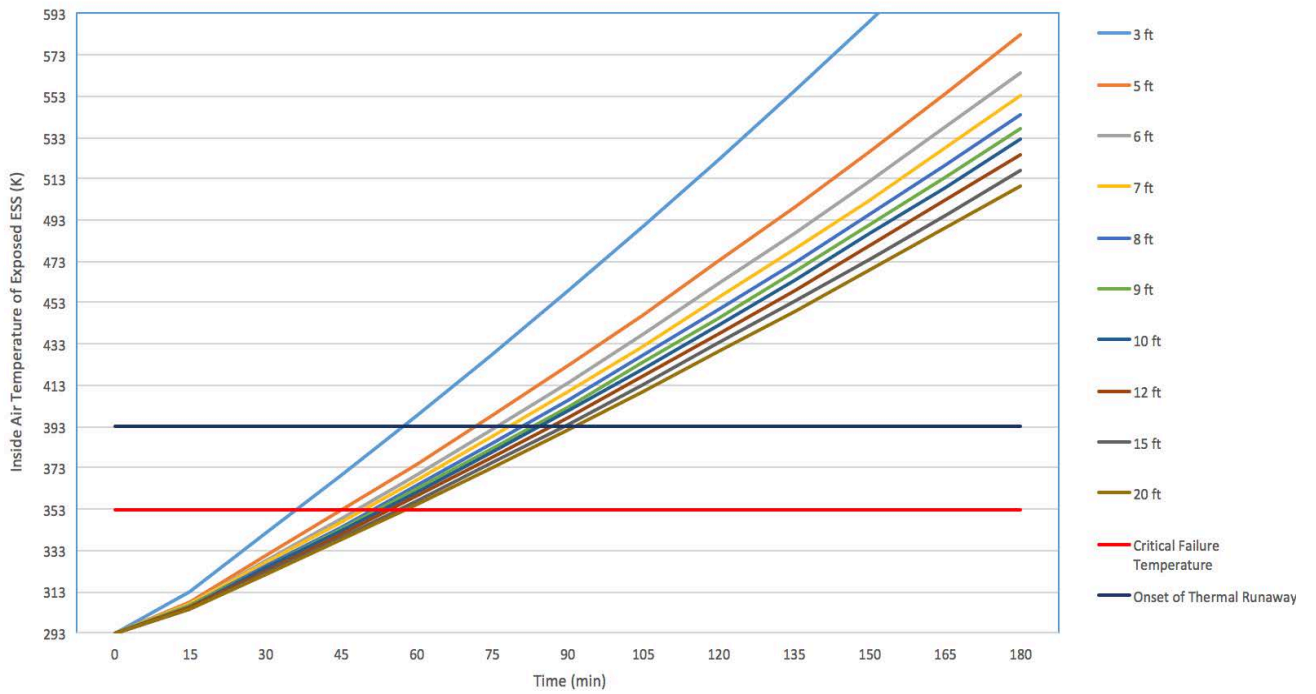


Figure 21 – Interior Temperature Profile of Exposed 20 ft ISO-Container (2 MWh)

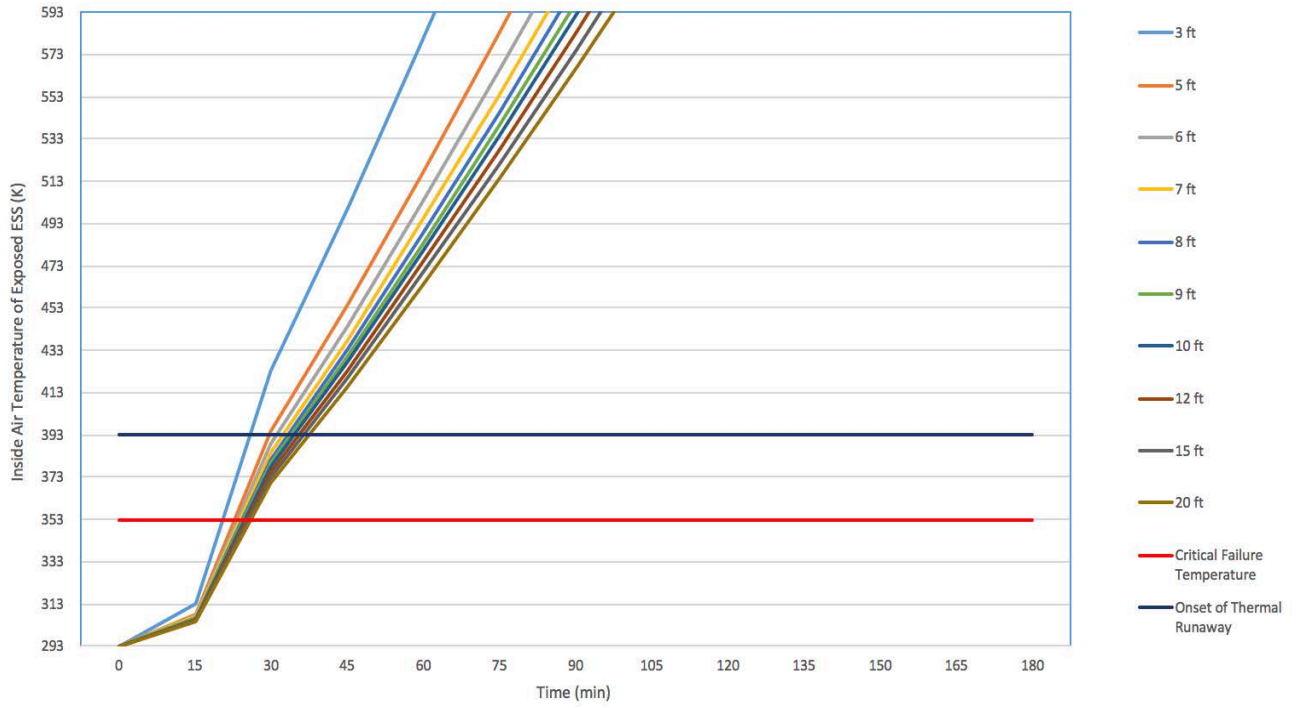


Figure 22 - Interior Temperature Profile of Exposed 20 ft ISO-Container (3 MWh)

4 MWh 20-ft ESS Inside Air Temperature

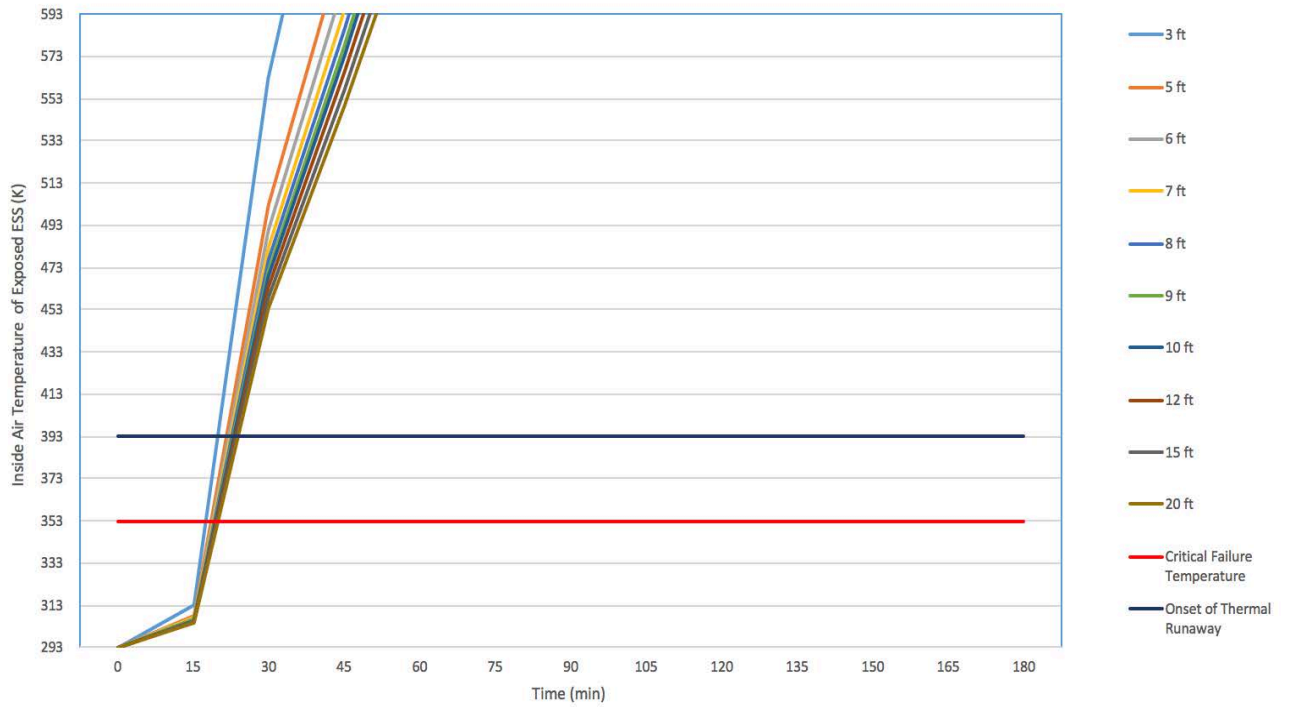


Figure 23 - Interior Temperature Profile of Exposed 20 ft ISO-Container (4 MWh)

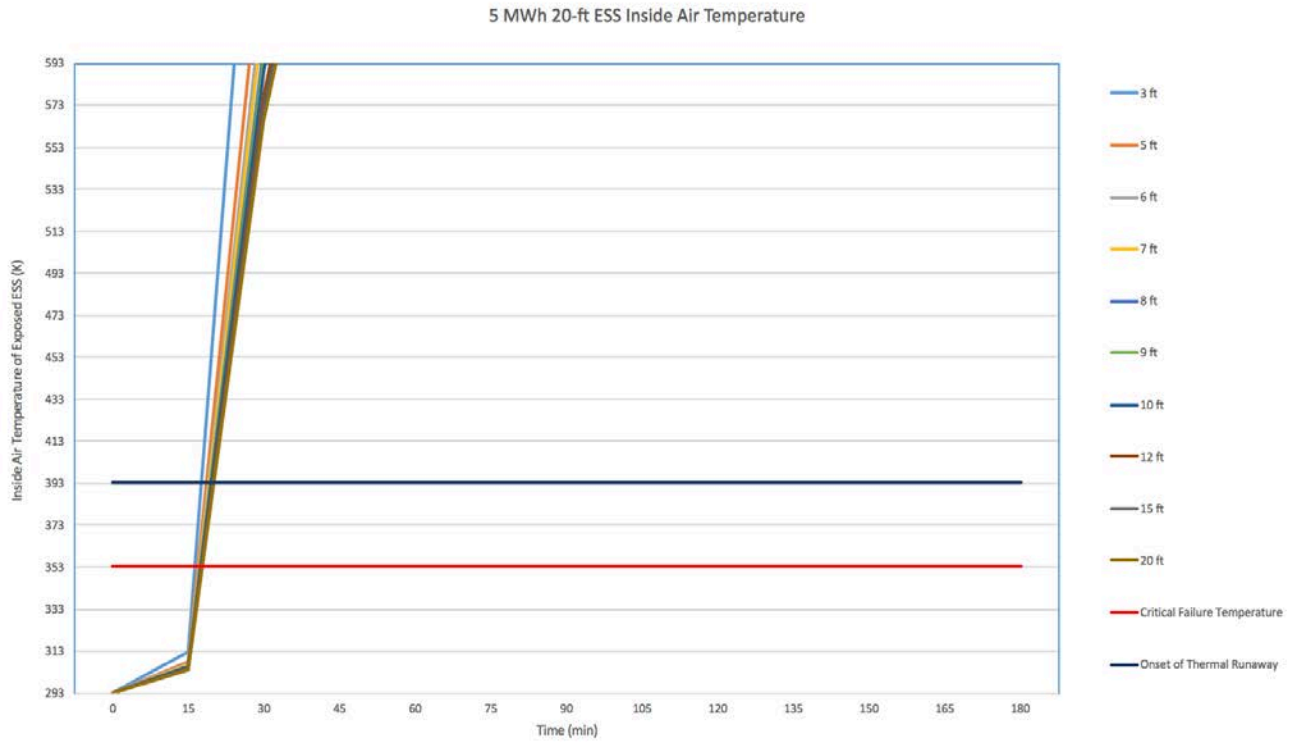


Figure 24 - Interior Temperature Profile of Exposed 20 ft ISO-Container (5 MWh)

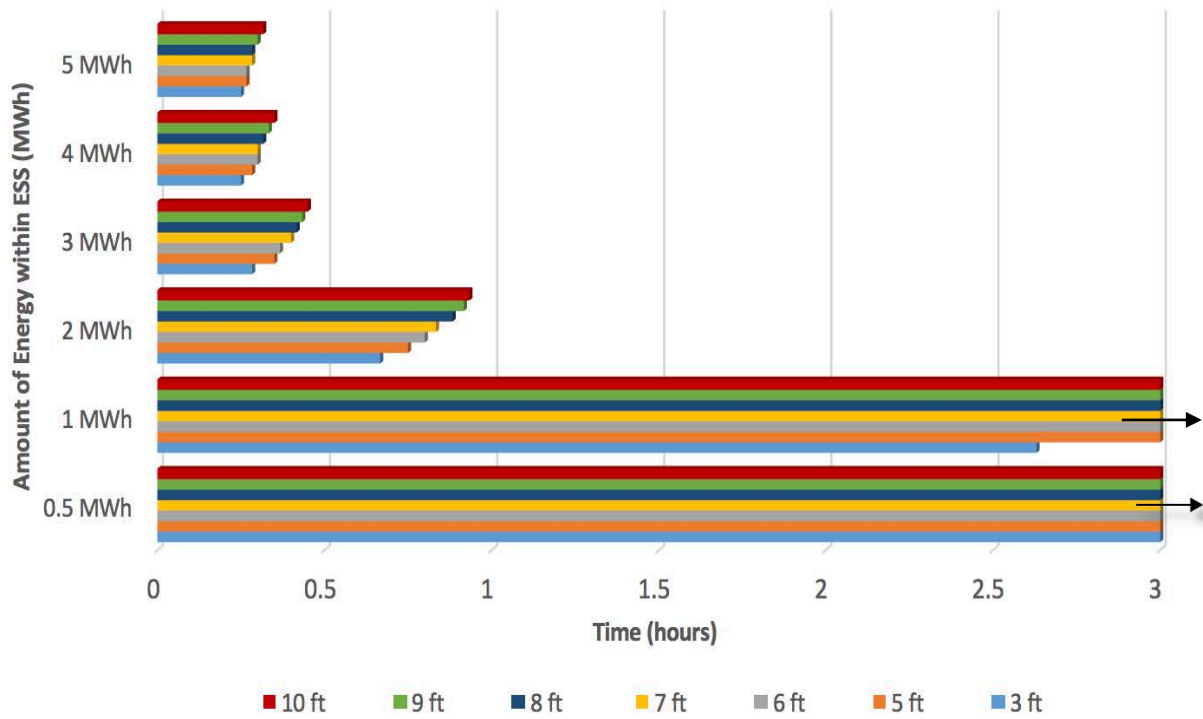


Figure 25 - Time to Reach Thermal Threshold for Exposed 20 ft ISO Containers

8.2 Results of 40 ft Exposed ESS Containers

Temperature profiles for 40 ft ESS containers exposed to radiant sources are provided in Figures 26 through 31. The figures indicate if and when the internal air temperature of the exposed 40 ft ESS container reach thermal thresholds of 80°C (353 K) and 120°C (393 K) over a three-hour period.

Figure 32 consolidates the results of the time to reach the thermal threshold of 80°C for 40 ft ESS containers when exposed to adjacent burning ESS containers of 500 kWh (0.5 MWh) to 5 MWh energy capacities.

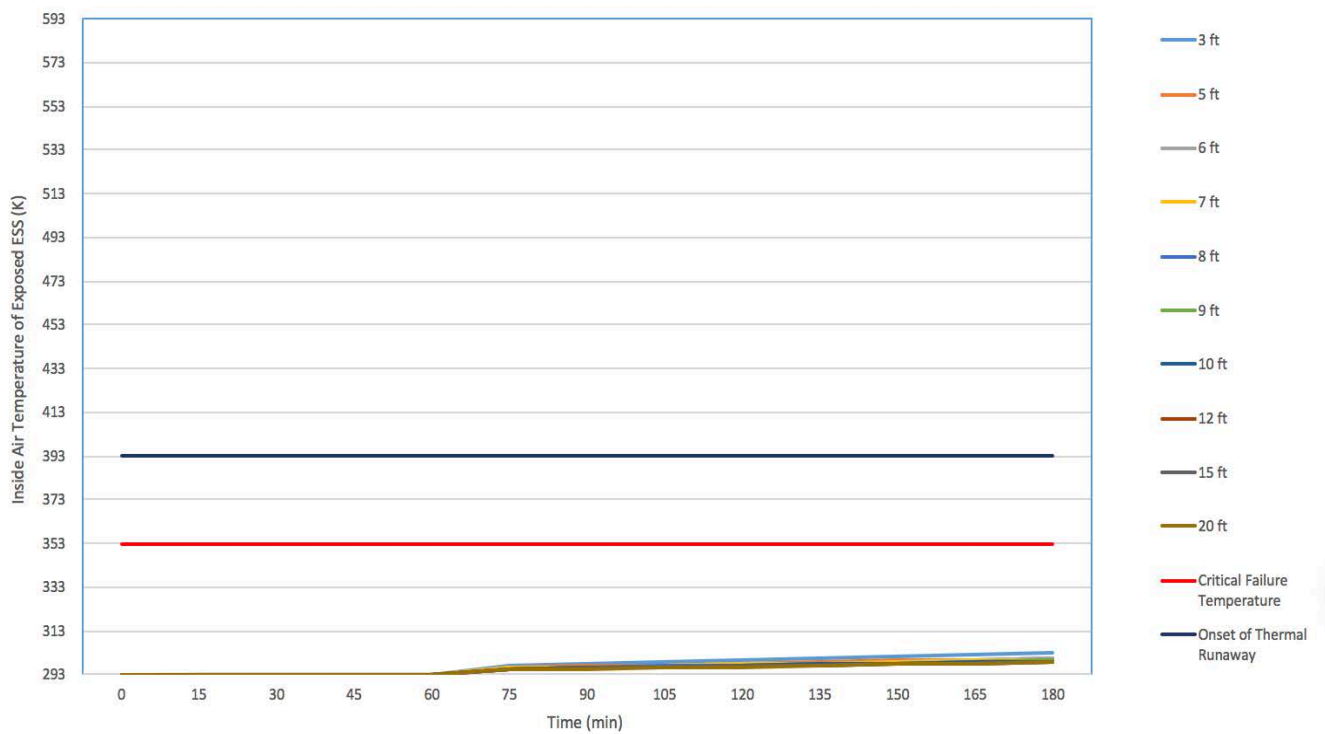


Figure 26 – Interior Temperature Profile of Exposed 40 ft ISO Container (500 kWh Exposure)

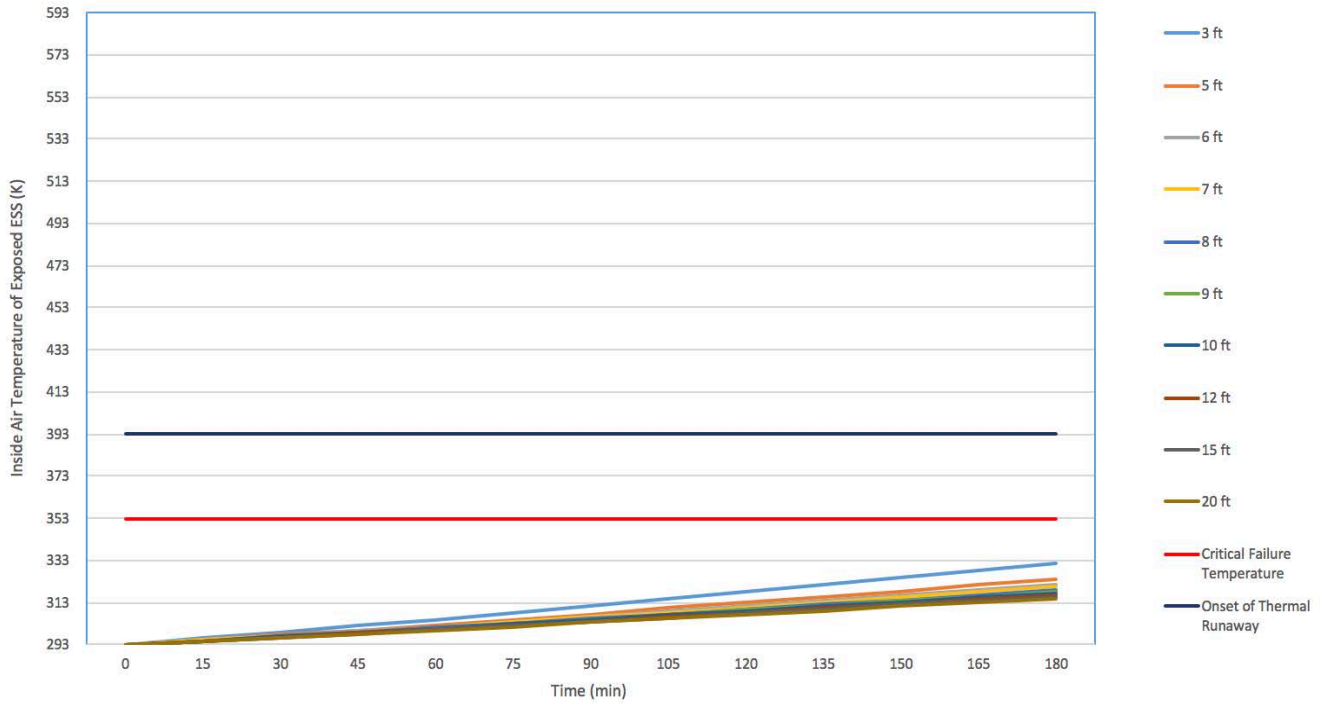


Figure 27 – Interior Temperature Profile of Exposed 40 ft ISO Container (1 MWh Exposure)

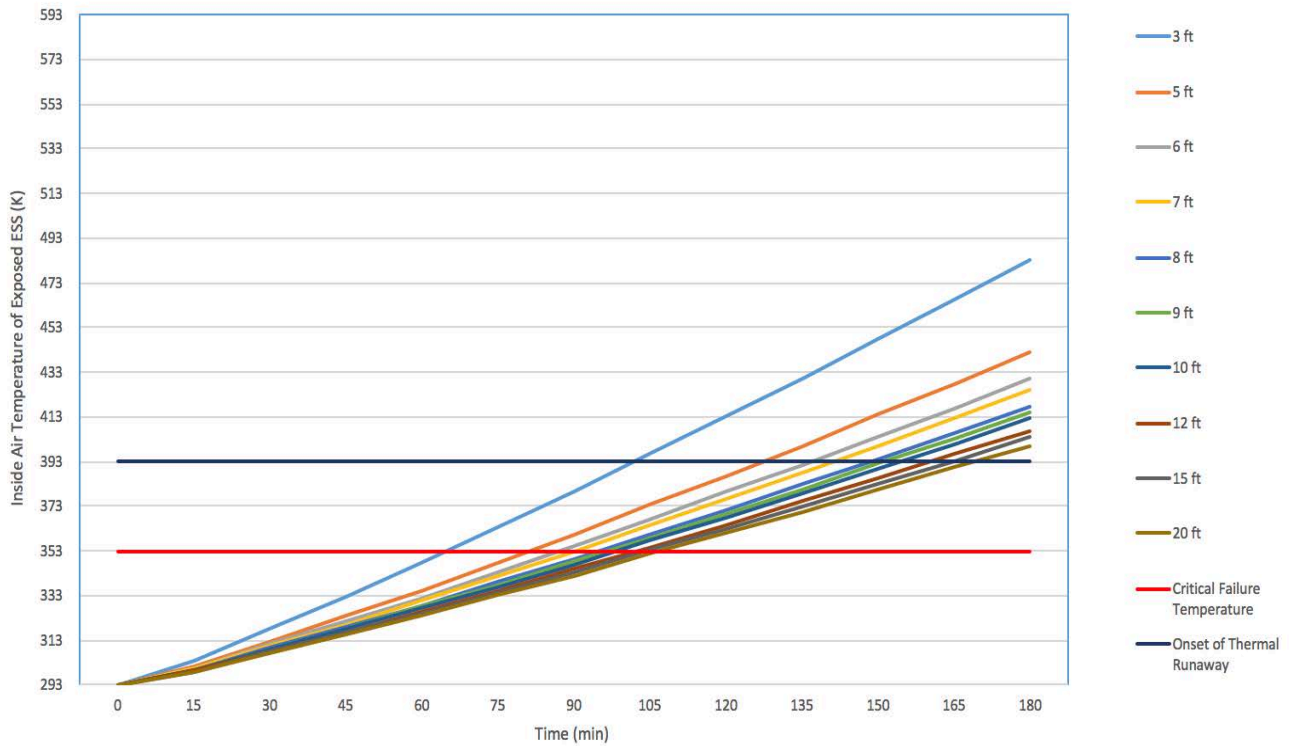


Figure 28 - Interior Temperature Profile of Exposed 40 ft ISO Container (2 MWh Exposure)

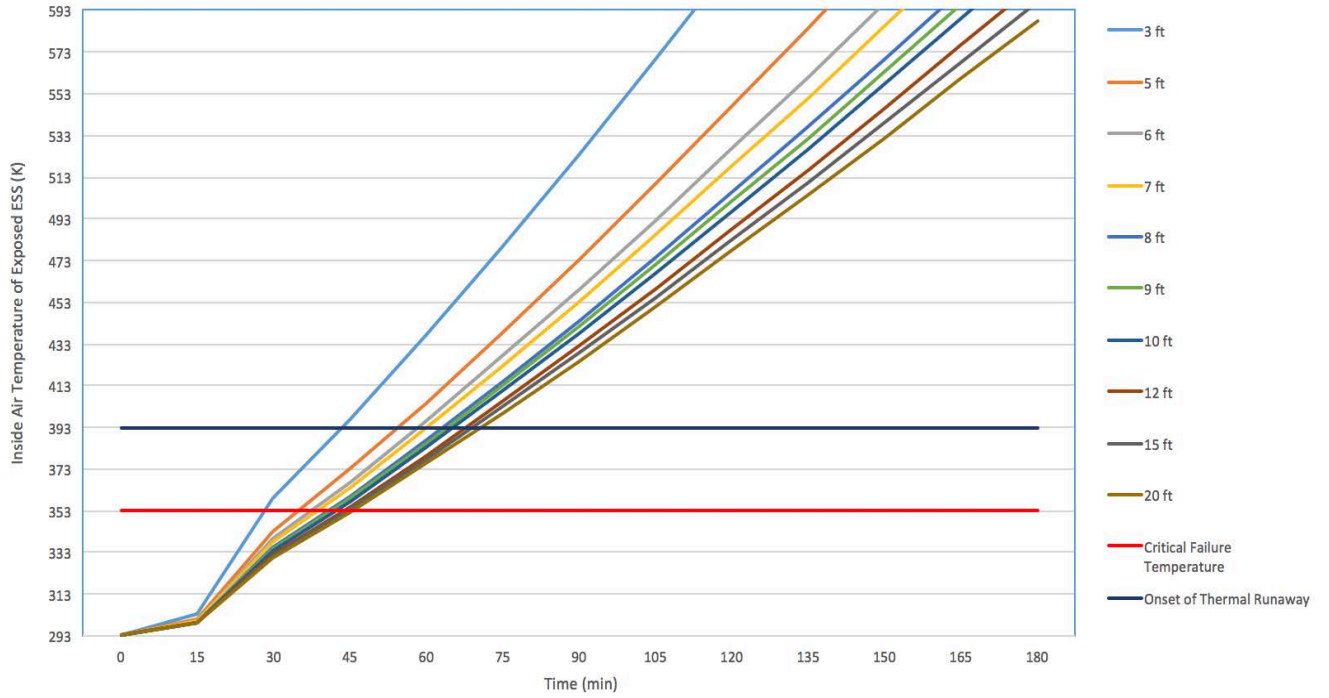


Figure 29 - Interior Temperature Profile of Exposed 40 ft ISO Container (3 MWh Exposure)

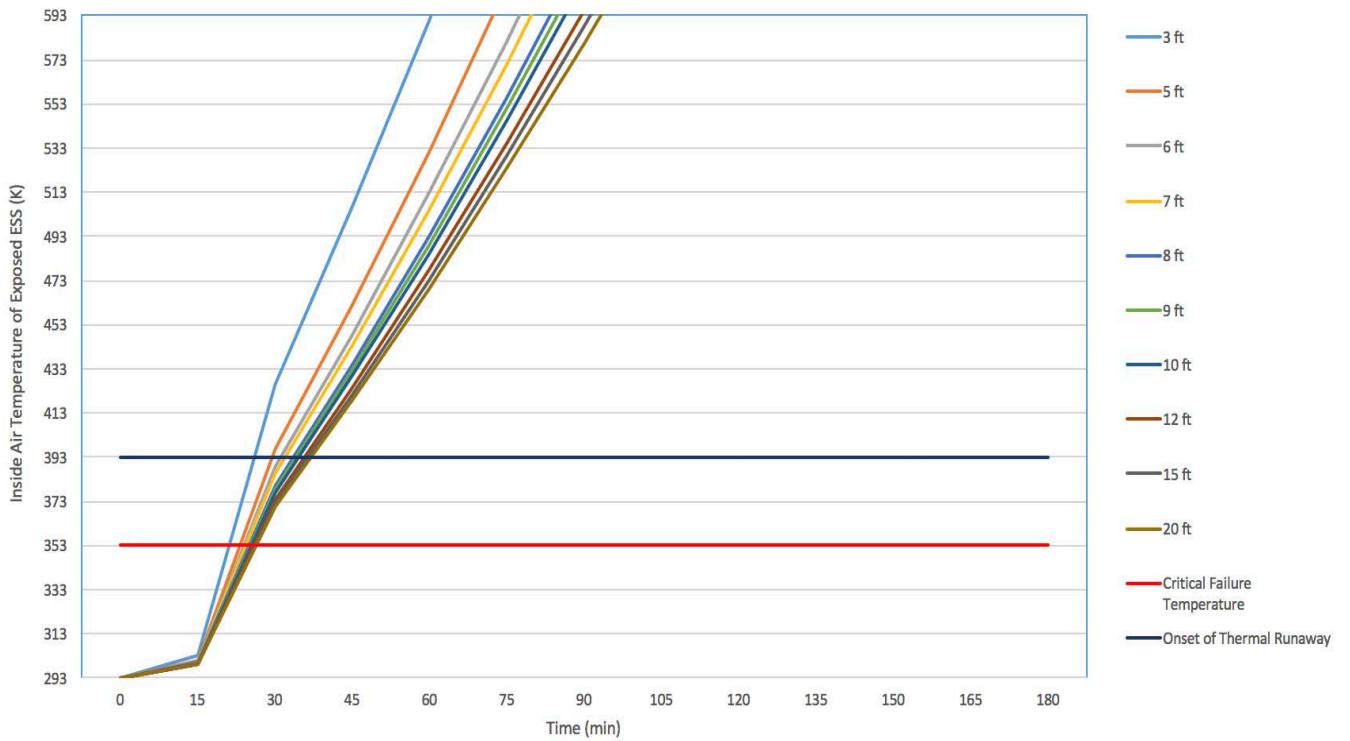


Figure 30 - Interior Temperature Profile of Exposed 40 ft ISO Container (4 MWh Exposure)

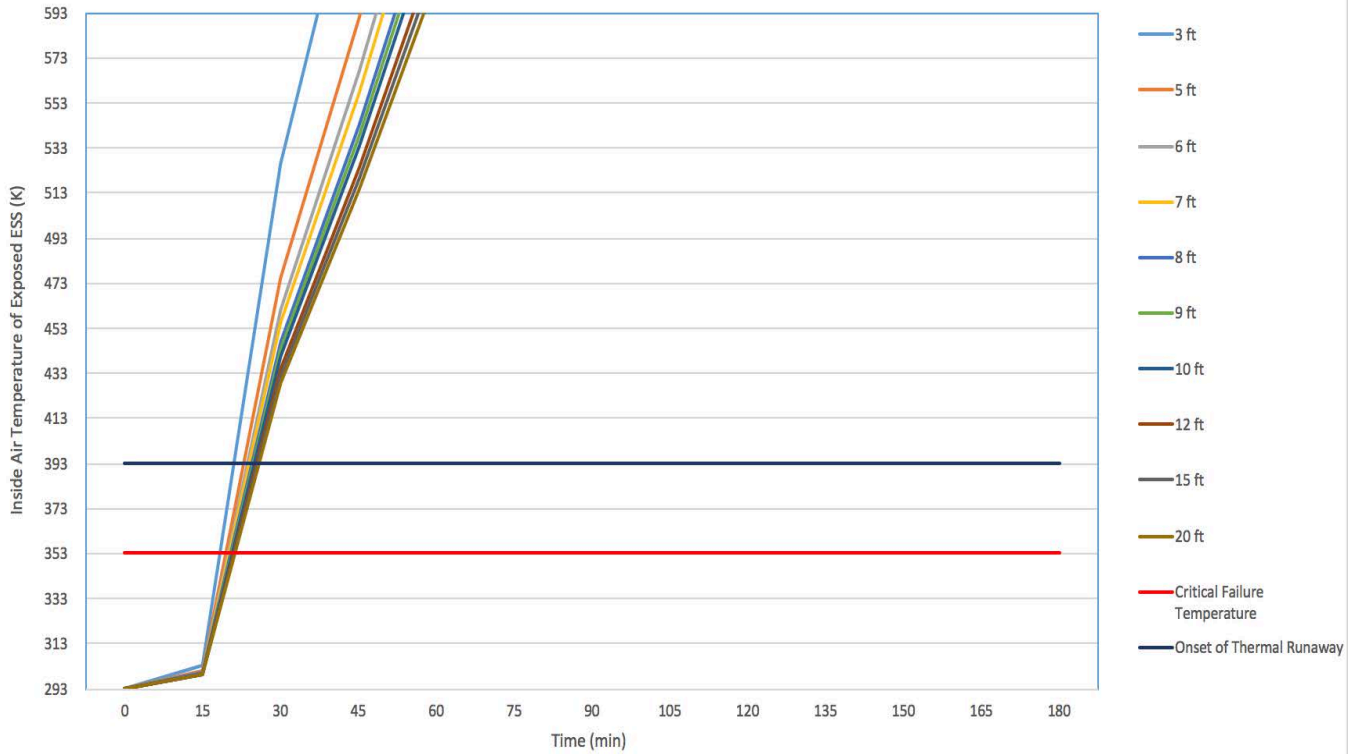


Figure 31 - Interior Temperature Profile of Exposed 40 ft ISO Container (5 MWh Exposure)

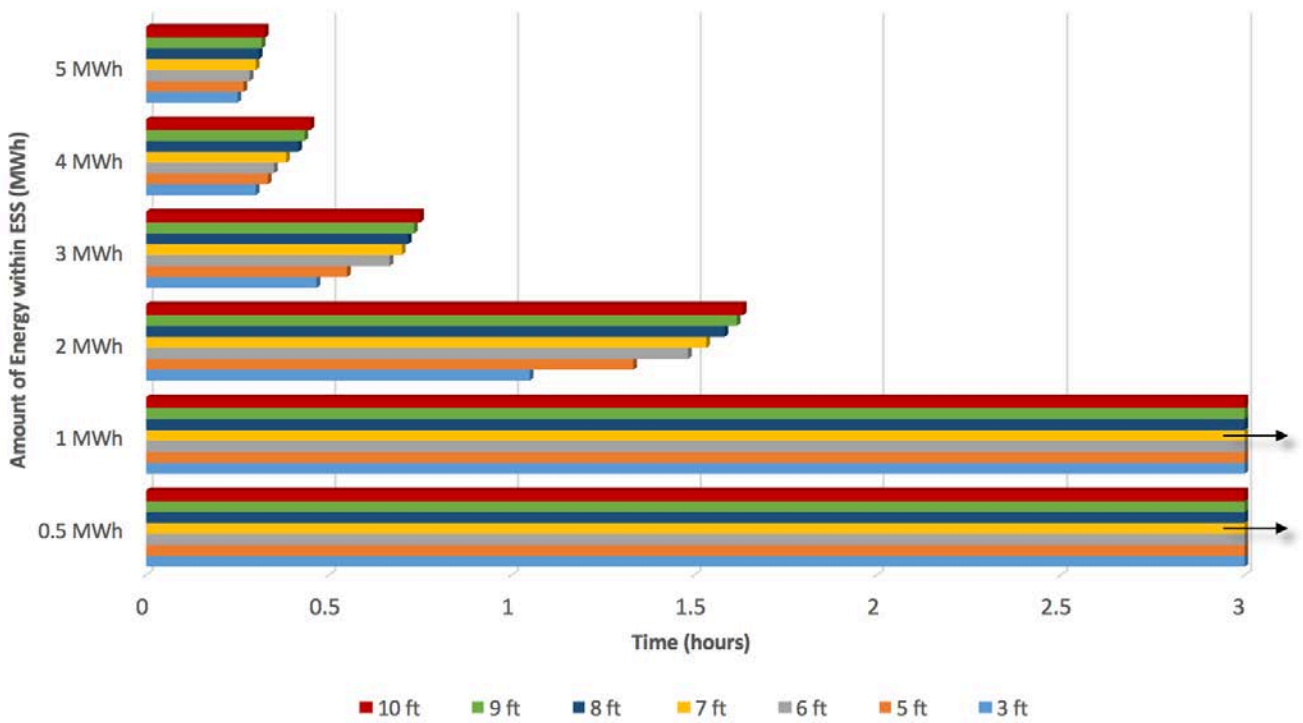


Figure 32 - Time to Reach Thermal Threshold for Exposed 40 ft ISO Containers

8.3 Results of 53 ft Exposed ESS Containers

Temperature profiles for 53 ft ESS containers exposed to radiant sources are provided in Figures 33 through 38. The figures indicate if and when the internal air temperature of the exposed 53 ft ESS container reach thermal thresholds of 80°C (353 K) and 120°C (393 K) over a three-hour period.

Figure 39 consolidates the results of the time to reach the thermal threshold of 80°C for 53 ft ESS containers when exposed to adjacent burning ESS containers of 500 kWh (0.5 MWh) to 5 MWh energy capacities.

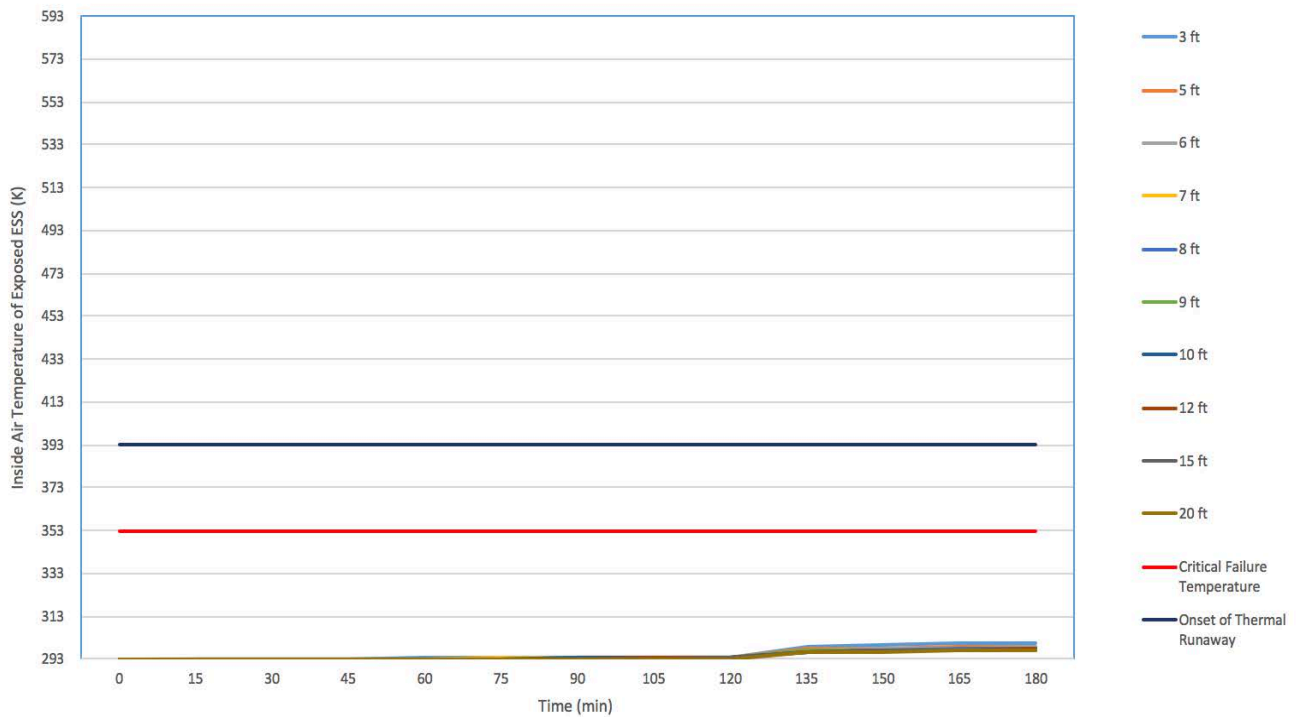


Figure 33 – Interior Temperature Profile of Exposed 53 ft ISO Container (500 kWh Exposure)

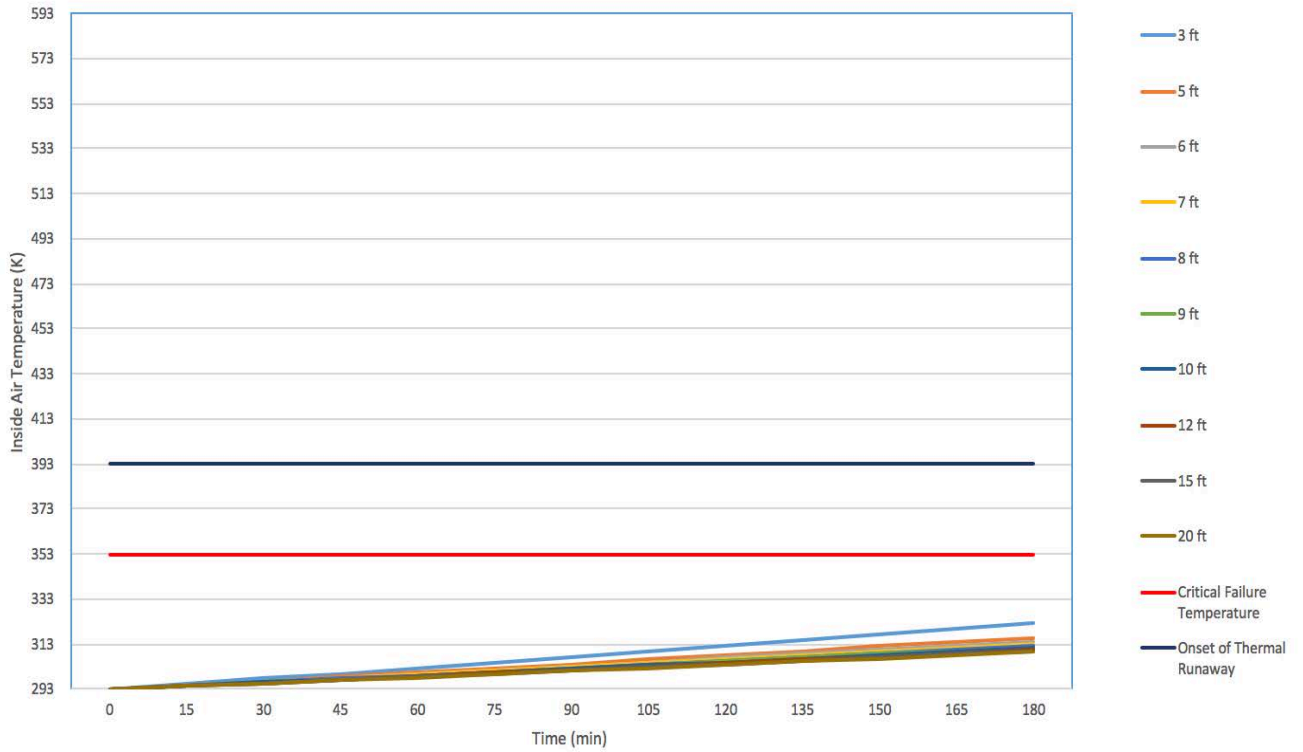


Figure 34 - Interior Temperature Profile of Exposed 53 ft ISO Container (1 MWh Exposure)

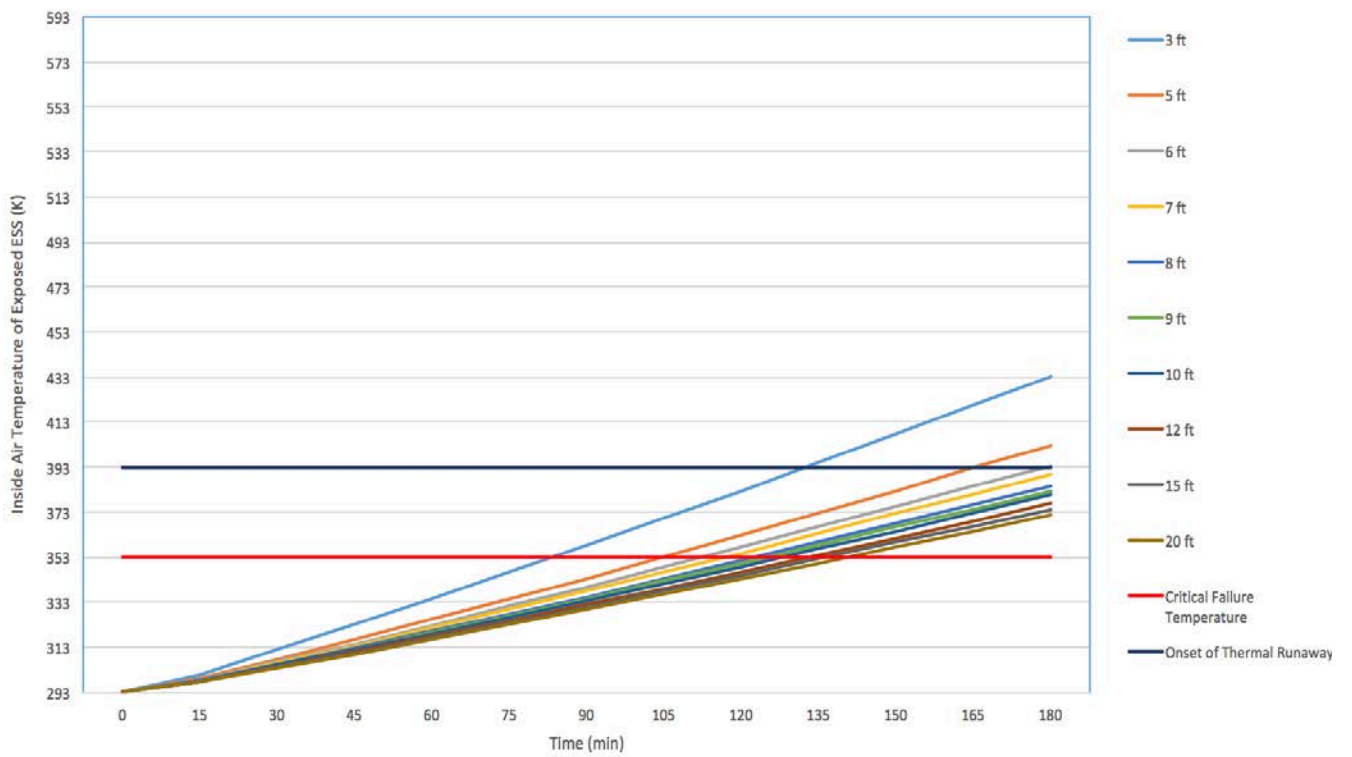


Figure 35 - Interior Temperature Profile of Exposed 53 ft ISO Container (2 MWh Exposure)

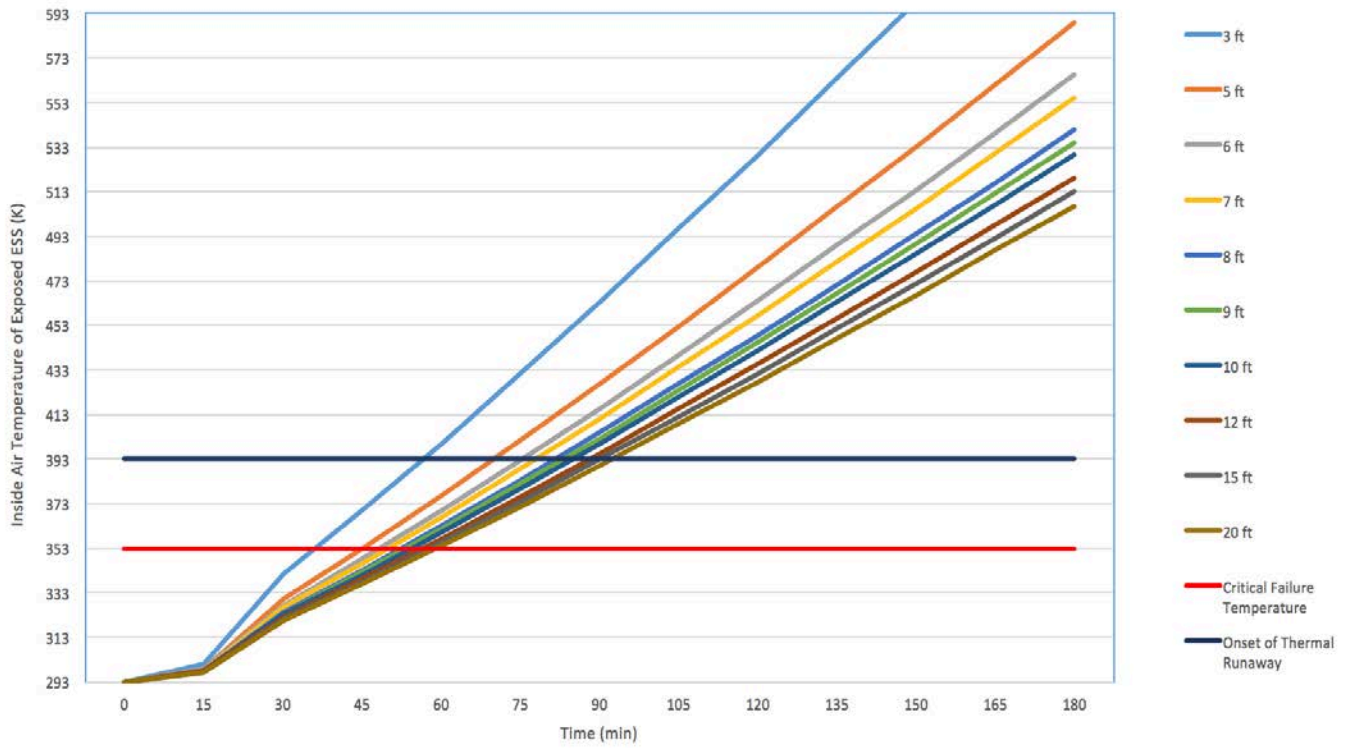


Figure 36 Interior Temperature Profile of Exposed 53 ft ISO Container (3 MWh Exposure)

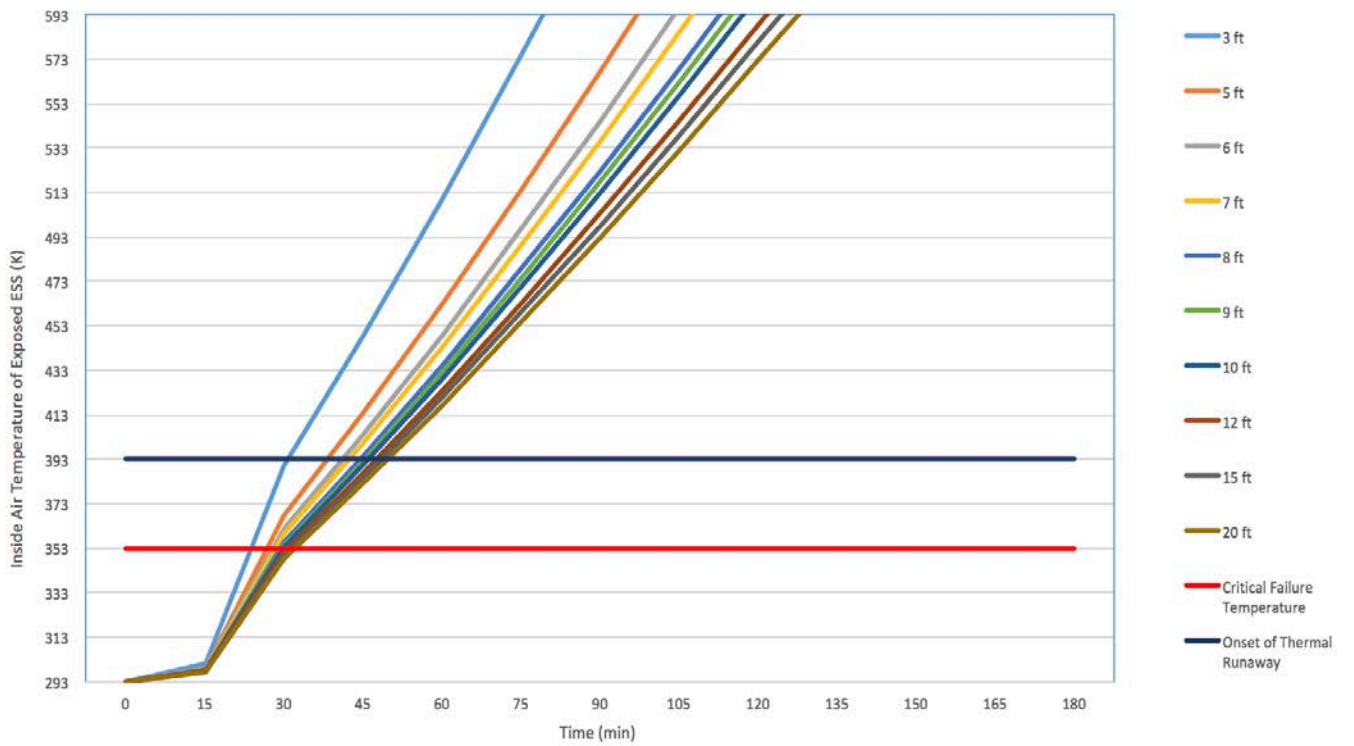


Figure 37- Interior Temperature Profile of Exposed 53 ft ISO Container (4 MWh Exposure)

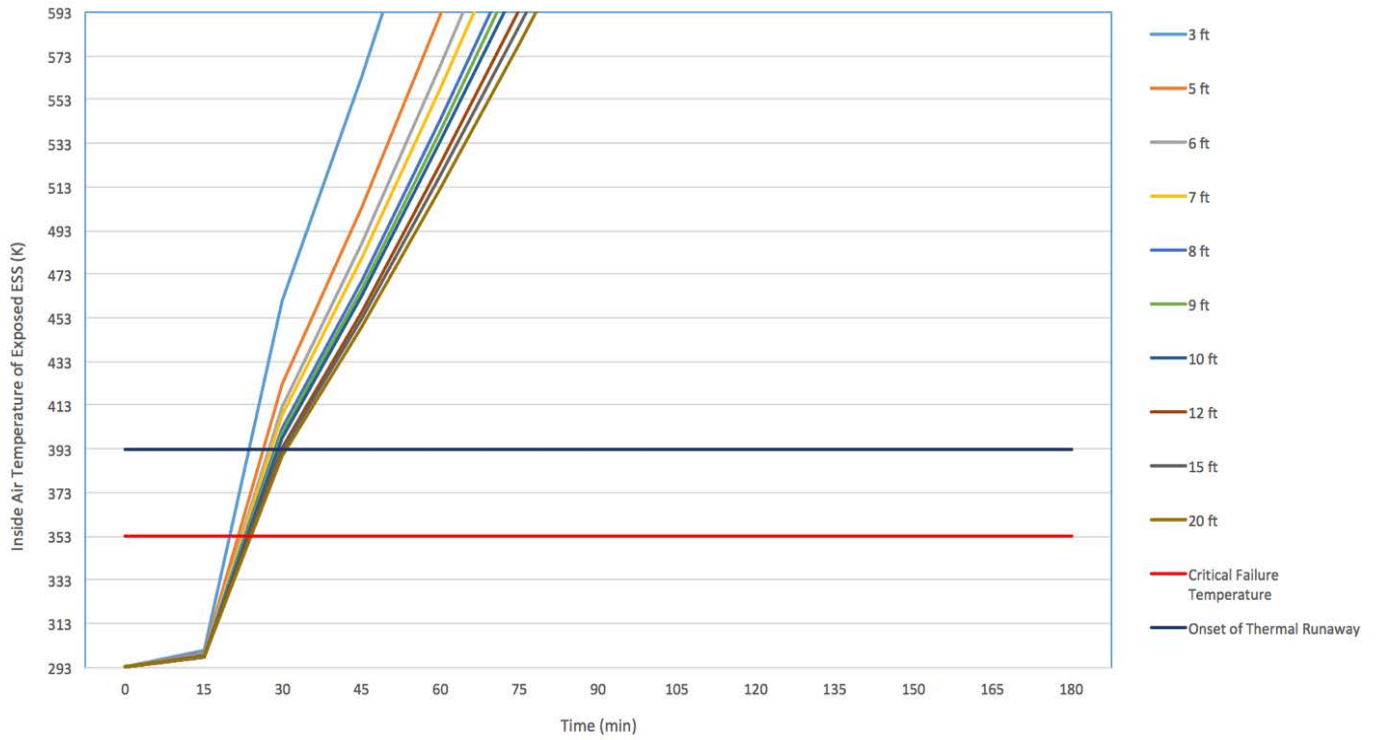


Figure 38 - Interior Temperature Profile of Exposed 53 ft ISO Container (5 MWh Exposure)

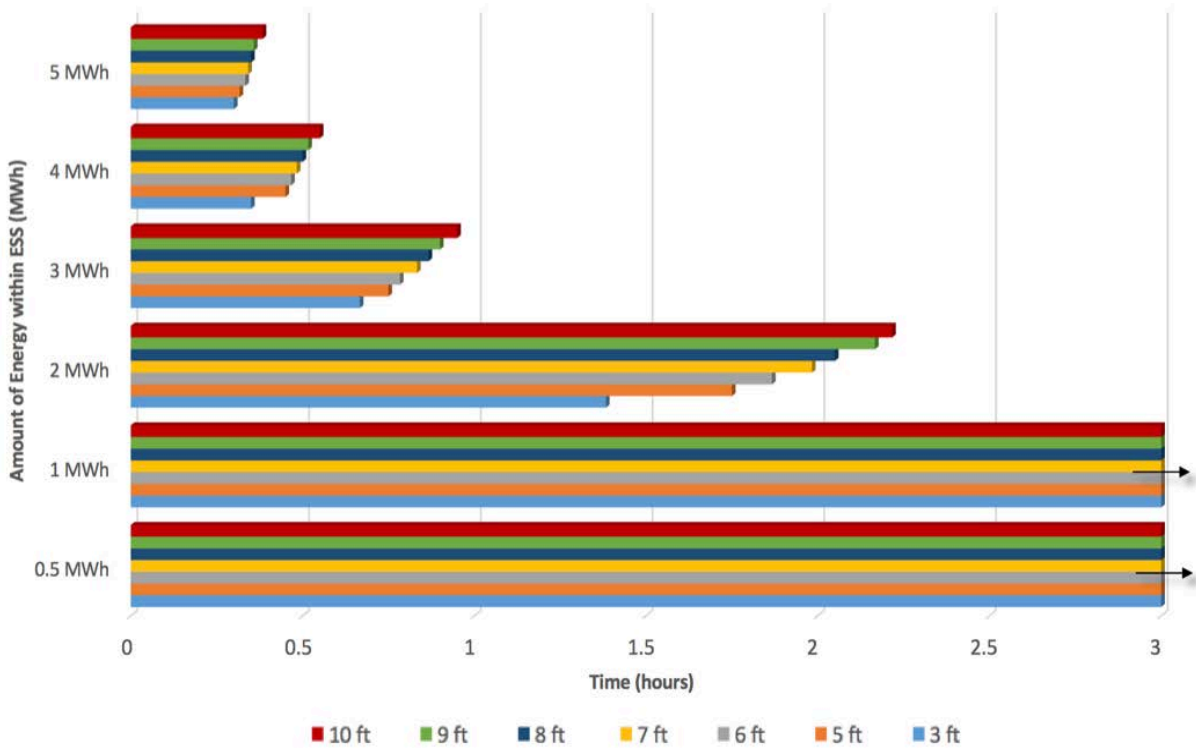


Figure 39 - Time to Reach Thermal Threshold for Exposed 53 ft ISO Containers

8.4 Discussion of Results

This section summarizes the results of the radiation heat transfer analysis. The results shown in section 8.1, 8.2, and 8.3 define the impact of an ESS container's energy density, relative size, and separation distance with respect to the time at which a thermal threshold within an exposed container is reached.

The time to reach the thermal threshold of 80°C within an exposed ESS container is directly related to the energy density of the exposing ESS container and the corresponding heat release rate. Radiation is primarily dependent on the temperature of the radiating bodies, so as the energy density of the ESS increased, the HRR increased which produced higher flame temperatures and heated surfaces. The rise in temperature resulted in higher heat fluxes emitted onto the exposed ESS containers, causing the radiant heat to be transferred through the exposed ESS more quickly and the internal air temperature of the exposed ESS to reach its thermal threshold sooner.

As can be seen in Figures 25, 32 and 39 a fire in an ESS container with an energy capacity of 0.5 MWh does not cause an adjacent container to reach its thermal threshold within the time duration examined under any condition of separation distance or container size. This is also true for ESS containers with an energy capacity of 1 MWh with the exception of a 20 ft container at a separation distance of 3 ft, at which the thermal threshold is reached in approximately 2.6 hours.

ESS containers with energy capacities ranging from 2 MWh to 5 MWh cause an adjacent container to reach its thermal threshold for all conditions of separation distance and container size. The results for containers with energy capacities ranging from 2 MWh to 5 MWh are rearranged and presented as a function of container size in Figures 40 through 43 below.

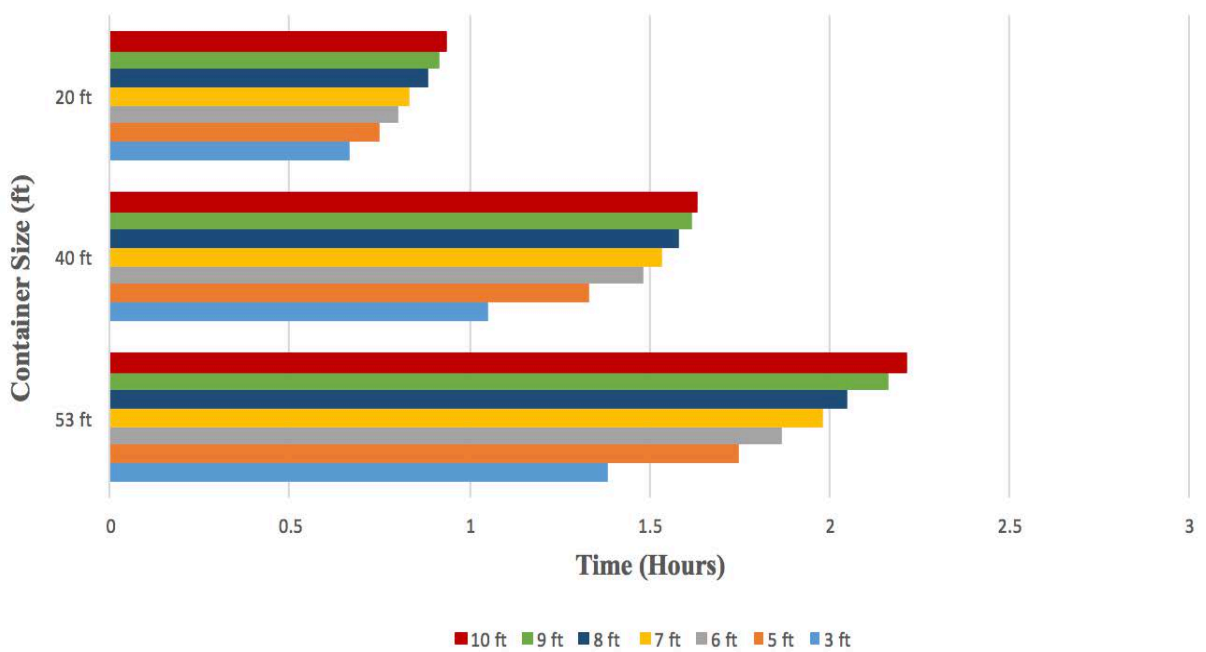


Figure 40 - Time to Failure for 20 ft, 40 ft, 53 ft ISO Containers (2 MWh Energy Capacity Exposure)

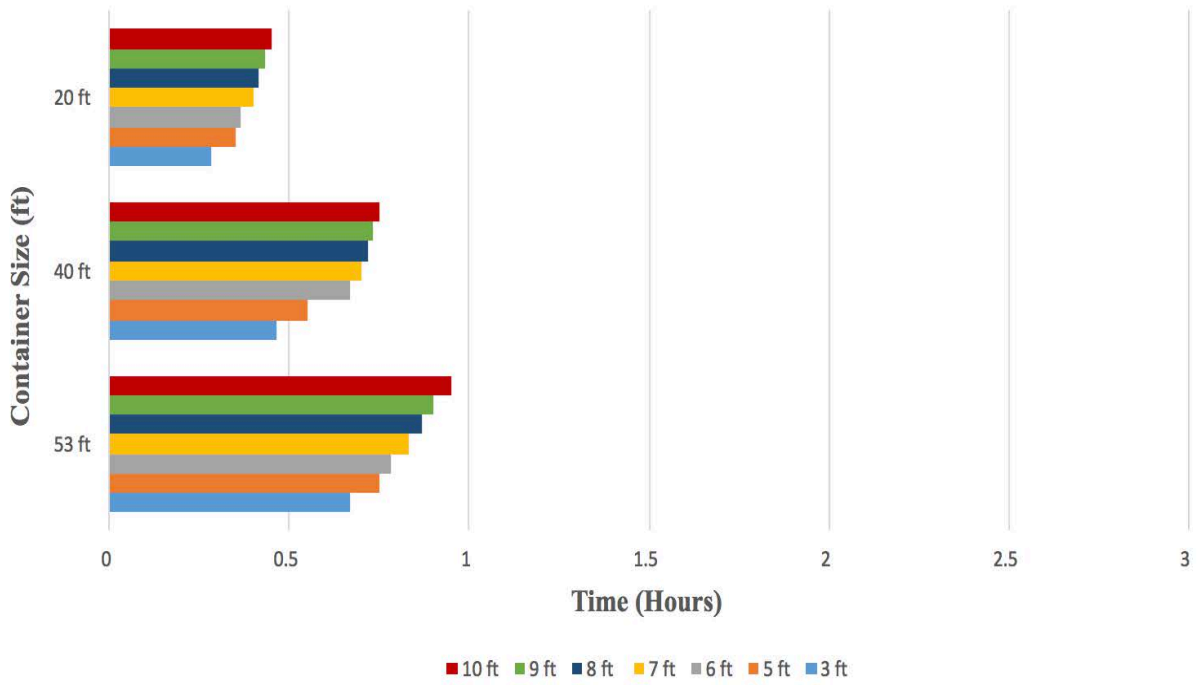


Figure 41 - Time to Failure for 20 ft, 40 ft, 53 ft ISO Containers (3 MWh Energy Capacity Exposure)

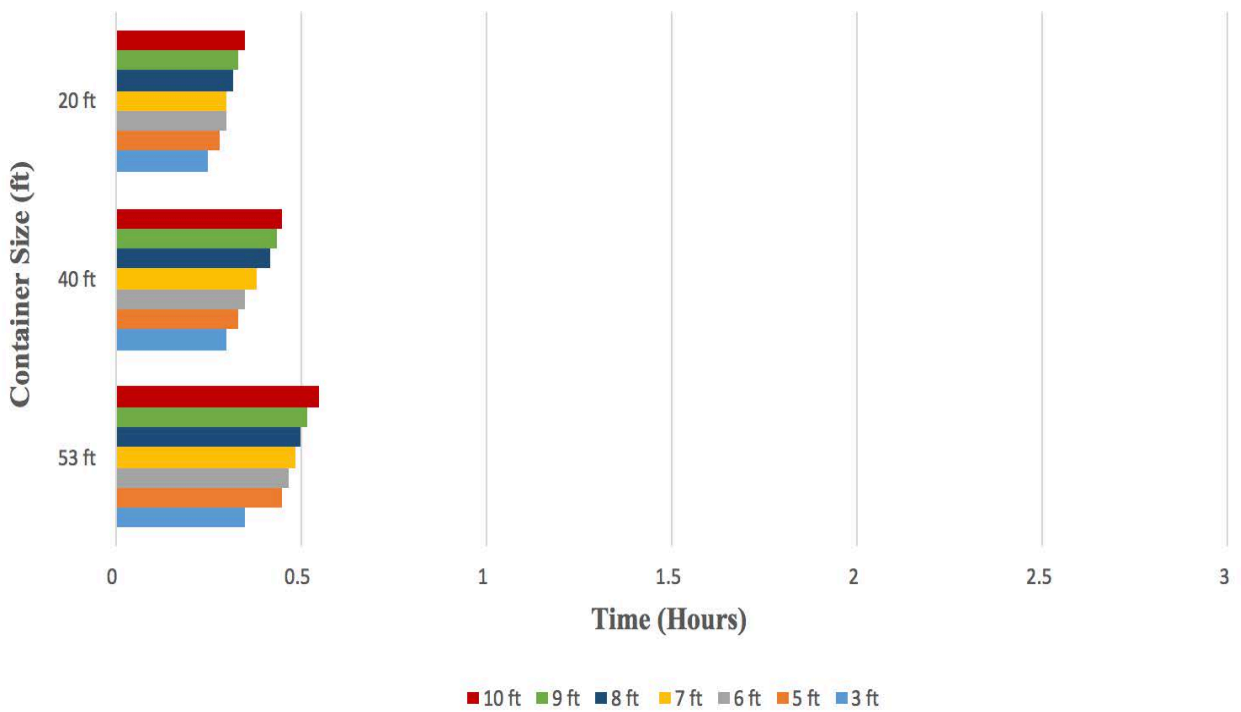


Figure 42 - Time to Failure for 20 ft, 40 ft, 53 ft ISO Containers (4 MWh Energy Capacity Exposure)

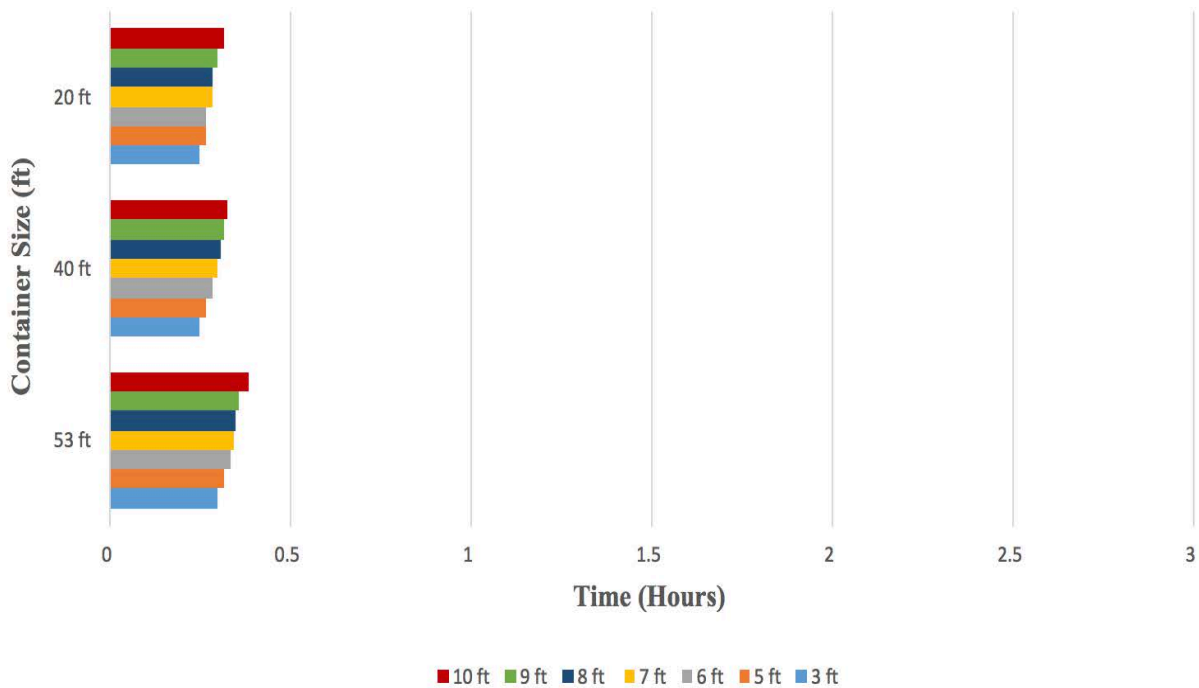


Figure 43 - Time to Failure for 20 ft, 40 ft, 53 ft ISO Containers (5 MWh Energy Capacity Exposure)

The variation in separation distances appears to have the most impact on time to reach the thermal threshold for 53 ft containers that are exposed to adjacent containers with energy capacities of 2 MWh. Figure 40 indicates that time to failures vary from 2.22 hours for a 10 ft separation to 1.38 hours for a 3 ft separation for 53 ft containers. Corresponding time for failures for a 20 ft container range from 0.9 hours (56 minutes) to 0.65 hours (39 minutes). While the time to reach a thermal threshold is generally greater in larger containers, as energy capacity increases the variation in time to failure becomes much less pronounced as a function of separation distance. Figure 43 shows that a 53 ft container exposed to an adjacent container with an energy capacity of 5 MWh has a variance in time to failure ranging between 0.383 hours (23 minutes) for a 10 ft separation and 0.3 hours (18 minutes) for a 3 ft separation. While a 20 ft container of a corresponding energy capacity exposure showed a difference in time to failure ranging between 0.316 hours (19 minutes) for a 10 ft separation and 0.25 hours (15 minutes) for a 3 ft separation. Therefore, the results indicate that at higher energy capacities the variation in separation distance becomes less impactful due to the intensity of the fire event.

9. Conclusions

This study generally indicates that as energy density in an ESS container is increased, the time to reach the thermal threshold in an adjacent ESS container decreases. Both separation distance and container size have a greater effect on the time to reach the thermal threshold in adjacent containers when energy capacities in the burning container are relatively small (2 MWh and less). As the energy capacity increases (3 MWh, 4 MWh, 5 MWh), the impact of container size and separation distance becomes less significant with respect to the time to reach the thermal threshold. Separation distances also appear to have a more significant impact on larger containers (i.e. 53 ft containers). The surface area of the exposed panels and volume of air to be heated is greater in larger containers thus requiring more energy to raise the temperature inside the container.

The results of this study further indicate that 500 kWh and 1 MWh systems do not show a significant fire propagation hazard between ESS containers during the 3-hour period analyzed. The majority of the installed lithium-ion ESS containers to date fall within the 500 kWh to 2 MWh capacity range [10]. As the lithium-ion battery technology evolves, the development and implementation of larger energy capacity systems is expected to increase. This study indicates that the fire hazard (heat release rate) intensifies within containers of larger energy capacities, thus significantly reducing the time to reach the thermal threshold of an adjacent ESS container. For larger energy capacity containers (3 MWh – 5 MWh), the difference in the time to reach the thermal threshold in adjacent containers becomes much less pronounced regardless of separation distance.

10. Recommendations for Future Work

This study put forth reasonable estimates on the radiative heat transfer between ESS storage containers due to an uncontrolled fire in one of the containers. However, ESS container fires and the behavior of lithium ion batteries during unstable conditions need to be better understood. There is limited literature and large scale test data available on these topics. As a result, certain assumptions about key factors were incorporated into this study to carry out the necessary calculations and analysis.

Greater confidence in the results of this study can be achieved by obtaining additional technical data on the following:

- Quantification of heat release rates of LIB and ESS
- Impact of ventilation on heat release rate and fire conditions within the container
- Production of gases and oxygen during LIB thermal runaway events
- Fire behavior and spread characteristics within ESS containers
- Effect of flame penetration through gaps in containers
- Emissivity of the container wall of the burning ESS container
- Emissivity of the flames emitted from the burning ESS container
- Heat of combustion of lithium-ion batteries (and ESS systems)
- Mass loss rate of lithium-ion batteries (and ESS systems)

Bibliography

- [1] U.S. Department of Energy. (2014). *Energy Storage Safety Strategic Plan*. Office of Electricity Delivery and Energy Reliability. U.S. Department of Energy.
- [2] City of New York. (2016). *NYC Sustainability*. Retrieved March 17, 2017, from nyc.gov: <http://www1.nyc.gov/site/sustainability/codes/80x50.page>
- [3] Shorris, A. (2016). *New York City's Roadmap to 80 x 50*. New York City: New York City Mayor's Office of Sustainability.
- [4] Blum, A. F., & Long, Jr., R. T. (2016). *Hazard Assessment of Lithium Ion Battery Energy Storage Systems*. Quincy: National Fire Protection Association.
- [5] Irfan, U. (2011, November 30). *Battery Fires Reveal Risks of Storing Large Amounts of Energy*. Retrieved 2016, from Scientific American: www.scientificamerican.com
- [6] *Fire Codes for Energy Storage Systems - Proposed Changes to IFC* (2017, January 4). Retrieved 2017, from Klausbruckner and Associates: www.klausbruckner.com/blog/fire-codes-for-energy-storage-systems/
- [7] NFPA. 2015. NFPA 1 The Fire Code. National Fire Protection Association. Quincy.
- [8] Cade, G. B. (2016). Code Solution: The government looks to NFPA for expertise on energy storage systems. *NFPA Journal*, 24.
- [9] *Lithium Ion (LI-ION) Batteries*. (2017). (E. S. Association, Producer) Retrieved from Energy Storage Association: energystorage.org/energy-storage/technologies/lithium-ion-li-ion-batteries
- [10] Department of Energy. (2016). *DOE Global Energy Storage Database*. (Sandia National Laboratories) Retrieved 2017, from DOE Global Energy Storage Database: www.energystorageexchange.org
- [11] A123 Design of Laurel Mountain. <http://www.a123systems.com>
- [12] LG Chem ESS Designs. <http://www.lgchem.com/global/main>
- [13] *BU-301a: Types of Battery Cells*. (2017). (Isidor Buchmann) Retrieved 2017, from Battery University: batteryuniversity.com/learn/article/types_of_battery_cells
- [14, 34] Factory Mutual Insurance Company. (2017). *FM Global Property Loss Prevention Data Sheets 5-33*. Factory Mutual Insurance Company.
- [15] Alevo Designs. <http://alevo.com>

- [16] Samsung Designs. <http://samsungsdi.com>
- [17] *Shipping Container Home Construction Globally*. (2015, April 24). Retrieved from Shipping Container Homes: www.containerhomes-info.com
- [18] SDG & E. (2017). *SDG&E Unveils World's Largest Lithium Ion Battery Storage Facility*. SDG & E.
- [19] Baldwin, D. (2017, March 13). *World's Largest Lithium-Ion Storage Facility in San Diego County May Help Solar Power*. Retrieved 2017, from Solar Tribune: solartribune.com/world's-largest-lithium-ion-storage-facility-in-san-diego-county-may-help-solar-power/
- [20] FCABC. (2014). *Intermodal Shipping Container Fire Safety*. Fire Chief's Association of British Columbia.
- [21] *Glossary*. (2017). Retrieved from Energy Storage Association: energystorage.org/energy-storage/glossary?search=energy+density
- [22] Reddy, T., & Linden, D. (Eds.). (2011). *Linden's Handbook of Batteries* (4th ed.). The McGraw-Hill Companies.
- [23] Wang, Q., Ping, P., Zhao, X., Chu, G., Sun, J., & Chen, C. (2012). Thermal Runaway caused fire and explosion of lithium ion battery. *Journal of Power Sources*, 211-222.
- [24] Ohsaki, T., Kishi, T., Kuboki, T., Takami, N., Shimura, N., Sato, Y., et al. (2005). Overcharge Reaction of Lithium-Ion Batteries. *Journal of Power Sources*, 146 (1-2), 97-100.
- [25] Ferguson, J. (2013, January 2). *APS Fire Probed*. Retrieved 2017, from Arizona Daily Sun: azdailysun.com/news/local/aps-fire-probed/article_1de2e924-ab0a-5e71-9a3a-6942c2d1c9bb.html
- [26] Smith, M. (2017, April 27). *Union Pacific Train Car Carrying Used Lithium Ion Batteries Explodes and Catches Fire Near Downtown Houston, Texas*. Retrieved 2017, from Metropolitan Engineering Consulting & Forensics - Expert Engineers: metroforensics.blogspot.com/2017/04/union-pacific-train-car-carrying-used.html
- [27] Kolly, J. M., Panagiotou, J., & Czech, B. A. (2013). *The Investigation of a Lithium-Ion Battery Fire Onboard a Boeing 787 by the US National Transportation Safety Board*. Boston: National Transportation Safety Board.
- [28] Kerley, D. (2013, March 8). *Report Details Dreamliner Battery Fire*. Retrieved 2016, from ABC News: abcnews.go.com/US/ntsb-report-details-dreamliner-battery-fire/story?id=18681266

- [29] Anderson, M., & DeLong, K. (2016, August 10). *Fire Departments from Across SE WI Called Out to Battle Blaze at Electric Company in Franklin*. Retrieved 2017, from Fox 6 Now: fox6now.com/2016/08/10/developing-crews-on-scene-of-structure-fire-at-industrial-park-in-franklin/
- [30] John, J. S. (2016, September 22). *S&C Electric Unveils Data Behind Last Month's Lithium-Ion Battery Fire*. Retrieved 2017, from Greentech Media: www.greentechmedia.com/articles/read/sc-electric-unveils-data-behind-last-months-lithium-ion-battery-fire
- [31] EnerDel. (2013). *EnerDel's approach to lithium-ion energy storage safety*. Indianapolis: EnerDel.
- [32] Mikolajczak, C. (2005). *US FAA-Style Flammability Assessment of Lithium Ion Cells and Battery Packs in Aircraft Cargo Holds*. Exponent. Menlo Park: Exponent.
- [33] Lyon, R. E., Walters, R. N., Crowley, S., & Quintiere, J. G. (2015). *Fire Hazards of Lithium Ion Batteries*. Federal Aviation Administration. Atlantic City: Federal Aviation Administration.
- [34] Jansen, A. N. (2013, October). Lithium Ion Batteries: Endless uses. *Chemical Engineering Progress*, 109.10, 57-64.
- [35] Pennsylvania Office of the State Fire Commissioner. (n.d.). *Fire Dynamics Terminology*. Retrieved 2017, from Pennsylvania Office of the State Fire Commissioner: www.osfc.pa.gov/Documents/Fire%20Dynamics%20Terminology.pdf
- [36] Federal Energy Regulatory Commission. (2013). *Recommended Parameters for Solid Flame Models for Land Based Liquefied Natural Gas Spills*. Department of Energy, Federal Energy Regulatory Commission. Washington, DC: Department of Energy.
- [37] Quintiere, J. G. (1998). *Principles of Fire Behavior*. Clifton Park: Delmar Cengage Learning.
- [38] McGrattan, K. B., Baum, H. R., & Hamins, A. (2000). *Thermal Radiation from Large Pool Fires*. National Institute of Standards and Technology.
- [39] Janna, W. S. (2000). *Engineering Heat Transfer* (2nd ed.). Boca Raton: CRC Press LLC.
- [40] Walton, W. D., & Thomas, P. H. (2008). Estimating Temperatures in Compartment Fires. In *The SFPE Handbook of Fire Protection Engineering* (4th ed., pp. 3-204-3-221). Quincy: National Fire Protection Association.
- [41] Brown, C. (2016). *Silatronix*. Retrieved October 10, 2016, from Technology. Li-Ion Battery Electrolytes: <http://silatronix.com/technology/li-ion-battery-electrolytes/>

- [42] Alhama, F., & Zueco, J. (2007). Application of a Lumped Model to Solids with Linearly Temperature-Dependent Thermal Conductivity. *Applied Mathematical Modelling*, 31 (2), 302-310.
- [43] Bell, K. J. (2011, February 2). *Overall Heat Transfer Coefficient*. Retrieved 2017, from Thermopedia: thermopedia.com/content/1007/
- [44] Wang, Y.C. *Steel and Composite Structures – Behavior and Design for Fire Safety*, Spon Press, 2002.
- [45] Underwriters Laboratory. (2013). Lithium-Ion Batteries. *New Science Sustainable Energy*, 1-27.
- [46] DNV GL. (2017). *Considerations for ESS Fire Safety*. Dublin: DNV GL.
- [47] Lisbona, D., & Snee, T. (2011). A review of hazards associated with primary lithium and lithium-ion batteries. *Process Safety and Environmental Protection*, 434-442.
- [48] Lamb, J., Orendorff, C. J., Steele, L. M., & Spangler, S. W. (2014). Failure Propagation in multi-cell lithium-ion batteries. *Journal of Power Sources*.
- [49] Mikolajczak, C., Kahn, M., White, K., & Long, R. T. (2011). *Lithium-Ion Batteries Hazard and Use Assessment*. Fire Protection Research Foundation.
- [50] Crowley, L. T., & Johnson, A. D. (1992). *Oil and Gas Fires: Characteristics and Impact*. The Steel Construction Institute. London: The Health and Safety Executive.
- [51] Anderson, J., Larsson, F., Andersson, P., & Mellander, B.-E. (2015). *Thermal Modeling of Fire Propagation in lithium-ion batteries*. Chalmers University of Technology. Göteborg: SP Technical Research Institution of Sweden.
- [52] Back, J., & Schwartz, J. (2016). *Modeling Conditions Produced During Battery Reactions*. Jensen Hughes. Jensen Hughes.
- [53] Custer, R. L. (2008). Dynamics of Compartment Fire Growth, Section 2, Chapter 4. In *Fire Protection Handbook* (20th ed., Vol. 1, pp. 2-49-2-58). Quincy: National Fire Protection Association.
- [54] Maloney, T. (2014). *Extinguishment of Lithium-Ion and Lithium-Metal Battery Fires*. Atlantic City: US DOT Federal Aviation Administration.
- [55] Biteau, H., Steinhaus, T., Schemel, C., Simeoni, A., Marlair, G., Bal, N., et al. (2008). *Calculation Methods for the Heat Release Rate of Materials of Unknown Composition*. International Association for Fire Safety Science.

- [56] Walton, W. D., Carpenter, D. J., & Wood, C. B. (2008). Zone Computer Fire Models for Enclosures. In SFPE, *The SFPE Handbook of Fire Protection Engineering* (pp. 3-222 - 3-228). Quincy: NFPA.
- [57] Drysdale, D. (2011). *An Introduction to Fire Dynamics* (3rd ed.). West Sussex, United Kingdom: John Wiley & Sons, Ltd.
- [58] Zhao, W. (2014). *Modeling of Large-Format Li-Ion Cell Performance and Safety*. The Pennsylvania State University, Department of Mechanical and Nuclear Engineering. State College: The Pennsylvania State University.
- [59] Ponchaut, N., Marr, K., Colella, F., Somandepalli, V., & Horn, Q. (n.d.). *Thermal Runaway and Safety of Large Lithium-Ion Battery Systems*. Exponent, Inc. Natick: Exponent Inc.
- [60] Ping, P., Wang, Q., Huang, P., Sun, J., Kong, D., & Chen, C. (2015). Study of the fire behavior of high-energy lithium-ion batteries with full-scale burning test. *Journal of Power Sources*, 285, 80-89.
- [61] Gottuk, D. T., & Lattimer, B. Y. (2008). Effect of Combustion Conditions on Species Production. In *The SFPE Handbook of Fire Protection Engineering* (4th ed., pp. 2-67-2-95). Quincy: National Fire Protection Association.
- [62] Marchetti, L. J. (2012). *Fire Dynamics Series: Predicting Hot Gas Layer Temperature and Smoke Layer Height in a Room Fire with Natural and Forced Ventilation*. Fairfax: PDH Center.
- [63] Quintiere, J. G. (2006). *Fundamentals of Fire Phenomena*. West Sussex, England: John Wiley & Sons, Ltd.
- [64] Feng, X., Sun, J., Ouyang, M., Wang, F., He, X., Lu, L., & Peng, H. (2014). Characterization of penetration induced thermal runaway propagation process within a large format lithium-ion battery module. *Journal of Power Sources*.
- [65] (2017). *Radiation Heat Transfer: Module 1*.
- [66] AZ Containers. (n.d.). *20 ft. Standard Container Dimensions*. Retrieved from AZ Containers:
www.azcontainers.com/sites/all/themes/azcontainers/images/containers/20Standard_lgb.jpg
- [67] AZ Containers. (n.d.). *40 ft. Standard Container Dimensions*. Retrieved from AZ Containers:
www.azcontainers.com/sites/all/themes/azcontainers/images/containers/40Standard_lgb.jpg

- [68] 3D Molier. (n.d.). *Subdivision Level 0*. Retrieved from 3D Molier: 3dsmolier.com/media/cache/9b/5c33fa238ae3c88e003a6bab76266c.jpg
- [69] Tien, C. L., Lee, K. Y., & Stretton, A. J. (2008). 1-4 Radiation Heat Transfer. In *The SFPE Handbook of Fire Protection Engineering* (4th ed., pp. 1-74-1-90). Quincy: National Fire Protection Association.
- [70] Drysdale, D. (2008). 1-5 Thermochemistry. In *The SFPE Handbook of Fire Protection Engineering* (4th ed., pp. 1-91-1-100). Quincy: National Fire Protection Association.
- [71] Friedman, R. (2008). 1-6 Chemical Equilibrium. In *The SFPE Handbook of Fire Protection Engineering* (4th ed., pp. 1-101-1-111). Quincy: National Fire Protection Association.
- [72] Heskestad, G. (2008). 2-1 Fire Plumes, Flame Height, and Air Entrainment. In *The SFPE Handbook of Fire Protection Engineering* (4th ed., pp. 2-1-2-20). Quincy: National Fire Protection Association.
- [73] Emmons, H. W., & Tanaka, T. (2008). 2-3 Vent Flows. In *The SFPE Handbook of Fire Protection Engineering* (4th ed., pp. 2-37-2-53). Quincy: National Fire Protection Association.
- [74] Lattimer, B. Y. (2008). 2-14 Heat Fluxes from Fires to Surfaces. In *The SFPE Handbook of Fire Protection Engineering* (4th ed., pp. 2-303-2-336). Quincy: National Fire Protection Association.
- [75] Babrauskas, V. (2008). 3-1 Heat Release Rates. In *The SFPE Handbook of Fire Protection Engineering* (4th ed., pp. 3-1-3-59). Quincy: National Fire Protection Association.
- [76] Tewarson, A. (2008). 3-4 Generation of Heat and Gaseous, Liquid and Solid Products in Fires. In *The SFPE Handbook of Fire Protection Engineering* (4th ed., pp. 3-109-3-194). Quincy: National Fire Protection Association.
- [77] Quintiere, J. G. (2008). 3-5 Compartment Fire Modeling. In *The SFPE Handbook of Fire Protection Engineering* (4th ed., pp. 3-195-3-203). Quincy: National Fire Protection Association.
- [78] Beyler, C. L. (2008). 3-10 Fire Hazard Calculations for Large, Open Hydrocarbons Fires. In *The SFPE Handbook of Fire Protection Engineering* (4th ed., pp. 3-271-3-319). Quincy: National Fire Protection Association.
- [79] Backovsky, J., Foote, K. L., & Alvares, N. J. (1988). Temperature Profiles in Forced-Ventilation Enclosure Fires. *Fire Safety Science - Proceedings of the Second International Symposium* (pp. 315-324). Livermore: International Association for Fire Safety Science.
- [80] Energy Storage Association. (2017). Come learn about SNO-PUD and Doosan's ESS Fleet Solution at ESACon17. Washington, DC: *Energy Storage Association*.

[81] Heritage Fire Protection, Inc. (2011). Photo. Ashland, KY: *Heritage Fire Protection, Inc.*

Appendix A: Additional Reference Material



Figure 44 Grid-tied MW scale Li-Ion ESS installations



Figure 45 20 ft ISO Container

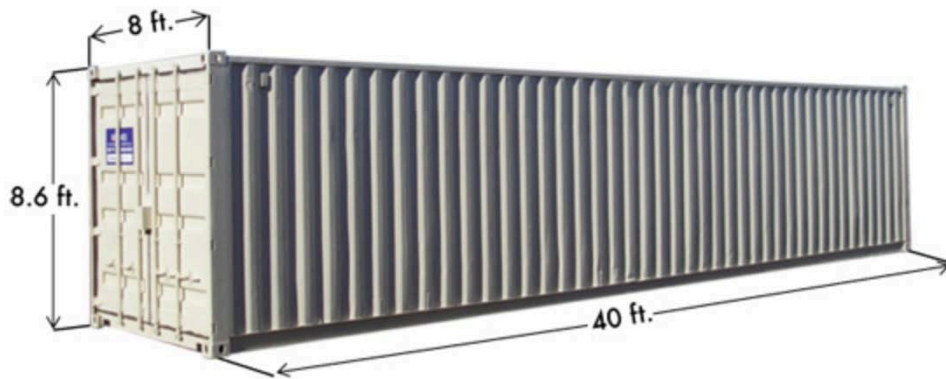



Figure 46 40 ft ISO Container



Figure 47 53 ft Modified ISO-Container

Appendix B: NFPA 2017 C&E Presentation




Lithium Ion Battery ESS: Fires and Protection Schemes

Presenters:

Victoria Hutchison
Graduate Student
WPI Fire Protection Engineering Dept.


Milosh Puchovsky, P.E., FSFPE
Professor of Practice
WPI Fire Protection Engineering Dept.
President SFPE 2016

NFPA 2017 Conference & Expo




Project Scope

A graduate research project applying an analytical radiation heat transfer analysis for the evaluation of separation distances between outdoor Lithium-Ion Energy Storage Systems (ESS).




Supported through an NFPA Fellowship

© 2017 Hutchison, Puchovsky



Agenda

- Overview of Energy Storage Systems (ESS)
- Fire Safety Concerns and Regulations
- Heat Transfer Methodology
- Quantification of LIB ESS Fires
- Evaluation Criteria (Thermal Thresholds)
- Discussion of Results and Recommendations for Future Work




© 2017 Hutchison, Puchovsky

Overview of ESS

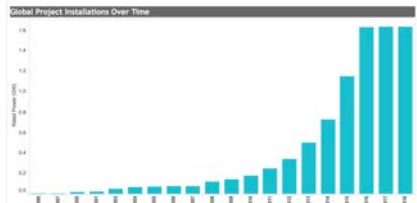
- Energy is King
- Energy Storage System (ESS) – A system that captures energy produced for use at a later time.
- Public Utilities, Commercial Enterprises, Residential Applications, etc.
- Focus:
 - Electrochemical Energy Storage Systems
 - Lithium-Ion Batteries

© 2017 Hutchison, Puchovsky



ESS Market


- Clean Energy Initiative*
- Key incentives for Renewable Energy
- ESS is a functional component of Renewable Energy



DOE Global Energy Storage Database (2017)


*United Nations Framework on Climate Change to Reduce 80% of Greenhouse Gas Emissions by 2050.

© 2017 Hutchison, Puchovsky




ESS Installations

- Large-Scale Lithium-Ion ESS Installations Worldwide
- Nearly 700 Installations: 1.64 GW of Power Deployed



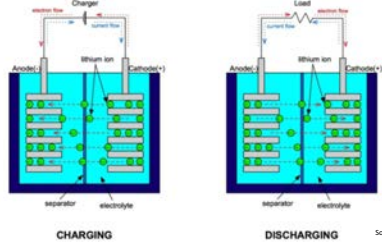
DOE Global Energy Storage Database (2017)

© 2017 Hutchison, Puchovsky



Battery Concept

- Battery – a container consisting of one or more cells in which chemical energy is converted to electricity and used as a source of power.



7 © 2017 Hutchison, Puchovsky



Battery Concepts

- Energy Density – how much energy the battery is capable of delivering per unit volume. Measured in Watt-hours per Liter (Wh/L).
- Power Density – the amount of power a battery can deliver per unit mass. Measured in Watt-hours per kilogram (Wh/kg).
- Energy Capacity of ESS – amount of power flowing for a specified period of time. Measured in Kilowatt-Hours (kWh) or Megawatt-Hours (MWh)

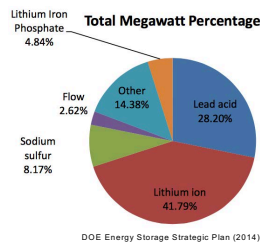
8 © 2017 Hutchison, Puchovsky



Lithium-Ion Battery Overview

Why Lithium-Ion Batteries?

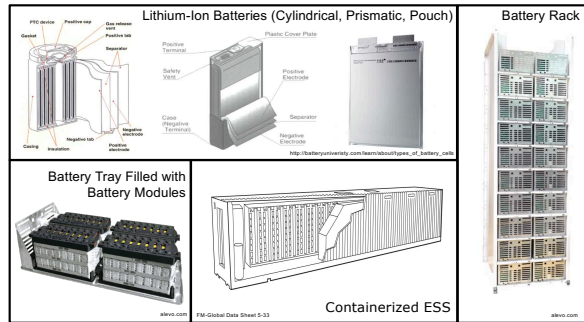
- High energy density
- Nearly 100% Charge/Discharge Efficiency
- High Power Rate Capability
- Large Storage Potential
- Rechargeable - Long Cycle Life (1000-3000+ Cycles)
- Scale flexibility among various applications



9 © 2017 Hutchison, Puchovsky



ESS Makeup



10 © 2017 Hutchison, Puchovsky



Variations in ESS Designs

- Different Types of Lithium-Ion Batteries Used
 - Format: Cylindrical, Prismatic, Pouch
 - Chemistry: LiCoO₂, LiFePO₄, LiMnNiCoO₂, etc.
 - Size: small format, large format
 - Energy Density (Wh/l) – amount of energy stored within specific volume
- Quantity of Batteries per module/tray/rack/system
- Orientation/Configuration of batteries within rack
- Rack Design – Enclosed Cabinet / Open Frame
- Ranges in Maximum Rated Energy (500kWh – 5 MWh+)

11 © 2017 Hutchison, Puchovsky



ESS Installations



12 © 2017 Hutchison, Puchovsky



ESS Installations



Picture from Energy Storage Association



ESS Container

- ESS Container
 - Typical ISO-Container (With modifications)
 - 20 ft x 8 ft x 8.5 ft
 - 40 ft x 8 ft x 8.5 ft
 - 53 ft x 8 ft x 8.5 ft
- Materials
 - Typically Corten Steel
 - ISO-Containers are not insulated
- Ventilation
 - Used for cooling within the compartment



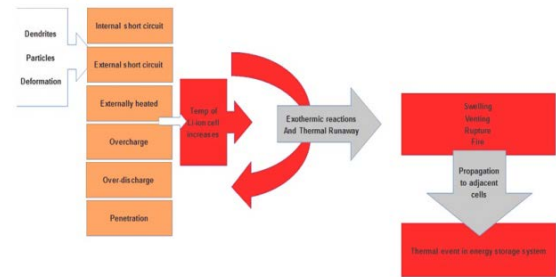
Inside an ESS Container



Pictures from Heritage Fire Protection, Inc.



Lithium-Ion Battery Failure Modes



The Fire Safety Concerns in ESS

- Large quantities of energy stored in a small space (i.e. high energy densities).
- Rapid Fires of Significant Heat Release
- Threat of propagating thermal runaway within ESS Container.
 - Batteries are heat sensitive
 - Difficult to dissipate heat generated from battery failure, resulting in fire growth
- Threat of radiation exposure from ESS fire causing fire propagation to adjacent ESS containers.



LIB Fire Events



Proposed Fire Safety Regulations

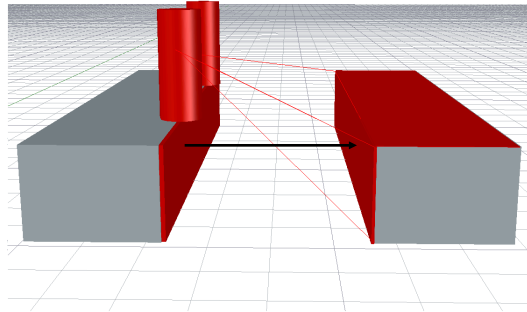
- NFPA 855 Standard for Stationary Energy Storage Systems
 - In Development
- NFPA 1 Fire Code
- International Fire Code (IFC)
- Provisions Recommended for 2018 editions:
 - 5 ft. separation between ESS containers and other exposure hazards
 - Other distances per "large scale" testing



19 © 2017 Hutchison, Puchovsky



Radiation Heat Transfer Approach



20 © 2017 Hutchison, Puchovsky



Radiation Heat Transfer Approach

$$\dot{q}'' = \epsilon \sigma F T^4$$

- \dot{q}'' – Radiation Heat Flux Impinging on Exposed Container
- ϵ – Emissivity of Surfaces and Flame of Burning Container
- σ – Stefan-Boltzman Constant
- F – View Factor (Geometric Dimensions)
- T – Temperature of Surfaces and Flames (Function of Burning Container)

Quintiere, Fundamentals of Fire Behavior

21 © 2017 Hutchison, Puchovsky



Radiation Heat Transfer Approach

- Container Sizes: 20 ft, 40 ft, 53 ft
- Range of Energy Capacities of ESS: 0.5 MWh – 5 MWh
- Separation Distances: 3 ft – 10 ft

22 © 2017 Hutchison, Puchovsky



Emissivity of Container Wall (ϵ_w)

Emissivity (ϵ) – a measure of the efficiency of a surface or flame as a radiator.

Steel Container – Opaque Surface – Behave as Radiant Blackbodies

Principle of Radiant Blackbodies – Perfect Emitter/Absorber

$$\epsilon = \alpha$$

$$\alpha = 1$$

$$\text{absorptivity } (\alpha) + \text{reflectivity } (\rho) + \text{transmissivity } (\tau) = 1$$

$$\text{Surface emissivity} = \epsilon_w = 1$$

SFPE HB Radiation Heat Transfer

23 © 2017 Hutchison, Puchovsky



Emissivity of Flames (ϵ_{fl})

$$\epsilon_{fl} = 1 - \exp(-kl)$$

- k – absorption coefficient (m^{-1})
 - measure of radiation's ability to penetrate through flame
- l – flame thickness (m)

Common to assume black-body behavior for luminous, turbulent, high temperature diffusion flames.

Fuels found in lithium-ion battery combustion products (such as total hydrocarbons) have flame emissivity's of nearly 1.

$$\text{Flame emissivity} = \epsilon \approx 1$$

Quintiere, Fundamentals of Fire Behavior

24 © 2017 Hutchison, Puchovsky



View Factor – Wall (F1_{p,2p})

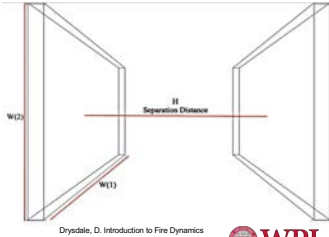
- View Factor between equal, parallel, rectangular plates of size W(1) x W(2) separated by a distance of H.

$$F_{1(p),2} = \frac{1}{\pi xy} \left[\ln \frac{x_1^2 y_1^2}{x_2^2 + y_2^2 - 1} + 2x(y_1 \arctan \frac{x}{y_1} - \arctan x) + 2y(x_1 \arctan \frac{y}{x_1} - \arctan y) \right]$$

$$x_1 = \sqrt{1+x^2}, \quad y_1 = \sqrt{1+y^2}$$

$$x = \frac{W_1}{H}, \quad y = \frac{W_2}{H}$$

View Factor between rectangular plates determines the amount of radiation received at the exposed panel based on the container size and their separation distance.

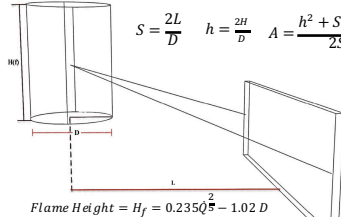


View Factor – Flame (F1_{fl,2p})

- View Factor from Cylindrical Flame to rectangular plate.

$$F_{1_{fl},2p} = \frac{1}{\pi S} \tan^{-1} \left(\frac{h}{\sqrt{S^2-1}} \right) - \frac{h}{\pi S} \tan^{-1} \sqrt{\frac{S-1}{S+1}} + \frac{Ah}{\pi S \sqrt{A^2-1}} \tan^{-1} \sqrt{\frac{(A+1)(S-1)}{(A-1)(S+1)}}$$

$$S = \frac{2L}{D}, \quad h = \frac{2H}{D}, \quad A = \frac{h^2 + S^2 + 1}{2S}$$



View Factor between cylindrical flame and rectangular plate determines the fraction of radiation received (visible) at the exposed panel based on the size of the flame, angle, and separation distance.



Wall Temperature (T_w)

- As temperature of walls rise, radiant heat will be emitted from the steel panel and absorbed by the exposed ESS.

$$\dot{q}'' = \epsilon \sigma F T_w^4$$

- The Temperature of Container Boundaries (Walls) rise through radiant and convective heating from the hot gas layer (fire plume).

$$\frac{dT_{w,1}}{dt} = \frac{1}{\rho_s c_s \Delta x A_s} \left[\epsilon \sigma (T_g^4 - T_w^4) + h A_w (T_g - T_w) - h_{\infty} A_w (T_w - T_{\infty}) \right]$$



Gas/Flame Temperature (T_g/T_{fl})

- Compartment Fire**

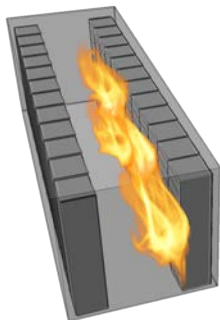
As the fire grows a hot gas layer (fire plume) will form inside the container and extend to the outside of the container.

- Calculated based on correlation for **Forced Ventilation Fires**.

$$\frac{\Delta T_g}{dt} = T_{\infty} + \left(0.63 * \frac{\dot{Q}}{\dot{m}_{air} c_p T_{\infty}} \right)^{0.72} * \left(\frac{h_k A}{\dot{m}_{air} c_p} \right)^{-0.36}$$



Development of Heat Release Rate



- Initiates with a thermal runaway in one battery.
 - Uncontrollable rapid release of energy (120 C) and temperature rise resulting in a fire
 - Spreads throughout modules and racks due to conduction, convection and radiation heat transfer.
 - Fire grows as internal temperature exceeds stable range of lithium-ion batteries.



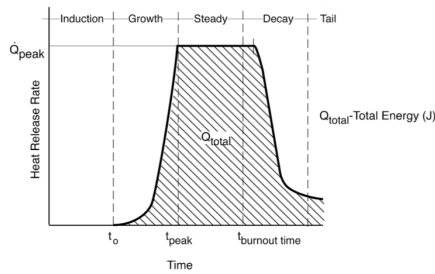
Impact of Forced Ventilation

- Mechanical ventilation system is assumed to be left on for means of cooling.
- Ventilation correlation factor of 0.32 cfm/kWh*
 - Function of Maximum Rated Energy of ESS
- Assumes all batteries within ESS become involved.
- Heat Release Rate is effected by the rate of forced air ventilation through the container (\dot{m}_{air}).

*Correlation from DNV GL/ Con-Edison Considerations for ESS Fire Safety



Approximated HRR Curve



31 © 2017 Hutchison, Puchovsky



Determination of Heat Release Rate

- **Peak Steady-State Heat Release Rate(HRR) - \dot{Q}** - the amount of energy released.

$$Peak\ HRR = \dot{m}_g \Delta H_c$$

$$\dot{m}_g = \dot{m}_{air} + \dot{m}_{fuel}$$

Fire Growth to Peak HRR

$$\dot{Q} = \alpha t^2$$

$$\alpha = 0.0118\ kW/s^3$$

Fire Protection Handbook 2-4
SFPE Handbook 1-6

32 © 2017 Hutchison, Puchovsky



Peak Heat Release Rate

Energy Capacity (MWh)	Ventilation Factor (cfm/kWh)	Air Flow Rate (cfm)	\dot{m}_{air} (kg/s)	\dot{m}_{fuel} (kg/s)	\dot{m}_g (kg/s)	ΔH_c (MJ/kg)	Peak HRR (MW)
0.5 MWh	0.32	160	0.0912	0.0015	0.0927	28	2.6
1 MWh	0.32	320	0.1812	0.0015	0.1837	28	5.1
2 MWh	0.32	640	0.3624	0.0015	0.3639	28	10.1
3 MWh	0.32	960	0.5436	0.0015	0.5451	28	15.2
4 MWh	0.32	1280	0.7248	0.0015	0.7263	28	20.3
5 MWh	0.32	1600	0.9060	0.0015	0.9075	28	25.4

33 © 2017 Hutchison, Puchovsky



When Flames Extend from ESS

- Heat Transfer Outside Container:
 - Flames and excess flammable gases can be ignited outside of the container through the vents once gas layer reaches ~ 775 K (500 C)
 - Temperature rises → internal pressure rises → forces flammable gases and flames out vents at temperature dependent velocity.
 - A radiant heat flux is emitted from the cylindrical flame exiting the vent.

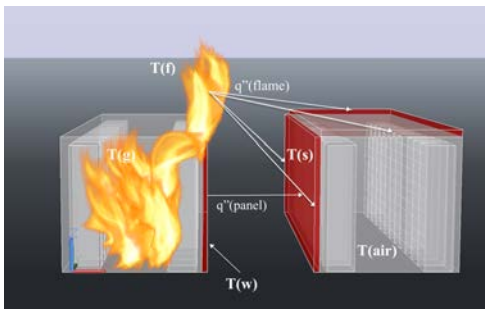
$$\dot{q}''_{fl} = \epsilon \sigma F_{fl,p} T_{fl}^4$$

Quintiere, Fundamentals of Fire Behavior

34 © 2017 Hutchison, Puchovsky



Radiation Heat Transfer



35 © 2017 Hutchison, Puchovsky



Thermal Threshold of Exposed ESS

It is assumed that when the internal air temperature of exposed ESS reaches 80°C lithium-ion batteries begin to thermally self-decompose.

- Measure when the internal air temperature of exposed container reaches 80°C based on heat transferred through heated surfaces.

- Heat transfer between heated steel panel and internal air temperature

$$\frac{dT_{air}}{dt} = \frac{1}{\rho c_p V} * [hA(T_{s,hot} - T_{air}) - (hA)_{cold}(T_{air} - T_{\infty})]$$

Oydsdale, D. Introduction to Fire Dynamics

36 © 2017 Hutchison, Puchovsky



Thermal Threshold of Exposed ESS

- Calculate rise in temperature of the surface of the exposed steel container based on summation of radiant exposure.

$$T_{s,hot} = T_{\infty} + \frac{\alpha \dot{q}'' \sqrt{t}}{A_s k \rho c_p}$$

- Function of Total Radiant Heat Flux: \dot{q}''_{total}

$$\dot{q}''_{total} = \epsilon \sigma F T_{fl}^4 + \epsilon \sigma F T_w^4$$

SFPE Handbook

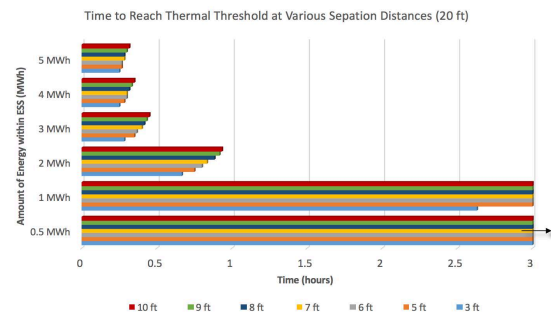


Conclusions

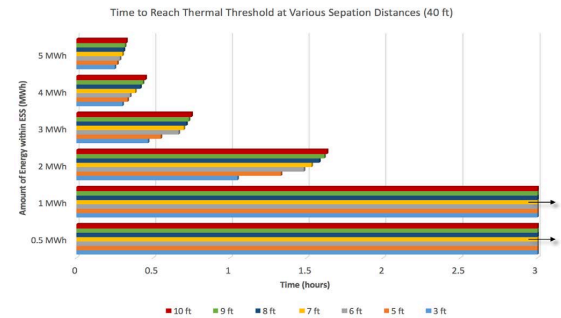
- Market is driving increased energy density of ESS units.
- The heat release rate is proportional to the energy density of the ESS.
- As energy density increases time to failure decreases.
- Container size has an impact on the absorbed radiation over time – smaller units fail sooner with same energy capacity.
- As energy density increases, container size and separation distances have less of an impact.



Results – 20 ft ESS



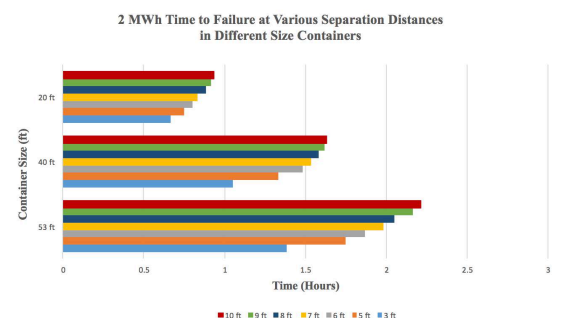
Results – 40 ft ESS



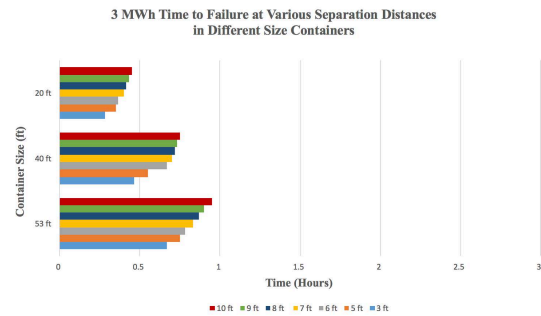
Results – 53 ft ESS



2 MWh Results



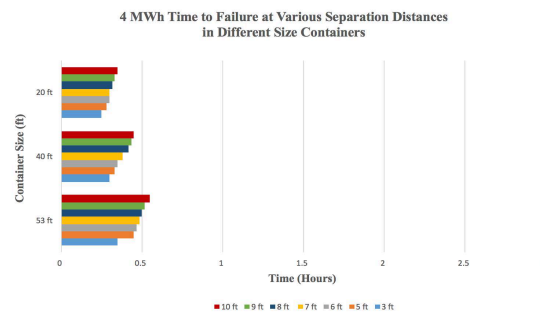
3 MWh Results



43 © 2017 Hutchison, Puchovsky



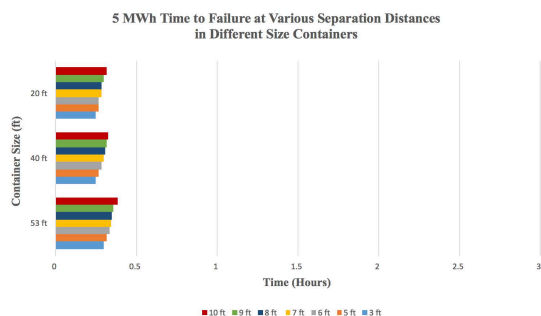
4 MWh Results



44 © 2017 Hutchison, Puchovsky



5 MWh Results



45 © 2017 Hutchison, Puchovsky



Recommendations for Future Work

- Full-Scale fire testing
- Quantification of heat release rates of LIB and ESS
- Impact of ventilation and oxygen production on fire conditions
- Fire behavior and spread characteristics within ESS container
- Effect of gaps in container on flame penetration
- Emissivity of wall container and flames
- ΔH_c and \dot{m}_{fuel} of LIB's



46 © 2017 Hutchison, Puchovsky



Thank You!

Victoria Hutchison
WPI Graduate Student
vnhutchison@wpi.edu

Milosh Puchovsky, P.E., FSFPE
WPI Professor of Practice
milosh@wpi.edu

Report and Presentation Available at:
wpi.edu/+FPE



47 © 2017 Hutchison, Puchovsky

2017 NFPA Conference & Expo

- CEUs:** To receive CEUs for this session scan your badge at the back of the room before leaving.
- Evaluation:** Complete a session evaluation on the mobile app. (Search app store for 'NFPA 2017 C&E'.)
- Handouts:** Handouts will be available via the mobile app and at nfpa.org/conference
- Recordings:** Audio recordings of all sessions will be available free of charge via NFPA Xchange.

48 © 2017 Hutchison, Puchovsky

